UNIVERSITÀ DEGLI STUDI DI PADOVA

Sede Amministrativa: Università degli Studi di Padova
Dipartimento di Scienze del Farmaco

SCUOLA DI DOTTORATO DI RICERCA IN
BIOLOGIA E MEDICINA DELLA RIGENERAZIONE

CICLO XXVI

Characterization and expression analysis of *ambra1a* and *ambra1b* genes in zebrafish and study of their roles during early development

Direttore della Scuola: Ch.ma Prof.ssa Maria Teresa Conconi

Supervisore: Ch.ma Dott.ssa Luisa Dalla Valle

Dottoranda: Dott.ssa Tatjana Škobo

Index

Abbreviations

AMBRA1, autophagy/beclin-1 regulator 1
ATG, autophagy related proteins
ATG5, autophagy related 5
ATG7, autophagy related 7
ATG14, autophagy related 14
^{ATG}MOs, translation blocking morpholinos
Baf A1, bafilomycin A_1
BCL2, B-cell CLL/lymphoma 2
BECN1, beclin 1, autophagy related
B. schlosseri, Botryllus schlosseri
cDNA, complementary DNA;
chd, chordin
chrm4, cholinergic receptor, muscarinic 4
C. intestinalis, Ciona intestinalis
CNS, central nervous system
D. rerio, Danio rerio
dpf, days post fertilisation
DIG, digoxigenin
dgkz, diacylglycerol kinase, zeta
DLCs, dynein light chains
DYNLL1, dynein, light chain, LC8-type 1
EGFP, Enhanced Green Fluorescent Protein
ER, endoplasmic reticulum
EST, Expressed Sequence Tags
gsc, goosecoid homeobox
hpf, hours post fertilisation
IDPs, Intrinsically Disordered Proteins
KIAA0226, RUBICON/RUN domain and cysteine-rich domain containing, Beclin 1-interacting protein
MAP1LC3/LC3, microtubule-associated protein 1A/1B-light chain 3
mdk, midkine (neurite growth-promoting factor 2)
^{MISM}MO, five-nucleotide-mismatched MOs
MOs, morpholinos;
mRNA, messenger RNA
NBT/BCIP, 5-nitro-blue tetrazolium chloride/bromo-4-chloro-3'-indolyphosphate p-toluidine salt
ORF, open reading frame
PBS, phosphate-buffered saline
PCR, polymerase chain reaction
PFA, paraformaldehyde

phf21a, PHD finger protein 21A

Abbreviations

PIK3C3, phosphatidylinositol 3-kinase, catalytic subunit type 3
PIK3R4/Vps15/p150, phosphoinositide-3-kinase, regulatory subunit 4
qPCR, real time-polymerase chain reaction
RACE, rapid amplification of cDNA ends
RT-PCR, reverse transcriptase-polymerase chain reaction
SEM, scanning electron microscopy
S.E.M., standard error of the mean
SL, splice leader sequence.
shha, sonic hedgehog a
SH3GLB1, SH3-domain GRB2-like endophilin B1
^{SPLIC}MOs, splicing blocking morpholinos
TP53, tumor protein p53
TUNEL, terminal deoxynucleotidyl transferase-mediated fluorescein-dUTP nick end labeling assay
UVRAG, UV radiation resistance associated
WMISH, Whole Mount In Situ Hybridization
WT, wild type

Summary

The study of autophagy is a new research field that has recently obtained great attention due to the involvement of autophagy in several developmental and pathophysiological processes. In the last years, zebrafish has become a powerful model organism to study the genes that play important roles during development, and thus, in this project, I used a reverse genetics approach and the zebrafish as a model organism to study the role and the functions of Ambra1, a key protein involved in the early steps of autophagosome formation. Ambra1-deficient mice are embryonic lethal, and show defects in the central nervous system, with hyperproliferation of the neuroepithelium, exencephaly and imperfect closure of the neural tube, thus suggesting that, in mouse, Ambra1 is crucial for the proper nervous system development.

In Chapter I, it is described the identification and characterization of the two paralogous genes, *ambra1a* and *ambra1b*, which encode the two isoforms of this protein in zebrafish. Transcripts of both genes are present as maternal RNAs in the early stages of development, while afterwards they are mainly localized in the head, suggesting a potential role for these proteins in the development of the central nervous system also in zebrafish. The knockdown of both proteins is associated with severe developmental abnormalities, early embryonic lethality and impairment of the autophagic process. Moreover, the results obtained suggest the possible acquisition of specific functions by the two paralogous genes that are both required during development and do not compensate each other following knockdown.

In Chapter II the possibility that, also in zebrafish, the functional silencing of Ambra1 could lead to uncontrolled cell proliferation was confirmed by Phospho-Histone-H3 immunohistochemistry in both *ambra1* zebrafish morphants. Moreover, the cell-autonomous capability of Ambra1-depleted cells to hyperproliferate was analysed by transplantation experiments that showed a higher proliferation rate in *ambra1a* and *ambra1b* chimeras with respect to controls.

Chapter III describes involvement of Ambra1a and Ambra1b on zebrafish skeletal muscle development and compares the phenotype of zebrafish ambra1-depleted embryos with that of Ambra1$^{gt/gt}$ mouse embryos. Morphological analysis of morphant embryos reveals that the silencing of *ambra1* impairs locomotor activity and muscle development. More severe phenotypes are obtained by knockdown of maternal transcripts, therefore, underlining the role of these proteins during development.

Finally, Chapter IV reports the cloning and characterization of *ambra1* in the tunicate *Botryllus schlosseri,* a model species of a colonial ascidian. This is the first characterization of *ambra1* transcripts in a non-vertebrate organism. The deduced amino acid sequence is shorter then vertebrate Ambra1 proteins but still contains the WD40 domain as well as other amino acid residues that are important for polyubiquitination or caspase cleavage of the protein. However, the *B. schlosseri* protein lacks other important domain such as the DLC1-binding consensus motifs (TQT) that, in vertebrates, docks the protein at its specific cytoskeletal site. Expression of these genes was found in all the different stages of the life cycle analysed.

Riassunto

Lo studio dell'autofagia costituisce un campo di ricerca che ha recentemente ottenuto una notevole attenzione grazie al coinvolgimento che questo processo sembra avere sia durante lo sviluppo sia nella vita adulta, in numerose condizioni fisiologiche e patologiche.

In questo progetto di ricerca ho utilizzato lo zebrafish come organismo modello e applicato un approccio di genetica inversa per la caratterizzazione e lo studio delle funzioni di Ambra 1, una proteina chiave coinvolta nelle fasi iniziali di formazione della vescicola autofagosomica. Nel topo, il silenziamento di Ambra1 porta non solo ad una riduzione dell'attività autofagica ma anche a letalità embrionale e al mancato sviluppo del sistema nervoso centrale. Gli embrioni presentano iperproliferazione del neuroepitelio, esencefalia e chiusura imperfetta del tubo neurale, risultati che suggeriscono un ruolo cruciale di Ambra1 per un corretto sviluppo del sistema nervoso.

La tesi è stata divisa in quattro capitoli, il primo dei quali descrive l'identificazione e la caratterizzazione dei due geni paraloghi *ambra1a* e *ambra1b*, che codificano per le due isoforme di questa proteina presenti nello zebrafish. I trascritti di entrambi i geni sono presenti, nell'ovocita e durante le prime ore dello sviluppo, come mRNA materno mentre a stadi successivi i trascritti materni vengono degradati e sostituiti da quelli embrionali. Questi si localizzano prevalentemente a livello cefalico suggerendo un potenziale ruolo di queste proteine anche nello sviluppo del sistema nervoso centrale dello zebrafish. Gli embrioni ottenuti dopo silenziamento delle due proteine presentano letalità a stadi di sviluppo precoci, numerose alterazioni morfologiche e una rilevante riduzione dell'attività autofagica. Inoltre, i risultati ottenuti suggeriscono la possibile acquisizione di funzioni specifiche da parte dei due geni paraloghi, geni che sono entrambi necessari per uno sviluppo corretto e che non si compensano uno con l'altro in seguito al silenziamento.

Nel Capitolo II è stato confermato, mediante colorazione immunoistochimica per l'istone H3 fosforilato, che il silenziamento di entrambi i geni porta ad un aumento della proliferazione cellulare. Inoltre, è stato dimostrato, mediante esperimenti di trapianto cellulare, che cellule prive di Ambra1 sono in grado di iperproliferare in maniera cellulo-autonoma. E' stata, infatti, osservata una maggiore proliferazione cellulare nelle chimere *ambra1a* e *ambra1b* rispetto ai controlli.

Il Capitolo III descrive il coinvolgimento di Ambra1a e Ambra1b nello sviluppo del muscolo scheletrico di zebrafish e compara la morfologia di questo tessuto nei morfanti per Ambra1a e Ambra1b e negli embrioni di topo Ambra1$^{gt/gt}$, nei quali è stato inattivato il gene per Ambra1. In entrambi i casi lo sviluppo del tessuto muscolare è chiaramente compromesso. Fenotipi più gravi sono ottenuti dal silenziamento dei trascritti materni, sottolineando così il ruolo fondamentale di queste proteine durante le prime fasi dello sviluppo embrionale.

Infine, il Capitolo IV descrive il clonaggio e la caratterizzazione di *ambra1* nel tunicato *Botryllus schlosseri,* una specie modello di ascidia coloniale. Si tratta della prima caratterizzazione di trascritti *ambra1* in un organismo non-vertebrato. La sequenza amminoacidica dedotta è più corta rispetto alle proteine Ambra1 dei vertebrati, ma contiene

sia il dominio WD40, tipico di questa proteina, che altri residui amminoacidici importanti per la poliubiquitinazione e per il taglio proteolitico catalizzato dalle caspasi. La proteina di *B. schlosseri* è però priva di altri domini importanti quali il motivo di consenso per il legame alla dineina che, nei vertebrati, lega la proteina al suo specifico sito citoscheletrico in assenza di induzione del processo autofagico. L'espressione di questo gene è stata verificata nei diversi stadi del ciclo vitale considerati ed è stata inoltre analizzata mediante microscopia elettronica.

AUTOPHAGY

Autophagy is an evolutionary conserved self-degradative process by which cells degrade and recycle, using the lysosomal machinery, various cellular constituents, including misfolded proteins and protein aggregates, lipids, intracellular pathogens and damaged organelles.

This process is crucial to maintain cellular homeostasis and represents an adaptive response to different stress stimuli, such as nutrient deprivation or cell damage. It has been demonstrated that autophagy plays important roles during embryo development and cellular differentiation [1, 2], normal physiology and survival during starvation and ageing [3]. Failure to remove aggregates of damaged toxic proteins could explain why autophagy is involved in several human disorders such as inflammatory diseases [4], and neurodegenerative conditions including Huntington's disease, Parkinson's disease, amyotrophic lateral sclerosis and Alzheimer's disease [5]. Autophagy has also been identified as a critical process in oncogenesis and cancer progression [6, 7]. The early stages of oncogenesis are associated with down-regulation of autophagy-related genes and several of these, such as Beclin 1, Bif-1, Atg4C, and UVRAG, have been found to possess tumor suppressor activity. By contrast, in later stages of tumorigenesis, autophagy could provide cancer cells with a survival strategy under unsuitable conditions, like nutrient shortage, chemotherapy or irradiation, therefore, acting in a tumor promoting way. Finally, in some congenital muscular dystrophies the increase of dysfunctional mitochondria and the subsequent loss or damage of muscle fibers were found to be linked to a misregulation of the autophagic process [8].

There are three major forms of autophagy: macroautophagy, usually referred as "autophagy", chaperone-mediated autophagy (CMA) and microautophagy, working with different cellular mechanisms and playing distinctive functions [9].

CMA is a selective form of autophagy that, to date, has been reported only in mammalian cells [10]. In this process the soluble cytosolic proteins containing a KFERQ-like sequence motif are recognized by a cytosolic chaperone complex, containing the heat shock cognate protein of 70 kDa (Figure 1). The complex then associates directly with the lysosomal membrane receptor Lamp2 that mediates, with the help of a second chaperone, translocation of the substrate proteins into the lysosomal lumen with subsequent degradation by lysosomal hydrolases [10].

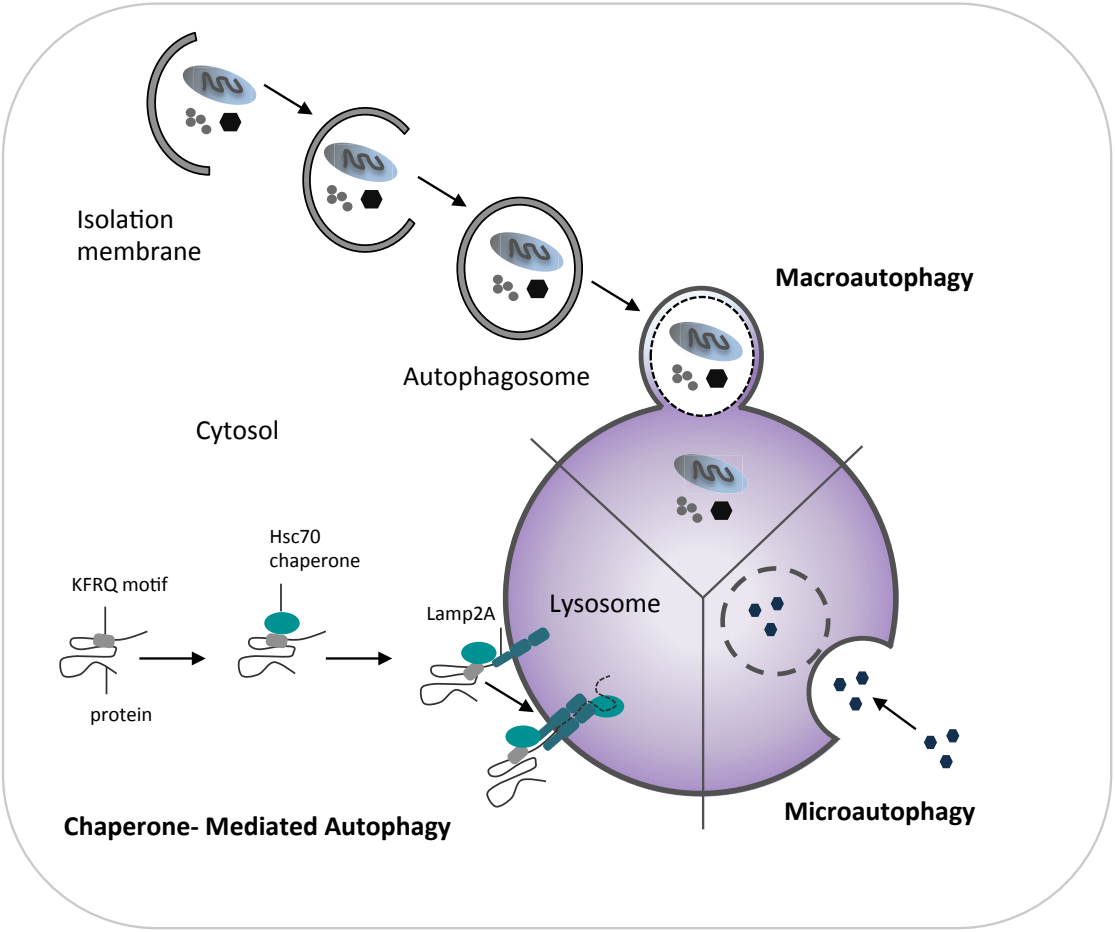

Figure 1. Schematic diagram illustrating three main types of autophagy in mammalian cells: macroautophagy, microautophagy and chaperone-mediated autophagy (CMA). Figure modified from [11].

In microautophagy, cytosolic contents are directly engulfed by invagination at the lysosomal membrane itself, without the formation of autophagosomes [12].

Macroautophagy is the process where portions of cytoplasm containing long-lived proteins and damaged organelles are isolated in a double membrane vesicle called autophagosome [13]. The autophagosomes fuse with the lysosomes, thereby forming autolysosomes, where lysosomal enzymes work on the degradation of cytosolic contents. The process consists of a cascade of steps that are finely regulated and relies upon a specific subset of AuTophaGy-related (Atg) genes first identified in yeast [14].

Autophagy induction

The target of rapamycin, mTOR, is a serine/threonine protein kinase that plays a key role in the induction of autophagy and regulation of cell growth [15]. This protein is able to respond and integrate different signals including nutrient availability, presence of growth factors, hypoxia and stress stimuli. In mammalian cells mTOR forms two functionally distinct protein complexes: the complex mTORC1 who plays a major role in the regulation of autophagy and the complex mTORC2. In the presence of nutrients or growth factors, mTORC1 blocks the autophagic process, by means of its association with the ULK1/2 complex (see later) and phosphorylation of the Atg13 protein [15]. mTORC2 is involved in skeletal muscle autophagy regulation in fasting condition via the Akt-FoxO3 pathway [16].

Initiation and nucleation of autophagosome

Autophagosome formation starts at the phagophore (autophagosome precursor, also defined as pre-autophagosomal structures) assembly sites (PAS) (Figure 2). As regards to membrane source, it has been hypothesized that autophagosomes could originate from intracellular membrane structures like the endoplasmic reticulum [17].

The autophagosome initiation requires the ULK1 complex (Atg1 in yeast) that is negatively regulated by mTORC1. In the absence of nutrient or growth factor mTORC1 is inactivated and dissociates from the ULK1/2 complex that is composed also by FIP200, Atg13 and Atg101. ULK1/2 complex is then activated and can move to the endoplasmic reticulum. Here the complex regulates the activity of Beclin1 (homologue of Atg6) complex that recruits the class III phosphoinositol-3-kinase Vps34 (Vacuolar protein sorting 34) to produce phosphatidylinositol-3-phosphate (PtdIns(3)P), a component that is crucial to the elongating phagophore. This activity is coordinated by the interaction of Beclin 1 with several other proteins such as p150, a homologue of Vps15, Atg14L or Barkor, a homologue of Atg14 and AMBRA1 [18]. The PtdIns(3)Ps recruit at the membrane the double FYVE-containing protein 1 (DFCP1) and other proteins [18], and the complex accumulate in specific structures of the ER named omegasome for their Ω−like form.

Autophagosome elongation

The elongation of the phagophore to form the omegasome is mediated by two ubiquitin-like conjugation systems that together promote the assembly of the ATG16L complex and the processing of LC3. The first ubiquitylation-like reaction in autophagy process involves ATG5 and ATG12 [19]. ATG12 is covalently tagged to ATG5 in a conjugation reaction catalyzed by two additional proteins, ATG7 [ubiquitin activating-enzyme (E1) like] and ATG10 [ubiquitin-conjugating-enzyme (E2) like] [20].

The second ubiquitylation-like reaction requires the conjugation of the soluble cytoplasmic protein, Atg8 (LC3 in mammals) with a lipid phosphatidylethanolamine (PE). LC3 is cleaved by the protease Atg4 [21], resulting in the cytosolic isoform LC3-I. LC3-I is conjugated to phosphatidiletanolamine (PE) in a reaction that requires Atg7 and Atg3 to form LC3-II [22]. LC3-II levels correlate with autophagic vacuole number that makes it an excellent marker for studying autophagy [23].

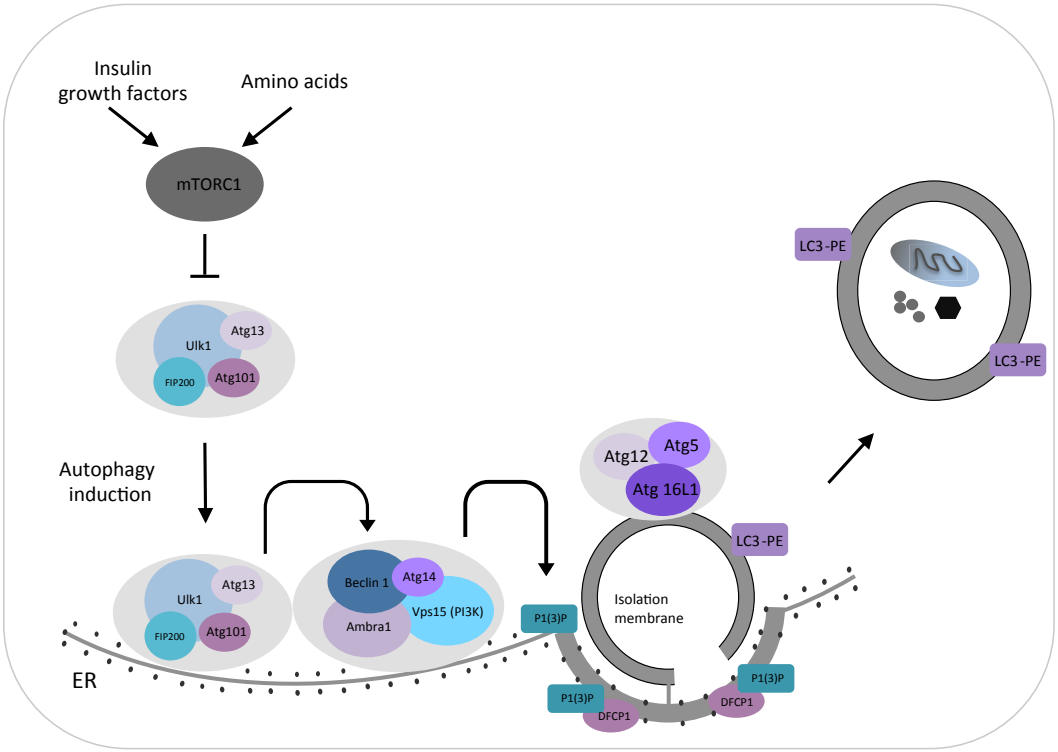

Figure 2. Schematic representation of autophagosome formation. mTOR complex 1 (mTORC1) blocks the ULK1 (Atg1 homolog) complex under nutrient-rich conditions. Upon autophagy induction, the ULK1 complex (including ULK1, Atg13, FIP200, and Atg101) is activated and translocates to a certain domain of the endoplasmic reticulum (ER). Once in the ER, the ULK1 complex regulates the class III phosphatidylinositol (PtdIns) 3-kinase complex (including Beclin 1, Atg14(L)/barkor, Vps15, Vps34, and Ambra1). Recruitment of Beclin 1 to the PtdIns3-kinase complex is also sensitive to starvation. Formation of PtdIns(3)P recruits double FYVE-containing protein 1 (DFCP1) and promotes the formation of the omegasome, from which autophagosomes appear to be generated. The Atg12–Atg5–Atg16L1 complex and the LC3 (Atg8 homolog)–phosphatidylethanolamine (PE) conjugate play important roles in the elongation and closure of the isolation membrane. The Atg12–Atg5 Atg16L1 complex is also required for formation of the covalent bond between LC3 and PE. Figure modified from [18].

Autophagosome maturation and fusion

Mature autophagosomes move along microtubules in a dynein-dependent manner to vacuoles (yeasts) or to lysosomes (mammals) clustered around the microtubule-organizing center (MTOC). Before they merge with a lysosome, the autophagosome may merge with an endosome, forming an anfisoma. The breakdown of the autophagic body results in the release of the load within the lumen, where the cytoplasmic components are degraded. The resulting macromolecules are recycled to overcome different stress conditions [24].

AMBRA1

AMBRA1 (activating molecule in Beclin1-regulated autophagy) is a highly conserved large protein (approximately 1300 amino acids) that presents a WD40 domain at its amino terminus [25].

This protein is expressed at high level in the mouse developing brain [25] and, in adult, in brain compartments, such as the hippocampus, cerebellum and striatum, which are all severely affected in neurodegenerative conditions [26]. According to this, during mouse embryogenesis, Ambra1 has shown to be crucial for the proper nervous system development (Figure 3). This was demonstrated by mouse Ambra1 knockout, an experimental approach that produces early embryonic lethality, severe abnormalities in the neural tube development, uncontrolled cell proliferation and excessive cell death [25].

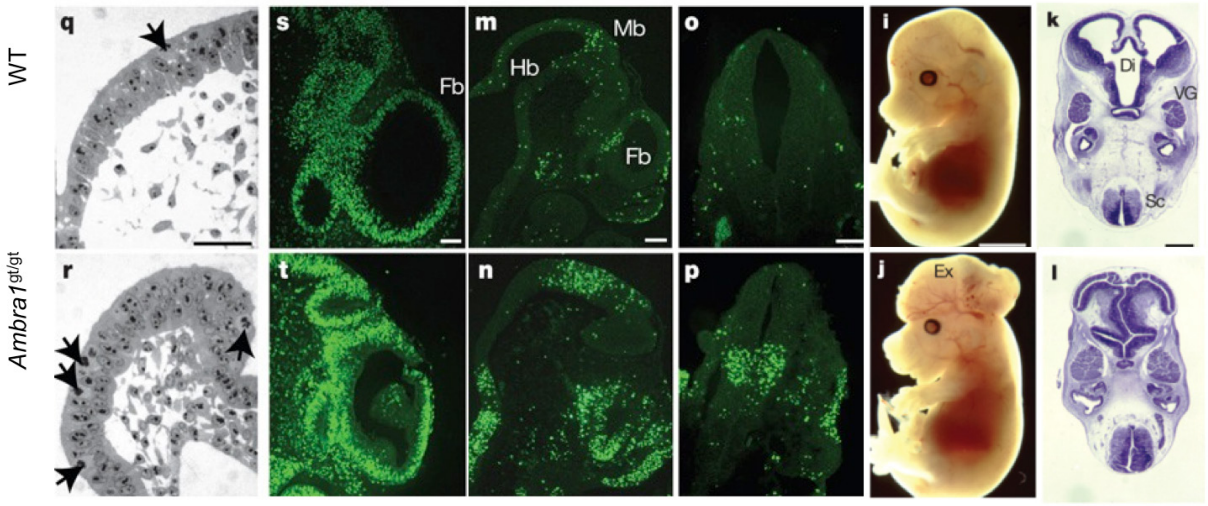

Figure 3. Neural tube defects in Ambra1 mutant embryos. Analysis of cell proliferation in wild-type (q, s) and Ambra1$^{gt/gt}$ (r, t) embryos on transverse sections of E8.5 cephalic neural folds in prospective hindbrain region (mitoses, arrows in q, r) and on sagittal sections of E10.5 forebrain (BrdU uptake, s, t). TUNEL (TdTmediated dUTP nick end labelling) staining of E10.5 brain (m, n) and E9.5 spinal cord (o, p) in wild-type (m, o) and Ambra1$^{gt/gt}$ (n, p) embryo sections. E14.5 wild-type (i) and Ambra1$^{gt/gt}$ (j) embryos are characterized by prominent exencephaly. Histological analysis of E12.5 wild-type (k) and Ambra1$^{gt/gt}$ (l) embryos on cross-section show the absence of a normal ventricular system, the extensive overgrowth of the proliferative neuroepithelium in the diencephalon (Di) and spinal cord (Sc), and the enlarged fifth ganglia (VG) in the Ambra1$^{gt/gt}$ embryo. Scale bars: c, g, h, k, 500 mm; d, 1 mm; e, 150 mm; i, 2 mm; m, s, 400 mm; o, 78mm; and q, 50mm. Figures as well as figure legends were taken from [25].

This protein, identified in mouse as a positive regulator of the Beclin 1-dependent program of autophagy, promotes the interaction of Beclin 1 with its target, the kinase Vps34, thus mediating the nucleation of autophagosome [25].

Ambra1 is an intrinsically disordered protein (IDP) [27], that is fine regulated by independent modifications and possesses the capability of binding a number of other regulatory partners involved in many cell processes including autophagy, apoptosis and cell proliferation [28].

In cell physiological conditions, Ambra1 is anchored, together with Beclin 1 and Vps34, to the dynein light chain, DLC1, by means of two DLC-binding consensus motifs (TQT) located at the C-terminal of the protein. After autophagy induction, the activated ULK1 complex can phosphorylate Ambra1 thus determining its release from dynein. The complex formed by Ambra1, Beclin 1 and Vps34 is now free to translocate to the ER where autophagosome nucleation takes place [26] (Figure 4). ULK1 is thus a direct regulator of Ambra1 activity.

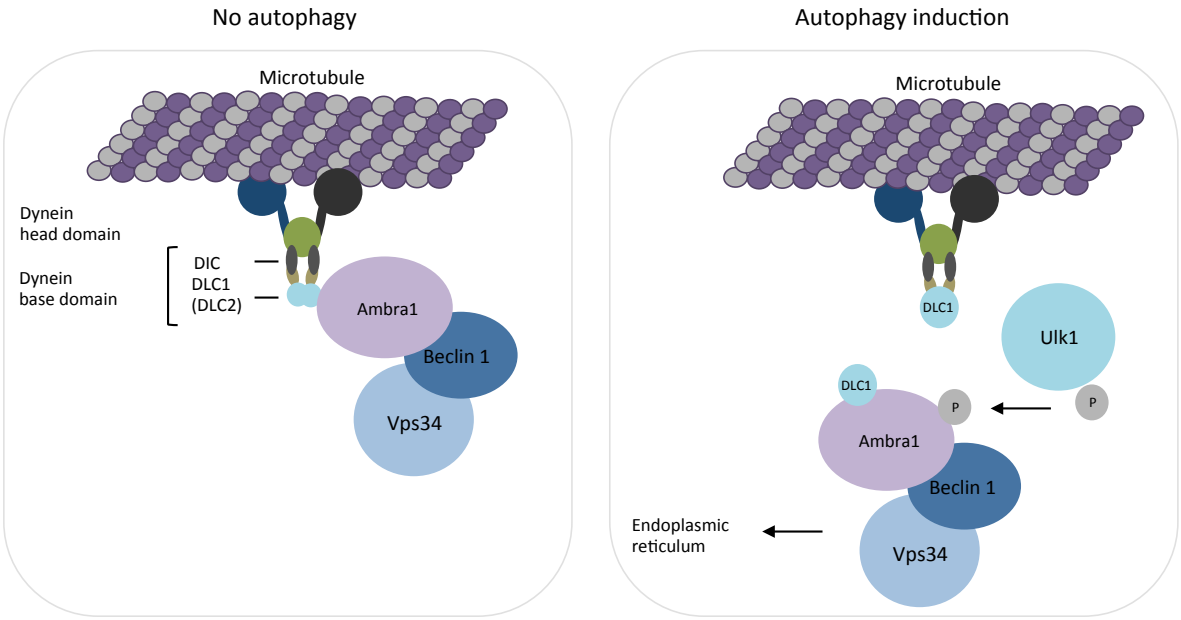

Figure 4. Dynamic interaction of AMBRA1 with the dynein motor complex in physiological cell conditions and after autophagy induction. Figure modified from [26].

Moreover, it has been demonstrated that the down-regulation of DLC1 expression determines the dissociation of Ambra1 from the dynein motor complex and leads to a significant increment of autophagosomes both in normal cell conditions and during starvation or treatment with rapamycin [26]. Likewise, Ambra1 mutants, lacking the DLC1 binding domain, have an increased ability to induce autophagy compared to the Ambra1 wild-type cells. Furthermore, the autophagy induction due to the down-regulation of DLC1 is prevented if Ambra1 is concomitantly inactivated thus confirming its direct involvement in this process [26].

The autophagic induction is regulated not only by the positive ULK1 phosphorylation of Ambra1 but also by means of other recently discovered protein interactions [27]. In basal condition, Ambra1 is linked to the dinein motor complex but also inhibited by phosphorylation, at the residue Ser52, catalyzed by the complex mTORC1. This prevents the Ambra1 specific activity in the autophagic process. As above described, after autophagy induction, ULK1 can phosphorylate Ambra1 thus allowing its release from dinein motor complex. However, the interaction between the two proteins is reciprocal, as Ambra1 has been shown to control and increase ULK1 stability and function by stimulation of the E3 ligase TRAF6 activity. This enzyme, which is able to interact with both ULK1 and Ambra1 proteins catalyzed a ubiquitylation reaction on ULK1-Lys-63 (Figure 5).

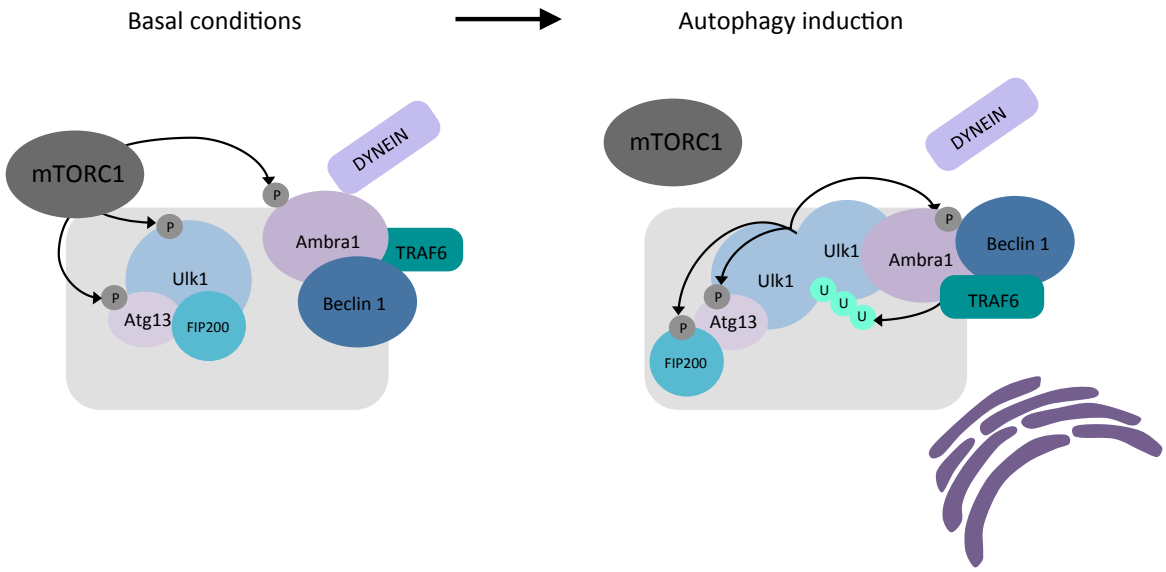

Figure 5. Proposed model of AMBRA1 regulation in ULK1 ubiquitylation. In basal conditions, AMBRA1 is maintained in an inactive state by mTOR phosphorylation and by its anchoring to the dynein motor complex. After autophagy induction, AMBRA1 and ULK1 are active. AMBRA1 enhances ULK1 kinase activity and stability by promoting its Lys-63-linked ubiquitylation and self-association through TRAF6. ULK1 primes AMBRA1 detachment from the dynein complex through a positive phosphorylation. Coupling these regulatory events may represent a positive feedback to sustain autophagy in a continuous loop. Figure modified and figure legend taken from [27].

Part of the cellular pool of Ambra1 is instead normally localized to mitochondria, where the proteins are linked to Bcl-2 by means of N- and C-terminal binding domains. If autophagy is induced, the proteins are released and free to interact with Beclin 1 and to promote the autophagic process [29]. Release of Ambra1 proteins from Bcl-2 occurs also after induction of the apoptotic process thus underlining the proposed crosstalk between the two cellular processes [28]. Recently it has been shown that levels of this protein are important for the cell in order to choose between an autophagic pro-survival response or the apoptotic process. Ambra1 proteolysis at the amino acid residue D482 is then required to interfere with the autophagic process and to direct the cell towards the dead program [30].

At the mitochondrial level Ambra1 interacts also with the Parkin protein that is involved in the induction of a selective form of the autophagic process, the mitophagy, by means of which damaged mitochondria are removed form the cell. Following mitochondria damage, Ambra1 is recruited near these organelles where it is involved in Vps34 enzyme activation and the induction of the mitophagy process [31].

ZEBRAFISH AS A MODEL ORGANISM

Kingdom: Animalia
Phylum: Chordata
Class: Acrinopterygii
Order: Cypriniformes
Family: Cyprinidae
Genus: Danio
Species: *Danio rerio*

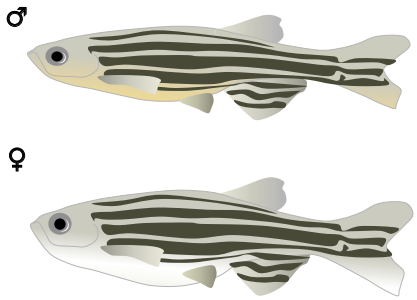

Figure 6. Schematic representation of an adult male and female zebrafish specimen with characteristic horizontal stripes running along the body and fins.

The zebrafish (*Danio rerio*) is a small tropical freshwater fish, native of the river Ganges, in the northeastern region of India and currently exported all over the world (Figure 6). In last years, it has become a favorite model organism to study biological processes.

Zebrafish is small, easy to breed and maintain in laboratory condition. Adult females spawn hundreds of eggs once every 5 days. Fertilization is external and allows an immediate analysis of the progeny at different stages of development, without the need of dissection and sacrifice of pregnant females as required in mammalian models.

The embryos and larvae of these fish are transparent and present rapid external development with all major organs developing within 36 h at 28.5°C [32], thus allowing micromanipulation and *in vivo* observation and analysis of embryogenesis and organogenesis. The zebrafish reaches sexual maturity in approximately 3-4 months [33].

These characteristics make this model particularly suitable for genetic and developmental biology techniques such as cell transplantation or microinjection of DNA or RNA, aimed at the production of transgenic lines, over-expression of mRNA or gene silencing by means of morpholino (MO) oligonucleotides. The microinjection of MOs is efficient and rapid, and it is the most commonly used and validated antisense zebrafish technology to investigate gene loss of function, signaling pathways and the roles of specific proteins in development or drug response. Injected MOs typically generate a graded severity of phenotypes, but not a complete loss-of-function. This, together with the possibility to modulate the concentration of the injected MOs, may be seen as a distinct advantage when complete knockout results in early lethality, as observed for most autophagic genes in mice [2].

As a vertebrate species, zebrafish is more closely related to humans than invertebrate models. Indeed, their genomes are highly conserved and approximately 70% of human genes have orthologs in zebrafish [34]. Among these genes, many are actually present as paralogs because Teleost underwent genome duplication [35]. This, due to the sub-functionalization of paralog genes, may be helpful to better understand their function.

Due to this high genomic conservation, zebrafish mutant lines have been prepared through chemical mutagenesis and identified by means of genetic screens. These lines have been demonstrated to serve as models for human diseases as well as to investigate the main

mechanisms of development, including those that determine the formation of the embryo, define the organization of distinct regions of the brain and allow the formation of specific neural circuits [36- 38].
These mutant lines can be found at the website:
http://www.sanger.ac.uk/resources/zebrafish/genomeproject.html.
Moreover, other mutant lines can be now obtained by using novel powerful gene targeting strategies, named CRISPR-Cas9 and TALEN, that are based on induced mutations and have already been successfully applied to zebrafish [39- 41].
A database that provides information on the genetics, genomics and the development of zebrafish is available at: http://www.zfin.org.

Zebrafish embryo development is similar to those of other teleost fish and has been described in detail by Kimmel and coo-workers [32]. The principal developmental stages are represented in Figure 7.
Differently from eutherian mammals, where maternal effects on embryos are exerted in real time at the placental boundary, in oviparous species, like zebrafish, maternal factors, both mRNA and proteins, are provided in their large oocytes to sustain and direct early development [42].
Maternal mRNAs are the almost unique translational templates for protein synthesis in the initial embryogenesis and are responsible for the maternal programming of subsequent development. Moreover, there is a timely interplay between maternal mRNA degradation, starting at the midblastula transition (MBT), at the 10th cleavage cycle (512-cell stage; 3 h post-fertilization) and carried out at different rates depending on the messenger, and the onset of zygotic transcription, including that of a number of micro-RNAs responsible for the clearance of several hundred of maternal messages [43, 44].

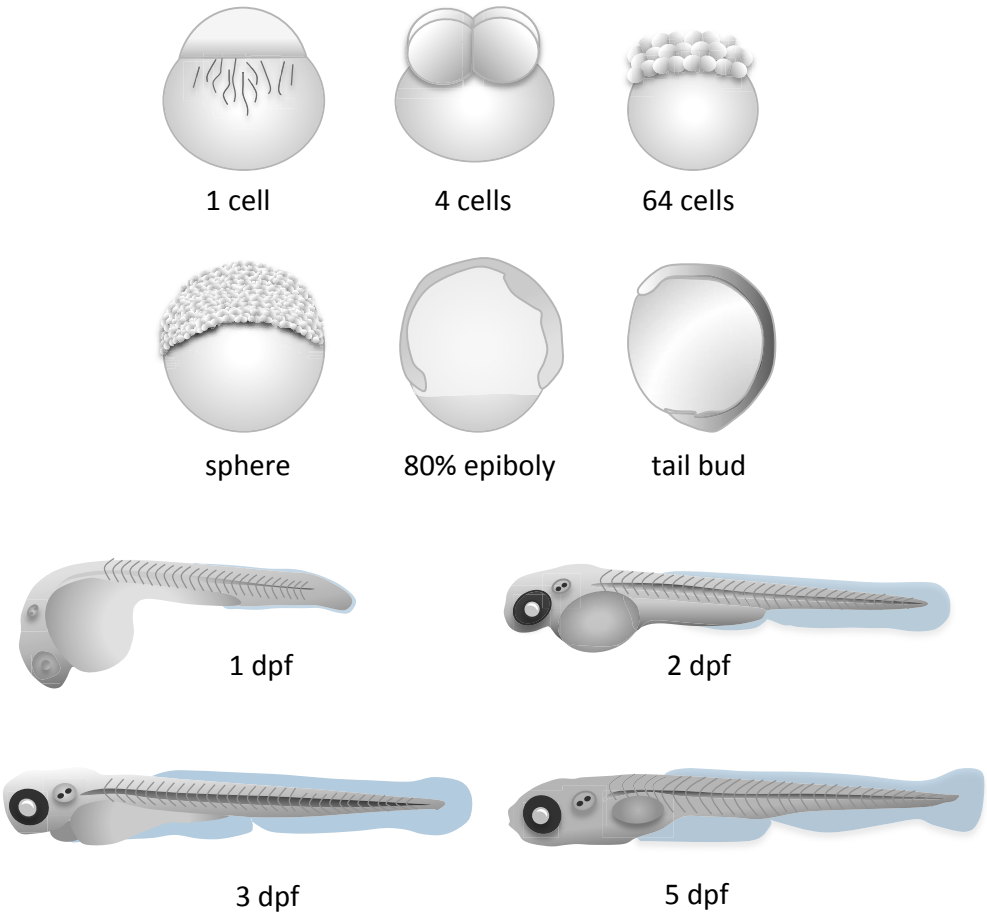

Figure 7. Schematic representation of several stages of zebrafish development. Hpf: hours post fertilization. Dpf: days post fertilization.

ZEBRAFISH SKELETAL MUSCLE

In vertebrates, skeletal muscle contains fibers of different type, with specific physiological and biochemical properties that make them suited to different functions [45]. Slow-twitch (Type I) or oxidative fibers contain a large number of mitochondria in which ATP is generated by oxidative metabolic processes, thus providing a higher resistance level and allowing the maintenance of contractile activity for long period [46]. These fibers present a typical red color that is given by high levels of myoglobin and high vascularization [47].

Fast-twitch (Type I) or glycolytic fibers contain a low number of mitochondria. In this case, ATP is generated very rapidly by anaerobic metabolic processes and muscle fibers contractile activity is reduced [46], The physiological difference in contraction activity between the two type of fibers is a consequence of the type of myosin isoform present in the thick filament [47].

Zebrafish is a great model organism to study muscle development due to the rapid external embryonic development, the large proportion of the body constituted by muscle (around 80%) and the spatial separation of fiber-type in the embryonic myotome [46] that is maintained throughout adult stages. Actually, fast muscle fibers are multinucleated and located inside the somite, whereas slow muscle contains mononucleated fibers and forms a subcutaneous layer [46, 48, 49]. Zebrafish muscle contains also muscle pioneer cells, belonging to the slow muscle and located in a medial position of the developing somite and the medial fast fiber cells [49].

Muscle activity beginning is temporally separated in the different types of fiber: the first spontaneous contraction in slow-twiched fibers appears in the embryo at 17 hpf [50] and the touch-evoked coiling behavior is initially detectable at 21 hpf [51], while the fast-twitch fibers start contraction after hatching [52].

Zebrafish's myogenesis is regulated by the Myogenic Regulatory Factors (MRFs) that are members of the basic helix-loop-helix transcription factor family [53]. In particular, the first genes to be expressed are *myogenic differentiation 1* (*myod1*) and *myogenic regulatory factor 5* (*myf5*).

In zebrafish myogenesis starts before somite segmentation, when midline hedgehog signals induce cells of the presomitic mesoderm to differentiate into adaxial cells [48, 53]. The adaxial cells, which represent the precursor of slow muscle as well as muscle pioneer cells [48], are initially aligned medially next to the notochord where they express the transcription factor *Myod1* (Figure 8, blue cells).

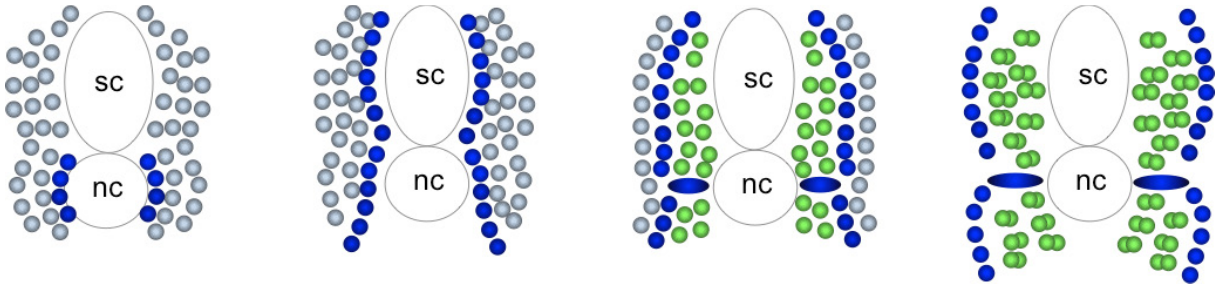

Figure 8. Schematic representation of transverse sections of developing somite showing the lateral migration of the adaxial cells (blue) followed by the onset of differentiation and fusion of the fast-twitch myoblasts (green), sc, spinal cord, nc, notochord. Figure modified from [46].

These cells migrate radially to reach the lateral surface of the somite where they form the superficial slow twich mononucleated fibers [54]. Moreover, a small portion of adaxial cells maintains its location adjacent the nothocord to differentiate into the muscle pioneer cells [49] that form the horizontal myoseptum. The slow fibers express the transcription factor *prox1* [54] and the slow isoform of the Myosin Heavy Chain (MyHC).

Fast twitch multinucleated fibers develop from the posterior half of each newly formed somite, by differentiation, independently of hedgehog signaling, of a second population of cells expressing *myoD* [48, 53] (Figure 8, green cells) and the fast MyHC isoform.

MORPHOLINO GENE KNOCKDOWN

The agents that inhibit or reduce the expression of a gene of interest are commonly called knockdown agents. Since they bind to the sense sequence of mRNA, they are also called antisense oligos [55].

There are three main types of knockdown agents:

- S-DNAs (phosphorothioate-linked DNAs) that use the enzyme RNase H to cut the RNA target sequence [56].
- siRNAs (short interfering RNAs) that are the mediators of sequence-specific degradation of mRNA. They consist of fragments of 21-22 nucleotides, generated by the cutting of longer dsRNAs (double strand RNAs). The technique of siRNA was discovered in 1990, and since then was widely used in the field of biological research [57].
- Morpholinos (MOs) that create a steric block and inhibit translation or splicing of the target gene [58].

MOs are synthetic molecules, typically 25 bases in length, designed and synthesized by Gene Tools (http://www.gene-tools.com). They bind to the target complementary sequences of RNA by nucleic acid base-pairing. Their name derives from the MO structure of the constituent units, each containing one of the four nitrogenous bases (A, C, G or T) linked to a six atoms morpholine ring instead of a ribose or deoxyribose molecule. The morpholine rings are then connected through phosphorodiamidate instead of phosphates groups [33]. MOs are resistant to nucleases degradation and thus more stable than other knockdown agents [58].

Normally MOs are complementary to a region between the 5'-CAP and the first 25 nucleotides after the translation initiation codon (AUG), beyond which the inhibitory activity of morpholino decade. MOs do not degrade the target RNA, but sterically invade the secondary structure of the mRNA thereby preventing the recognition of the ribosome and, as a consequence, blocking the protein translation (Figure 9). These knockdown agents reduce in a very efficient and specific manner gene expression, in particular, the translation of the target mRNAs [55] When a specific antibody is available, a Western Blot analysis can demonstrate the effective reduction of the protein translation. Otherwise, efficiency of MOs must be obtained with other alternative strategies [59].

Besides inhibiting the translation, a MO can also act on the maturation of the pre-mRNA in the nucleus (splice-blocking MO). These MOs are complementary to splice acceptor (intron-exon boundary) or donor (exon-intron boundary) sites in the unspliced RNA and therefore are in competition for these binding sites with the splicing apparatus (Figure 9). The binding of these MOs may result in the loss of an exon or in the intron retention, in the resulting mRNAs [60] This knockdown has the advantage of allowing an easy quantification of the efficiency of MO, by RT-PCR analysis of the RNA extracted from microinjected embryos [61].

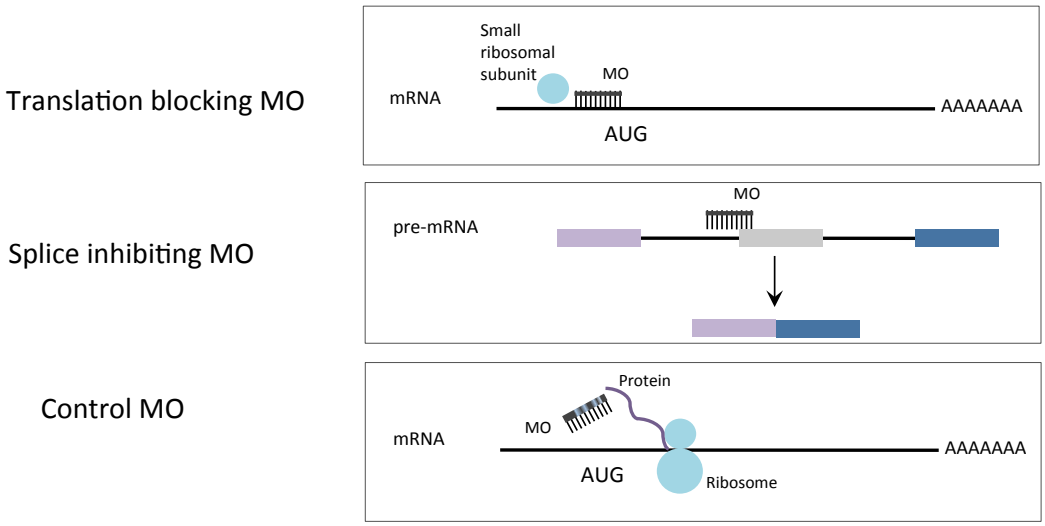

Figure 9. Schematic representation of different types of MO oligos.

This technology is particularly used in zebrafish and allows the study of the function of genes. The MO is microinjected in fertilized eggs at the stage of one/two cells to blocks translation of the target genes. The embryos phenotypically modified by MO are called morphants [62].

Sometimes MOs can be toxic to cells and produce off-target effects. It can cause stress-induced apoptosis in central nervous system and somites. Although the MOs act in a sequence-specific way, there is always the possibility that it also blocks translation of other genes with similar sequences [59]. Therefore, specificity of morphants phenotypes requires some checks phenotype [59]:

- two morpholinos, non-overlapping and therefore complementary to different portions of the target transcript, should produce the same phenotypic effects;
- use of a mismatch MO (a modified oligonucleotide which differs for 4-5 bases from the specific MO) that is unable to bind to the target gene and, consequently, should not produce a morphant.
- rescue experiments in which MOs are co-injected with an mRNA encoding the target protein should recover, at least partially, the normal phenotype. To prevent the MOs from blocking the injected messenger, this must derives from another organism, or the transcript should be modified in the region recognized by the MO.

REFERENCES:

1. Levine B, Klionsky DJ. 2004. Development by self-digestion: Molecular mechanisms and biological functions of autophagy. Dev Cell 6: 463–477.
2. Cecconi F, Levine B. 2008. The role of autophagy in mammalian development: cell makeover rather than cell death. Dev Cell 15, 344–357.
3. Rubinsztein DC, Mariño G, Kroemer G. 2011. Autophagy and aging. Cell 146, 682-695.
4. Rubinsztein DC, Gestwicki JE, Murphy LO, Klionsky DJ. 2007. Potential therapeutic applications of autophagy. Nat Rev Drug Discov 6, 304–412.
5. Levine B, Kroemer G. 2008. Autophagy in the pathogenesis of disease. Cell 132: 27-42.
6. Mizushima N, Levine B, Cuervo AM, Klionsky DJ. 2008. Autophagy fights disease through cellular self-digestion. Nature 451, 1069–1075.
7. Zhineng JY, Cheng EC, Shengbing H, Frank A. 2011. Sinicrope Review: The Role of Autophagy in Cancer: Therapeutic Implications. Mol Cancer Ther 10, 1533–1541.
8. Sandri M., Coletto L., Grumati P., Bonaldo P. 2013. Misregulation of autophagy and protein degradation system in myopathies and muscular dystrophies. J Cell Science, 126, 5325–5333.
9. García-Arencibia M, Hochfeld WE, Toh PPC, et al., 2010. Semin Cell Dev Biol, 21, 691–8.
10. Kaushik S, Cuervo AM. 2012. Chaperone-mediated autophagy: a unique way to enter the lysosome world. Trends Cell Biol 22, 407–417.
11. Boya P, Reggiori F, Codogno P. 2013. Emerging regulation and functions of autophagy. Nat Cell Biol 15, 713–20.
12. Li W-W, Li J, Bao J-K. 2012. Microautophagy: Lesser-known self-eating. Cell Mol Life Sci 69, 1125–1136.
13. Yang Z, Klionsky DJ. 2010. Eaten alive: A history of macroautophagy. Nat Cell Biol 12, 814–822.
14. Huang WP, Klionsky DJ. 2002. Cell Struct Funct, 27, 409–20.
15. Jung CH, Ro SH, Cao J, Otto NM, Kim DH. 2010. mTOR regulation of autophagy. FEBS Lett 7, 1287–95.
16. Mammucari C, Milan G, Romanello V, Masiero E, Rudolf R, Del Piccolo P, Burden SJ, Di Lisi R, Sandri C, Zhao J, Goldberg AL, Schiaffino S, Sandri M. 2007. FoxO3 controls autophagy in skeletal muscle in vivo. Cell Metab 6, 458–71.
17. Axe EL, Walker SA, Manifava M, Chandra P, Roderick HL, Habermann A, Griffiths G, Ktistakis NT. 2008. Autophagosome formation from membrane compartments enriched in phosphatidylinositol 3- phosphate and dynamically connected to the endoplasmic reticulum. J Cell Biol 182, 685–701.
18. Mizushima N, Komatsu M. 2011. Autophagy: renovation of cells and tissues. Cell 147, 728–741.
19. Ravikumar B, Futter M, Jahreiss L, Korolchuk VI, Lichtenberg M, Luo S, Massey DC, Menzies FM, Narayanan U, Renna M, Jimenez-Sanchez M, Sarkar S, Underwood B, Winslow A, Rubinsztein DC. 2009. Mammalian macroautophagy at a glance. J Cell Sci 122, 1707–11.

20. Mizushima N, Sugita H, Yoshimori T, Ohsumi Y. 1998b. A new protein conjugation system in human. The counterpart of the yeast Apg12p conjugation system essential for autophagy. J Biol Chem 273, 33889–33892.
21. Hemelaar J, Lelyveld VS, Kessler BM, Ploegh HL. 2003. A single protease, Apg4B, is specific for the autophagy-related ubiquitin-like proteins GATE-16, MAP1-LC3, GABARAP, and Apg8L. J Biol Chem 278, 51841–51850.
22. Ohsumi Y, Mizushima N. 2004. Two ubiquitinlike conjugation systems essential for autophagy. Semin Cell Dev Biol 15, 231–236.
23. Klionsky DJ, Abeliovich H, Agostinis P, Agrawal DK, Aliev G, Askew DS. et al. 2008. Guidelines for the use and interpretation of assays for monitoring autophagy in higher eukaryotes. Autophagy 4, 151–175.
24. Yang Z, Klionsky DJ. 2009. An overview of the molecular mechanism of autophagy. Curr Top Microbiol Immunol 335, 1–32.
25. Fimia GM, Stoykova A, Romagnoli A, Giunta L, Di Bartolomeo S, Nardacci R, Corazzi M, Fuoco C, Ucar A, Schwartz P, Gruss P, Piacentini M, Chowdhury K, Cecconi F. 2007. Ambra1 regulates autophagy and development of the nervous system. Nature 447, 1121–1125.
26. Di Bartolomeo S, Corazzari M, Oliverio S, Nazio F, Lisi G, Antonioli M, Pagliarini V, Matteoni S, Fuoco C, Giunta L, D'Amelio M, Nardacci R, Romagnoli A, Piacentini M, Cecconi F, Fimia GM. 2010. The dynamic interaction of Ambra1 with the dynein motor complex regulates mammalian autophagy. J Cell Biol 191, 155–168.
27. Nazio F, Strappazzon F, Antonioli M, Bielli P, Cianfanelli V, Bordi M, Gretzmeier C, Dengjel J, Piacentini M, Fimia GM, Cecconi F. 2013. mTOR inhibits autophagy by controlling ULK1 ubiquitylation, self-association and function through AMBRA1 and TRAF6. Nat Cell Biol 4, 406–16.
28. Fimia GM, Corazzari M, Antonioli M, Piacentini M. 2013. Ambra1 at the crossroad between autophagy and cell death. Oncogene 32, 3311–3318.
29. Strappazzon F, Vietri-Rudan M, Campello S, Nazio F, Florenzano F, Fimia GM, Piacentini M, Levine B, Cecconi F. 2011. Mitochondrial BCL-2 inhibits AMBRA1-induced autophagy. EMBO J 30, 1195–208.
30. Pagliarini V, Wirawan E, Romagnoli A, Ciccosanti F, Lisi G, Lippens S et al. 2012. Proteolysis of Ambra1 during apoptosis has a role in the inhibition of the autophagic pro-survival response. Cell Death Differ 19, 1495–1504.
31. Van Humbeeck C, Cornelissen T, Hofkens H, Mandemakers W, Gevaert K, De Strooper B et al. 2011. Parkin interacts with Ambra1 to induce mitophagy. J Neurosci 31, 10249–10261.
32. Kimmel CB, Ballard WW, Kimmel SR, Ullmann B, Schilling TF. 1995. Stages of embryonic development of the zebrafish. Dev Dyn 203, 253–310.
33. Dahm R, Geisler R, Nüsslein-Volhard C. 2006. Zebrafish (Danio rerio) Genome and Genetics. In: Encyclopedia of Molecular Cell Biology and Molecular Medicine, Editor(s): R.A. Meyers, Wiley Online Library, DOI: 10.1002/3527600906.

34. Howe K, Clark MD, Torroja CF, Torrance J, Berthelot C, Muffato M, et al. 2013. The zebrafish reference genome sequence and its relationship to the human genome. Nature 496, 498–503.
35. Volff JN. 2005. Genome evolution and biodiversity in teleost fish. Heredity 94, 280-94.
36. Walker C, Streisinger G. 1983. Induction of Mutations by gamma-Rays in Pregonial Germ Cells of Zebrafish Embryos. Gen 103, 125-136.
37. Kimmel CB. 1993. Patterning the brain of the zebrafish embryo. Annu Rev Neurosci 16, 707-732.
38. Driever W, Solnica-Krezel L, Schier AF, Neuhauss SC, Malicki J, Stemple DL, Stainier DY, Zwartkruis F, Abdelilah S, Rangini Z, Belak J, Boggs C. 1996. A genetic screen for mutations affecting embryogenesis in zebrafish. Development 123, 37-46.
39. Hwang WY, Fu Y, Reyon D, Maeder ML, Tsai SQ, Sander JD, Peterson RT, Yeh JR, Joung JK. 2013. Efficient genome editing in zebrafish using a CRISPR-Cas system. Nat Biotechnol 3, 227–9.
40. Chang N, Sun C, Gao L, Zhu D, Xu X, Zhu X, Xiong JW, Xi JJ. 2013. Genome editing with RNA-guided Cas9 nuclease in zebrafish embryos. Cell Res 4, 465–72.
41. Cade L, Reyon D, Hwang WY, Tsai SQ, Patel S, Khayter C, Joung JK, Sander JD, Peterson RT, Yeh JR. 2012. Highly efficient generation of heritable zebrafish gene mutations using homo- and heterodimeric TALENs. Nucleic Acids Res 16, 8001–10.
42. Pelegri F. 2003. Maternal factor in zebrafish development. Dev Dyn 228, 535–554.
43. Abrams EW, Mullins MC. 2009. Early zebrafish development: it's in the maternal genes. Curr Opin Genet Dev 19, 396–403
44. Giraldez AJ. 2010. microRNAs, the cell's Nepenthe: clearing the past during the maternal-to-zygotic transition and cellular reprogramming. Current Opinion in Genetics & Development 20, 369–375
45. Schiaffino S, Reggiani C. 2011. Fiber types in mammalian skeletal muscles. Physiol Rev 91, 1447–1531.
46. Jackson HE, Ingham PW. 2013. Control of muscle fibre-type diversity during embryonic development: the zebrafish paradigm. Mech Dev 130, 447–457.
47. Scott W, Stevens J, Binder-Macleod SA. 2001. Human skeletal muscle fiber type classification. Physical Therapy 81, 1810–1816.
48. Devoto SH, Melançon E, Eisen JS, Westerfield M. 1996. Identification of separate slow and fast muscle precursor cells in vivo, prior to somite formation. Development 122, 3371–3380.
49. Ochi H, Westerfield M. 2007. Signaling networks that regulate muscle development: Lessons from zebrafish. Develop Growth Differ 49, 1–11.
50. Saint-Amant L, Drapeau P. 2000. Motoneuron activity patterns related to the earliest behavior of the zebrafish embryo. J Neurosci 20, 3964–3972.
51. Pietri T, Manalo E, Ryan J, Saint-Amant L, Washbourne P. 2009. Glutamate drives the touch response through a rostral loop in the spinal cord of zebrafish embryos. Dev Neurobiol 69, 780–795.

52. Naganawa Y, Hirata H. 2011. Developmental transition of touch response from slow muscle-mediated coilings to fast muscle-mediated burst swimming in zebrafish. Dev Biol 355, 194–204.
53. Coutelle O, Blagden CS, Hampson R, Halai C, Rigby PW, et al. 2001. Hedgehog signalling is required for maintenance of myf5 and myoD expression and timely terminal differentiation in zebrafish adaxial myogenesis. Dev Biol 236, 136–150.
54. Glasgow E, Tomarev SI. 1998. Restricted expression of the homeobox gene prox 1 in developing zebrafish. Mech Dev 76, 175–178.
55. Summerton J. 1999. Morpholino antisense oligomers: The case for an RNase H independent structural type. Biochim Biophys Acta 1489, 141–158.
56. Cohen JS. 1993. Phosphorothioate oligodeoxynucleotides.Crooke, S.T.,Lebleu, B., Eds., CRC Press: Boca Raton 1993. In Ant Res Appl 205–219.
57. Dorsett Y, Tuschl T. 2004. siRNAs: application in functional genomics and potential as therapeutics. Nat Rev Drug Discov 3, 318–329.
58. Summerton J. 2007. Mopholino, siRNA, and S-DNA compared: impact of structure and mechanism of action on off-target effects and sequence specifity. Med Chem 7, 651–660.
59. Eisen JS, Smith JC. 2008. Controlling morpholino experiments: don’t stop making Antisense. Development 135, 1735–1743.
60. Sazani P, Kang S-K, Maier MA, Wie C, Dillman J, Summerton J, Manoharan M, Kole R. 2001. Nuclear antisense effects of neutral, anionic and cationic oligonucleotide analogs. Nucl. Acids Res 29, 3965–3974.
61. Draper BW, Morcos PA, Kimmel CB. 2001. Inhibition of Zebrafish fgf8 Pre-mRNA Splicing With Morpholino Oligos: A Quantifiable Method for Gene Knockdown. Genesis 30, 154–156.
62. Nasevicius A, Ekker SC. 2000. Effective targeted gene knockdown' in zebrafish. Nat Genet 26, 216–20.

Ambra1 knockdown in zebrafish leads to incomplete development due to severe defects in organogenesis

Francesca Benato[1*], **Tatjana Skobo**[1*], Giorgia Gioacchini[2], Isabella Moro[1], Fabiola Ciccosanti[3], Mauro Piacentini[3, 4], Gian Maria Fimia[3], Oliana Carnevali[2§], Luisa Dalla Valle[1§].

[1] Department of Biology, University of Padova, Padova, Italy.
[2] Department of Life Science and Environment, Marche Polytechnic University, Ancona, Italy.
[3] National Institute for Infectious Diseases IRCCS 'L. Spallanzani', Rome, Italy.
[4] Department of Biology, University of Roma Tor Vergata, Rome, Italy.

*These authors contributed equally to this work.
§These authors contributed equally to this work.

Autophagy 9, 476-495

ABSTRACT

AMBRA1 is a positive regulator of the BECN1-dependent program of autophagy recently identified in mouse. In this study, we cloned the full-length cDNAs of *ambra1a* and *ambra1b* zebrafish paralogous genes. As in mouse, both Ambra1 proteins contain the characteristic WD40 repeat region. The transcripts of both genes are present as maternal RNAs in the eggs and display a gradual decline until 8 hpf, being replaced by zygotic mRNAs from 12 hpf onwards. After 24 hpf, the transcripts are mainly localized in the head, suggesting a possible role in brain development. To check their developmental roles, we adopted morpholino knockdown to block either translation (ATGMOs) or splicing (SPLICMOs). Treatment with ATGMOs causes severe embryonic malformations, as prelarvae could survive for only 3 and 4 days in *ambra1a* and *b* morphants, respectively. Treatment with SPLICMOs led to developmental defects only at a late stage, indicating the importance of maternally supplied *ambra1* transcripts. Analysis of the levels of Lc3-II, an autophagosome-specific marker, in the presence of lysosome inhibitors evidenced a reduction in the rate of autophagosome formation in both MOs-injected embryos at 48 hpf, more pronounced in the case of *ambra1a* gene. Although some defects, such as body growth delay, curved shape and haemorrhagic pericardial cavity were present in both morphants, the occurrence of specific phenotypes, such as major abnormalities of brain development in *ambra1a* morphants, suggests the possible acquisition of specific functions by the two paralogous genes that are both required during development and do not compensate each other following knockdown.

INTRODUCTION

Autophagy is an evolutionarily conserved catabolic process used to break down and recycle, through the lysosomal machinery, long-lived proteins and organelles in order to maintain a homeostatic environment within the cell. This process is tightly regulated and plays several important roles in embryo development, differentiation, normal physiology, survival during starvation and ageing [1,2]. Three types of autophagy are known: macroautophagy (usually referred as "autophagy"), microautophagy, and chaperone-mediated autophagy, working with different cellular mechanisms and playing distinctive functions [3]. Macroautophagy is responsible for the bulk degradation of macromolecules and damaged cytoplasmic organelles in a double-membrane-bound vesicle, the autophagosome [4]. Failure to remove aggregates of mutated toxic proteins could explain the key pathogenic effect of impaired autophagy in neurodegenerative diseases, including Huntington disease, Parkinson disease, amyotrophic lateral sclerosis, and Alzheimer disease [5,6]. Autophagy has also been identified as a critical process in oncogenesis and cancer progression [7,8]. Moreover, in some congenital muscular dystrophies, defective activation of the autophagic machinery causes accumulation of dysfunctional mitochondria, leading to damage and the subsequent loss of muscle fibers [9].

A great number of papers, reviewed by Di Bartolomeo and coworkers [10], suggest that autophagy, in eukaryotes, represents a crucial mechanism during the development of multicellular organisms. Several proteins, called AuTophaGy-related proteins (ATG), first identified in yeast [11], participate in the different steps of the autophagic process: vacuole initiation, elongation and fusion with the lysosomes. Autophagosome formation requires a BECN1-containing complex that recruits the class III phosphatidylinositol 3-kinase (PIK3C3) to produce phosphatidylinositol-3-phosphate. This activity is coordinated by the interaction of BECN1 with several other proteins, including the regulatory protein kinase PIK3R4/Vps15/p150, the UV radiation resistance-associated protein (UVRAG), SH3GLB1 (endophilin B1/Bif-1), AMBRA1 (autophagy/beclin-1 regulator 1), BCL2 (B-cell CLL/lymphoma 2), ATG14 (autophagy related 14), and KIAA0226 (RUN domain and cysteine-rich domain containing, Beclin 1-interacting protein /RUBICON) to form different protein complexes that mediate distinct functions in membrane trafficking [12,13].

A positive regulator of the BECN1-dependent program of autophagy has been recently identified in mouse as AMBRA1 [14]. AMBRA1 is normally docked in mammalian cells at a specific cytoskeletal site (the dynein light chain, DYNLL1), wherefrom it is unleashed upon autophagy induction to translocate to the autophagosome origin sites on the ER [15]. AMBRA1 is primarily expressed, during mouse embryogenesis, in the neural plate of the CNS and it is crucial for the proper nervous system development. AMBRA1-deficiency in mouse embryos is lethal, due to neural tube developmental defects as well as abnormal neural cell proliferation [14].

Currently, zebrafish is one of the leading models for studying not only early development, a phase of the life cycle in which zebrafish has a recognized superiority, but also cellular and physiological processes involved in human diseases. Zebrafish is more

closely related to humans than invertebrate models and, at the same time, it offers numerous advantages, such as external fertilization, the rapid development of transparent embryos, and the large number of offspring, compared with non-fish vertebrate models. Within six days, the transparent embryos and larvae complete their development, allowing *in vivo* visualization and analysis of all developmental stages and organogenesis. Moreover, the zebrafish often contains duplicate copies of genes that are instead present as single copies in mammals. This is helpful to obtain additional insight into the multiple functions of the human counterpart [16]. Herein, two zebrafish *ambra1* genes were identified and analysed for their function in embryonic development. *Ambra1a* and *ambra1b* genes appear to be paralogous and their expression was detected throughout embryonic development. Morpholino-based silencing of both genes resulted in developmental defects similar to those observed in the AMBRA1-deficient mouse model. Presence of paralog-specific alterations suggests the possibility of subfunctioning of the two genes and demonstrates that zebrafish is a viable model for the study of AMBRA1 functions.

METHODS

Fish maintenance and embryo collection

Zebrafish of wild-type (WT) strain, purchased from local pet shops, were maintained according to Westerfield and Lawrence [29,30]. Embryos were obtained by natural spawning and cultured in zebrafish Fish Water solution at 28.5°C with a photoperiod of 14 h light/10 h dark. The developmental stages were determined according to the hpfs and morphological features [31].

RNA extraction, reverse transcription and quantitative polymerase chain reaction (qPCR)

Total RNA was extracted from pools of 20 to 60 embryos at the desired stages of development using TRIzol reagent (15596-018, Invitrogen) according to the manufacturer's instructions. The number of embryos was chosen according to the embryo size at each time point. The RNA samples were kept at -80°C until use.

For qPCR, 1 µg of total RNA obtained from three different pools of embryos at each developmental stage was used for cDNA synthesis, employing iScript cDNA Synthesis Kit (Bio-Rad) and following the manufacturer's protocol. PCRs were performed with SYBR green method in a iQ5 iCycler thermal cycler (179-8891, Bio-Rad). All samples were analysed in triplicate in 20 µl volumes. Each reaction mixture consisted of 2 µl of diluted (1/10) cDNA, 10 µl of 2X concentrated iQ TM SYBR Green Supermix (170-8882, Bio-Rad), containing SYBR Green as a fluorescent intercalating agent, 0.3 µM of forward primer and 0.3 µM of reverse primer. Real-time PCR conditions were optimized after trying various times and temperatures for each cycling step. The reaction conditions were as follows: enzyme activation at 95°C for 3 min followed by 45 cycles of denaturation (30 s at 95°C), annealing (30 s at 60°C for *arginine rich protein*, *arp*, 30 s at 54°C for *ambra1a* and *ambra1b*, 30 s at 55°C for *18S,* and 30 s at 60°C for *becn1,* and extension (20 s at 72°C). Fluorescence monitoring occurred at the end of each cycle. The extension phase of the last cycle was prolonged by 10 min. Primer specificity and the absence of primer-dimer formation during real-time PCR analysis was indicated in each sample by the presence of a single peak in the dissociation (melt) curve at the end of the amplification program. The specificity of each primer set was also analysed by sequencing of the obtained fragment. *18S* and *arp* mRNAs were used as normalizers in each sample in order to standardize the results by eliminating variations in mRNA and cDNA quantity and quality. The data obtained were analysed using the iQ5 optical system software version 2.0 (Bio-Rad) including GeneEx Macro iQ5 Conversion and genex Macro iQ5 files. Modification of gene expression is represented with respect to the control sampled at the same time of the treatment. The primer sequences are reported in supplementary Table 4.

Cloning of zebrafish *ambra1a* and *ambra1b* cDNAs

A BLASTN search for zebrafish *ambra1* cDNA sequence was performed in the NCBI database (http://www.ncbi.nlm.nih.gov) using the amino acid sequence of mouse AMBRA1

(NP_766257) as query. Two *Danio rerio* cDNA sequences were obtained: XM_002667669 (coding for *ambra1a*, as named in this paper) and XR_084457 (coding for *ambra1b*). ESTs databases were also analysed but, due to the length of the *ambra1* cDNA, no full-length clones were found, but only fragments of both sequences.

Based on the predicted sequences, primers covering overlapping fragments were designed for RT-PCR and to obtain the 5'- and 3'-UTR regions according to the cloning strategy described in Supplementary Figure 1. RNA ligase-mediated rapid amplification of cDNA 5'-ends (RLM-5'-RACE) and 3'-RACE were performed using the FirstChoice RLM-RACE kit (AM1700M, Ambion), following the manufacturer's instructions, with the primers reported in supplementary Figure 1. These analyses were accomplished using RNA extracted from 2- and 48-hpf-old embryos. The full-length open reading frame (ORF) of zebrafish *ambra1a* (accession number: XM_002667669) and *ambra1b* (accession number: XR_084457) were amplified from 2-hpf zebrafish embryo total cDNA with pair of primers located outside of the start and stop codon regions (see Supplementary Figure 1) and cloned into pCR®-Blunt vector. Both strands were sequenced for each gene.

Synteny and phylogenetic analyses

Genomic analysis of conserved syntenies between human and zebrafish *ambra1* genes were examined using the Synteny database with zebrafish as the source genome (release Sanger Zv9) and the human genome (release GRCh37.p2) as the outgroup. The sliding window size was settled at 25 genes [17]. This program is designed for analysing genomes that have undergone complete duplication during evolution. It identifies pairwise clusters of orthologs and paralogs simultaneously.

Phylogenetic relationships of zebrafish *ambra1* genes were derived by aligning their deduced amino acidic sequences together with *AMBRA1* sequences reported for other vertebrate species using the Clustal W program [32]. All alignment positions were included in the analysis. The tree was generated by the Maximum likelihood method [33], as implemented in the RaxML 7.2.6 program [34]. Insertions and deletions were not taken into account. Bootstrap resamplings were also performed to test the robustness of the trees and 1000 replicates were done.[35] Program setting is detailed in the figure legend.

Morpholinos

All the MOs were obtained from Gene Tools (Philomath, OR, USA). The antisense MOs used for the silencing of zebrafish *ambra1a* and *ambra1b* were designed against the ATG translation initiation site according to the following sequences: MO1-*ambra1a* (5-CTC CAA ACA CTC TTC CTC ACT CCC T -3') and MO1-*ambra1b* (5'-TTT TCC TCT TTA GTG CTC CAC GGC C-3').

The antisense splice variant MOs were designed for both genes on the sequence at the exon 3-intron 3 junction: MO2-*ambra1a*: 5'-TGT AAT CAA AGT GGT CTT ACC TGT C-3' and MO2-*ambra1b*: 5'- TGA AAT TGA TTG TTA CCT ATC TGG A-3' (the exon complementary sequence is underlined).

As controls, we used five-nucleotide-mismatched control MOs: MO1-*ambra1a*-5m (5'-CTC gAA AgA CTg TTC CTg AgT CCC T-3') and MO1-*ambra1b*-5m (5'-TTa TgC TgT TTA GTc CTC CAC cGC C-3') (lowercase bold letters indicate the mismatch changes). Finally, we used an MO against the ATG translation initiation site of *tp53* mRNA, *tp53* MO: 5'-GCG CCA TTG CTT TGC AAG AAT TG-3' (MO4-*tp53*) [19].

All the MOs were reconstituted at 1 mM in nuclease-free water. Different MOs concentrations were tested in a range between 1 and 2.5 µg/µl. MOs and mRNAs (see below) were injected into the yolk mass of 1- or 2-cell embryos. These were then incubated in 1X Fish Water (50X: 25 g Istant Ocean, 39.25 g $CaSO_4$, and 5 g $NaHCO_3$ for 1 l) at 28.5°C. MOs- and/or mRNAs-injected embryos were raised to the desired stages for observations or collected for further analysis.

In order to verify the knockdown effectiveness of MO1-*ambra1a* and MO1-*ambra1b*, the 5'-UTR region of both paralogs, containing the MOs target sequence, was cloned in pCR®-BluntII-TOPO vector (K280002, Invitrogen), in-frame upstream of the fluorescent protein EGFP coding region. The nucleotide portion including MOs target sequence and EGFP was *Xba*I and *EcoR*I digested and subcloned into pCS2+ expression vector. The resulting expression vectors were verified by sequencing. Linearized plasmids (1 µg) were used as templates for the synthesis of capped synthetic mRNAs with the mMESSAGE mMACHINE® SP6 Kit (AM1340, Ambion). Synthetic mRNAs were precipitated by centrifugation in LiCl and their integrity confirmed by formaldehyde-agarose electrophoresis. Stock of synthetic mRNAs solutions were quantified by absorbance and diluted to desired concentrations in 1X Danieau's buffer for microinjection.

The effectiveness of SPLICMOs for exon skipping was confirmed by the presence of a significant amount of shorter RNA products detected by RT-PCR with two set of specific primers flanking the splice site (Am1a-F5 with Am1a-R6 for *ambra1a* and Am1b-F5 with Am1b-R4 for *ambra1b*, see supplementary Table 4).

In vitro transcription

For rescue experiments, since the injected synthetic mRNAs should not contain the MOs target sequences, modified cDNAs were amplified for *ambra1a1*, *ambra1a3* and *ambra1b* with forward primers containing silent mutations and the restriction site of *Cla*I and reverse primers containing the restriction site of *Xho*I (see supplementary Figure 1 and supplementary Table 4 for details). The resulting PCR products were cloned into the pCR®-Blunt vector and, after complete sequencing to check for lack of nucleotide changes that could alter the amino acidic sequence or interrupt the translation reading frame, subcloned into pCS2+ expression vector using *Cla*I and *Xho*I restriction enzymes.

Linearized plasmids (1 µg) were used as templates for the synthesis of capped synthetic mRNAs, which were purified as described above.

The pGEM plasmids containing the last 280 and 267 nucleotides plus the 3'-UTR regions of *ambra1a1* and *ambra1b*, respectively, were used to synthesize digoxigenin (DIG)-labelled riboprobes for whole-mount *in situ* hybridization (WMISH). The PCR fragments were then

cloned into pGEM-T Easy vector. DIG-labeled riboprobes were synthesized by *in vitro* transcription with SP6 and T7 RNA polymerases, respectively (Sp6 RNA polymerase, 10 810 274 001; T7 RNA polymerase, 10 881 767 001, Roche), following the manufacturer's instructions.

Whole-mount *in situ* hybridization and microscopy analyses

WMISH was performed, on normal and treated embryos, essentially as reported by Thisse and Thisse [36]. Embryos were fixed overnight in 4% paraformaldehyde (PFA, P6148, Sigma) in phosphate-buffered saline (PBS) at the desired stage of development. For embryos older than 24 hpf, pigmentation was suppressed by raising embryos in 0.03% PTU (1-phenyl-2-thiourea, P7629, Sigma) in Fish Water. Afterwards, the embryos were washed in PBT (PBS plus 0.1% Tween 20, P1379, Sigma) and dechorionated with forceps. They were treated with methanol and stored at -20°C. Methanol-stored embryos were rehydrated in methanol/PBS series, permeabilized by proteinase K (10 µg/ml), prehybridized, and then hybridized overnight at 65°C with 1 ng/µl of the appropriate riboprobe in the Hybridization Mix (HM: 50% formamide, 5×SSC, 0.1% Tween 20, 50 µg/ml heparin and 500 µg/ml tRNA). After HM/SSC and SSC/PBT washing series, embryos were preincubated in blocking solution (2% sheep serum, and 2 mg/ml BSA in PBT) and then incubated overnight at 4°C with alkaline phosphatase (AP)-conjugated anti-DIG antibodies (11 093 274 910, Roche) diluted 1:3,000 in blocking solution. After PBT washing, embryos were pre-soaked in staining buffer and then incubated in NBT/BCIP (5-nitro-blue tetrazolium chloride/bromo-4-chloro-3'-indolyphosphate p-toluidine salt Stock solution, 11 681 451 001, Roche) for blue staining. WMISH-stained embryos were mounted in 80% glycerol in PBT or cleared and mounted in 2:1 benzyl benzoate/benzyl alcohol, observed under a Leica DMR microscope (Leica Microsystems Srl, Milano, Italy) and photographed with a Leica DC500 digital camera (Leica Microsystems Srl, Milano, Italy)

All riboprobes for WMISHs are listed in supplementary Table 5.

For histology analysis, zebrafish WMISH-stained larvae at 6 dpf were fixed in 4% paraformaldehyde at RT for 2 h and processed into an alcohol–xylene series followed by paraffin embedding.

Blood vessels were visualized by endogenous alkaline phosphatase activity at 3 dpf following the protocol of Serbedzija et al [37].

For scanning electron microscopy (SEM) material was fixed in 6% glutaraldehyde in 0.1 M cacodylate buffer (pH 6.9) overnight at 4°C. The post-fixed samples were dehydrated in a graded ethanol series, dried at the critical point and coated with gold. The samples were observed with a Stereoscan 260 (Cambridge Instruments Ltd, Cambridge, UK) scanning electron microscope, operating at 12 kV. For semithin section, material was fixed in 6% glutaraldehyde in 0.1 M cacodylate buffer (pH 6.9) overnight at 4°C. After washing in cacodylate buffer, the specimens were post-fixed in 1% OsO_4 in the same buffer for two h and dehydrated in a graded ethanol series followed by propylene oxide. The specimens were stained with uranyl acetate while undergoing dehydration in 75% ethanol. The samples were

embedded in Araldite resin. Thin sections were cut with an Ultracut S, Reichert ultramicrotome (New York, USA), stained with toluidine blue and examined with a light microscope.

Immunoblotting analysis

Embryos were homogenized in CelLytic Mammalian Tissue extraction reagent (C3228, Sigma-Aldrich). Twenty micrograms of protein extracts were separated on a 13.5% SDS-polyacrylamide gel and electroblotted onto PVDF (IPVH20200, Millipore) membranes. Blots were incubated with a rabbit anti-LC3 antibody, (#2775, Cell Signaling) and a rabbit anti-BECN1 antibody (Santa Cruz H-300 #11427) in 5% non-fat dry milk in TBS plus 0,1% Tween20 overnight at 4°C. Detection was achieved using horseradish peroxidase-conjugate anti mouse IgG antibody (711-036-152, Jackson Immunoresearch) and visualised with ECL PRIME (RPN2232, GE Healthcare) using ECL-Hyperfilm (28-9068-37, GE Healthcare). Rabbit anti-Actin antibody (A2066, Sigma Aldrich), was used to monitor equal protein loading. The antibody is made against the SGPSIVHRKCF peptide that is 100% identical in beta and gamma Actin and 91% in alpha Actin.

To assess the rate of autophagic flux upon Ambra1 downregulation, Lc3-II levels were analysed in 48 hpf embryos incubated with the lysosome inhibitor bafilomycin A_1 (1 mM) (Sigma Aldrich #B1793) for 6 h and then fixed for immunoblotting analysis.

Quantification of chemiluminescent signals was performed with the Gel Doc densitometer (BioRad,) using the Quantity One imaging software, version 4.4.0. All samples were run in triplicate and averaged.

Apoptotic assays

Apoptotic cells in the embryos were detected by the TdT-mediated fluorescein-dUTP nick end labeling (TUNEL) assay. The TUNEL assay was performed using alkali stable digoxigenin-dUTP and TdT (terminal deoxynucleotidyl transferase) (03 333 574 001, Roche). Embryos were fixed in 4% PFA (overnight, 4°C), treated with methanol and stored at -20°C. Methanol-stored embryos were rehydrated in methanol/PBS series and permeabilized by proteinase K (10 µg/ml). Afterwards, the embryos were washed in PBT (5x5 min, RT) and in ethanol/acetic acid (2:1) (20 min RT). After incubation with TUNEL buffer (30 min, RT), embryos were incubated in 100 µl TUNEL reaction mixture (overnight, RT). The reaction was stopped by washing samples with PBT/EDTA 1mM (2x1 h, RT). Samples were then processed as for the whole-mount *in situ* hybridization and stained with the AP substrate Fast Blue (Fast Blue BB 4-benzoylamino-2,5-diethoxybenzenediazonium chloride hemi [zinc chloride] salt, F3378, Sigma) plus NAMP (3-hydroxy-2-naphthoic acid 2,4-dimethylanilide phosphate N5000, Sigma). Stained embryos were mounted in 80% glycerol in PBT and examined with Leica SP5 confocal microscope.

Apoptotic cells were estimated within the same area in five embryos of each experimental condition. All data were represented as the mean ± S.D. Statistical significance was tested by Student's t-test. Groups were considered significantly different if $P < 0.05$.

Nucleotide sequencing

Sequencing was performed on double-stranded DNA using the ABI PRISM Dye Terminator Cycle Sequencing Core Kit (Applied Biosystems, Monza, Italy). Electrophoresis of sequencing reactions was completed on the ABI PRISM model 377, version 2.1.1 automated sequencer.

RESULTS

Isolation and characterization of the zebrafish *ambra1* genes and deduced proteins

Two predicted sequences, XM_002667669 (coding for *ambra1a*, as named in this paper) and XR_084457 (coding for *ambra1b*), were identified by bioinformatics tools using the mouse AMBRA1 amino acid sequence (NP_766257) as query. The whole coding region of the two transcripts, as well as the 5'- and 3'-untranslated terminal regions (UTRs), were then sequenced using RNA extracted from 2- and 48-hpf (hours post-fertilization) embryos, according to the cloning strategy reported in supplementary Figure 1. Sequences obtained by RT-PCR and cloning display differences with the above-predicted sequences as well as the presence or absence of predicted exons. Data on the nucleotide features of the different transcript variants identified and sequenced in this work are described in Table 1.

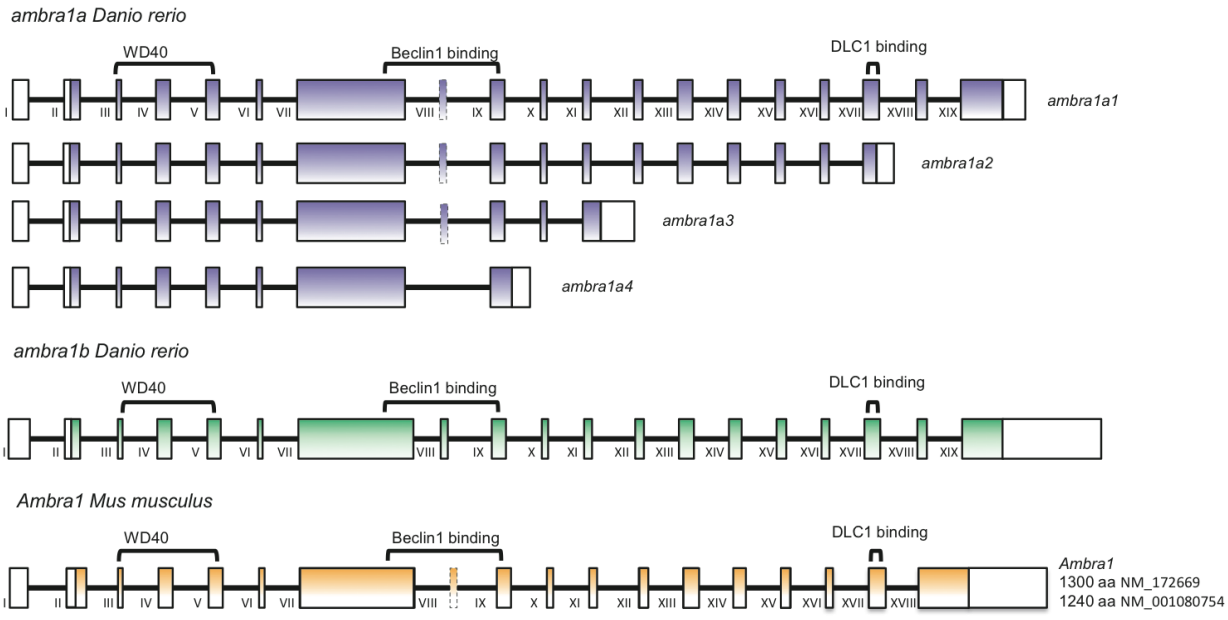

Figure 1. Genomic structure and organization of zebrafish and mouse *ambra1* genes. Plain boxes indicate exons. The coding region is in colour and numbered with Roman numerals. Boxes of exon 8 are dashed in transcripts where it may be absent. The positions of the WD40 domain, BECN1 and DYNLL1 binding regions are indicated. Introns, represented as lines, are not drawn to scale, but the corresponding lengths can be found in supplementary Table 1 together with the exon sizes. Exons in zebrafish *ambra1a* and *b* are similar in size to orthologous exons in mouse *Ambra1*.

The genomic organization of the two genes, obtained by sequence analysis of the new cDNAs with the BLAT program, is described in Figure 1 and compared with that of the mouse *Ambra1* gene. In supplementary Table 1, we report the sizes of each of the exons and introns. The canonical splice consensus sites "GT" and "AG" are present in all zebrafish *ambra1* introns.

The zebrafish gene *ambra1a* is alternatively spliced, generating four variant carboxy-terminal sequences. The entire coding sequence of the four *ambra1a* transcripts was obtained by overlapping fragments of different lengths. Given the long and alternatively spliced transcripts, all the four variants were also amplified with a set of primers localized before and after the start and stop codons (see supplementary Figure 1). The fragments were then cloned and sequenced to verify the accuracy of the overlapping processes. All the four variants cloned lacked exon 8, as it occurred in one of the two transcripts encoded by mouse *Ambra1* gene (see Figure 1, exon boxed with dashed line). However, PCR performed with a sense primer located on exon 7 and an antisense primer specific for each *ambra1a* form showed that exon 8 could be transcribed, but at very low levels with respect to the forms lacking this exon (data not shown). The presence of exon 8 as well as the expression of all the identified transcripts were checked at 2- and 48-hpf (see Table 1). No transcript containing exon 8 was found for the *ambra1a4* variant at both 2- and 48-hpf.

Ambra1b gene contains 19 exons as *ambra1a,* with the same genomic organization. Though several 3'-RACE analyses using sense primers localized on different regions of its coding sequence were performed, only one transcript was identified for this gene. Moreover, no transcript variant lacking exon 8 was sequenced or identified by PCR analysis. The mouse *Ambra1* gene (sequence used NP_766257), as the human one (not shown, sequence used Q9C0C7), presents the same genomic organization as the zebrafish genes, but it contains only 18 exons. Nevertheless, the mouse last exon (18^{th}) contains a longer coding region with respect to the corresponding exon 18 of zebrafish *ambra1* genes. This difference explains the low identity in the C-terminal regions of mammals and zebrafish full-size Ambra1 deduced proteins (Figure 2). Cloning results show that, although there is no consistency with respect to intron size (supplementary Table 1), the overall gene architecture has been conserved across species.

	5' UTR	3'UTR	Coding region	Predicted ORF	GenBank Accession	2 hpf	48 hpf
ambra1a1	307 bp	182 bp	3948 bp	1315 aa	HE602022	x	x
			4035 bp	1344 aa	-	x	x
ambra1a2	307 bp	266 bp	3297 bp	1098 aa	HE602023	x	x
			3384 bp	1127 aa	-	x	x
ambra1a3	307 bp	540 bp	2367 bp	788 aa	FR846231	x	x
			2454 bp	817 aa	-	-	x
ambra1a4	307 bp	362 bp	2175 bp	724 aa	HE602022	-	x
			2262 bp	753 aa	-	-	-
ambra1b	350 bp	1269 bp	4083 bp	1360 aa	FR846230	x	x

Table 1. Summary of the principal features of the cloned transcripts for zebrafish *ambra1* genes.

Alignment of the zebrafish Ambra1a1 and b amino acid sequences with those of human and mouse indicates that the primary structure of Ambra1 proteins is highly conserved among vertebrates (Figure 2) and is represented by a WD40 protein of about 1,300 amino acids. Zebrafish Ambra1a1 and Ambra1b polypeptides exhibit 55% identity to each other, and 56 and 58% identity with human and mouse AMBRA1s, respectively (Table 2). The WD40 motif (amino acids 49–175 of human AMBRA1) shows very high identity among the human, mouse and zebrafish AMBRA1 polypeptides (Table 2). The region involved in the binding with the BECN1 protein presents a lower identity ranging from 45 to 52%, according to the presence or absence of exon 8. Binding sites to the dynein light chain (DYNLL1) are present only in Ambra1a1, Ambra1a2 and Ambra1b proteins, all three containing the double TQT domain (Table 2).

Figure 2. Multiple sequence alignment of human (Hs, *Homo sapiens,* Q9C0C7), mouse (Mm, *Mus musculus,* NP_766257) and zebrafish (Dr, *Danio rerio*) Ambra1 proteins was originated with the program ClustalW. Zebrafish Ambra1 amino acid sequence is inferred from the coding sequences cloned in this study (Ambra1a1, HE602022; Ambra1a2, HE602023; Ambra1a3, FR846231; Ambra1a4, HE602024; Ambra1b, FR846230). In the alignment, identical residues in all sequences are indicated by '*'. Conservative and semi-conservative substitutions are indicated by ':' and '.', respectively. The WD40 repeats-region at the N-terminus is shadowed in yellow, the region involved in the BECN1 interaction in green and the binding site to the dynein light chain (DYNLL1) in light blue, with the TQT-domain in red. Position of exon 8, inside BECN1 binding region, is underlined.

	Dr-*ambra1b*				M*m-Ambra1*				Hs-*AMBRA1*			
	Tot. identity	WD40	Becn1 b	DYNLL1 b	Tot. identity	WD40	BECN1 b	DYNLL1 b	Tot. identity	WD40	BECN1 b	DYNLL1 b
Dr-*ambra1a*	55	88	45/50	69	56	90	46/51	61	56	90	47/52	66
Dr-*ambra1b*	-	-	-	-	58	90	49	74	58	90	50	79
Mm-*ambra1*					-	-	-	-	95	100	94	92

Table 2. Percentage of identity between Zebrafish Ambra1a1 and Ambra1b polypeptides and with human and mouse AMBRA1s.

Conserved syntenies for *ambra1* genes and phylogenetic analysis

Analysis of conserved synteny between zebrafish and human genomes was performed using the Syntheny Database set up on the zebrafish genome assembly Zv9 and the Ensembl version 61 [17]. The duplicated *ambra1* genes share strong synteny with the human *AMBRA1*. As shown in Figure 3, panel A, zebrafish *ambra1a* and *b* lie on chromosomes 7 (Dre7) and 25 (Dre25), respectively. Their genomic neighbourhoods contain 20 and 12 genes, respectively, with conserved synteny to the orthologous region in human chromosome 11 (Hsa11) in which the single *AMBRA1* gene is located as expected if zebrafish *ambra1* genes are co-orthologous to the human gene *AMBRA1*. Moreover, the Synteny Database analysis (sliding window size 25 genes) shows that the linkage fragments of chromosomes 7 and 25 containing *ambra1a* and *b* enclose other genes that are duplicated in zebrafish and present as single gene in mammals, such as: *midkine* (*mdk*), *diacylglycerol kinase-zeta* (*dgkz*), *M4 muscarinic cholinergic receptor* (*chrm4*) and *PDH finger protein 21A* (*phf21a*). These findings suggest that the zebrafish *ambra1a* and *ambra1b* genes are paralogs, which most likely arose as a result of the genome-wide duplication that occurred at the base of the teleost radiation [18].

To determine whether the presence of two *ambra1* genes is a general feature of teleost genomes, genomic database from *Tetraodon nigroviridis, Takifugu rubripes, Gasterosteus aculeatus* and *Oryzias latipes* were screened on the BLAT program (http://genome.ucsc.edu/cgi-bin/hgBlat?command=start) using Ambra1a and b sequences as queries. However, no duplicated *ambra1* genes could be detected in these genomes, suggesting that, in these species, one of the duplicated genes was silenced and subsequently lost. Moreover, analysis of teleost fishes EST libraries did not suggest the presence of transcripts deriving from duplicated genes.

A phylogenetic analysis was performed to study the evolutionary relationships among the *AMBRA1* genes using the amino acid sequence of zebrafish Ambra1a and b and other published Ambra1 sequences. The resulting tree (Figure 3, panel B) shows that tetrapods and teleostean fishes share a common ancestor for the *AMBRA1* gene family. Moreover, the tree suggests that a duplication arose within the teleostean clade giving birth to the paralogous forms of *ambra1* found in zebrafish. The separation of the two paralogous zebrafish genes is very well supported (bootstrap value: 1000/1000). Moreover, *Danio rerio ambra1b* gene is the orthologous form of the other teleostean *ambra1s*.

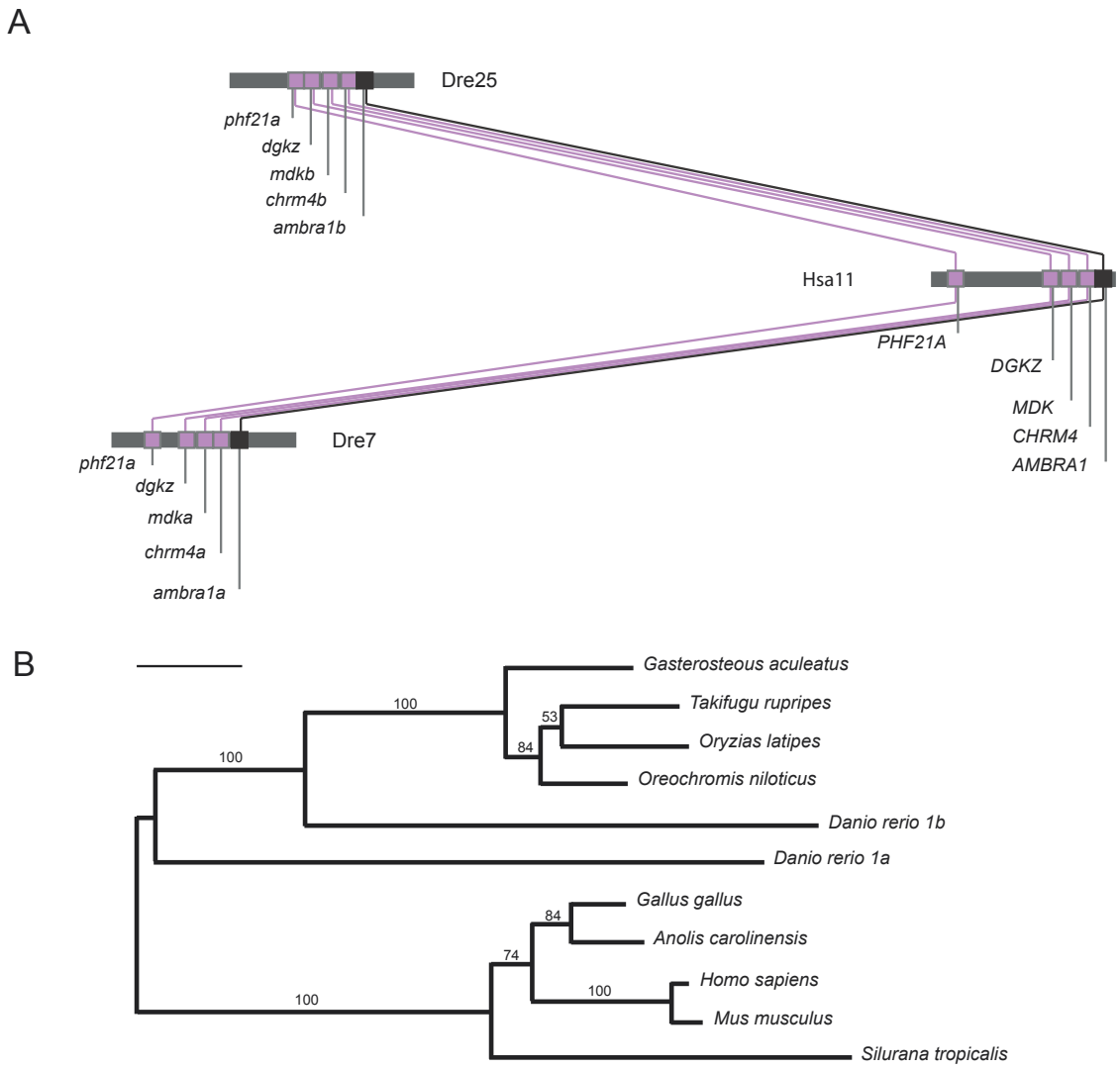

Figure 3. Conserved synteny neighbouring the *AMBRA1* locus and evolutionary relationship of the known *ambra1* genes. (A) Graphical representation of conserved synteny neighbouring the *AMBRA1* locus between *D. rerio* chromosomes 7 (Dre7) and 25 (Dre25) and *H. sapiens* chromosome 11 (Hsa11). The analysis was performed with the Synteny Database program (http://teleost.cs.uoregon.edu/acos/synteny_db/) with a sliding window size of 25 genes. Synteny analysis shows that the portion of zebrafish chromosome 7 (Dre7) that contains *ambra1a* and the portion of zebrafish chromosome 25 (Dre25) that contains *ambra1b* possess other four genes that are orthologous to genes in the portion of human chromosome 11 (Hsa11) that contains *AMBRA1*. Gene names are from Ensembl (http://www.ensemblgenomes.org/) or NCBI (http://www.ncbi.nlm.nih.gov/gene/). Genes are drawn as squares. The figure depicts the relative locations of genes, but is not drawn to physical scale. The positions of *ambra1a*, *ambra1b* and *AMBRA1* are marked in green. Oblique lines connect presumed paralogs within chromosome groups. (B) Evolutionary relationship of the known *ambra1* genes. The phylogenetic tree was calculated using the Maximum likelihood method with the RaxML 7.2.6 program and by applying the evolutionary model JTT+G [41]. Bar represents 0.1 substitutions per site. Comparisons were made to the amino acid sequences of *D. rerio* Ambra1a (CCE04070), *D. rerio* Ambra1b (CCA61107), *Takifugu rubripes* (ENSTRUG00000013113), *Gasterosteus aculeatus* (ENSGACG00000007844), *Orizyas latipes* (ENSORLP00000017709), *Silurana tropicalis* (XP_002934144), *Anolis carolinensis* (XP_003214662), *Gallus gallus* (ENSGALP00000013594), *Oreochromis niloticus* (XP_003458340), *Mus musculus* (NP_766257), *Homo sapiens* (Q9C0C7). Numbers indicate the values supporting the branching pattern from 1000 bootstraps.

Expression patterns of *ambra1a* and *b* mRNAs during zebrafish development

To investigate the temporal expression pattern of zebrafish *ambra1* genes, together with *becn1*, we performed qPCR analysis on cDNA obtained from different developmental stages (Figure 4). Gene-specific primer sets were designed to span known introns, thus revealing any contaminating genomic DNA as larger sized PCR fragments. For *ambra1a*, a set of primers was designed to simultaneously amplify the four transcript variants, whereas a second set could amplify only the two longer forms, *ambra1a1* and *ambra1a2* (see supplementary Figure 1). Due to constraints in fragment length for qPCR amplification, it was not possible to select more specific primer sets for the shorter forms, *ambra1a3* and *ambra1a4*.

Simultaneous detection of *arp* and *18S rRNA* gene expression was used to normalize the expression level of *ambra1* variants. For the comparison of differences in gene expression over time, all values were adjusted to the stage with the lowest expression level, corresponding to *becn1* expression at 8 hpf which was set at an arbitrary unit of 1. Similarly, all *ambra1* variants present the lowest expression at this stage.

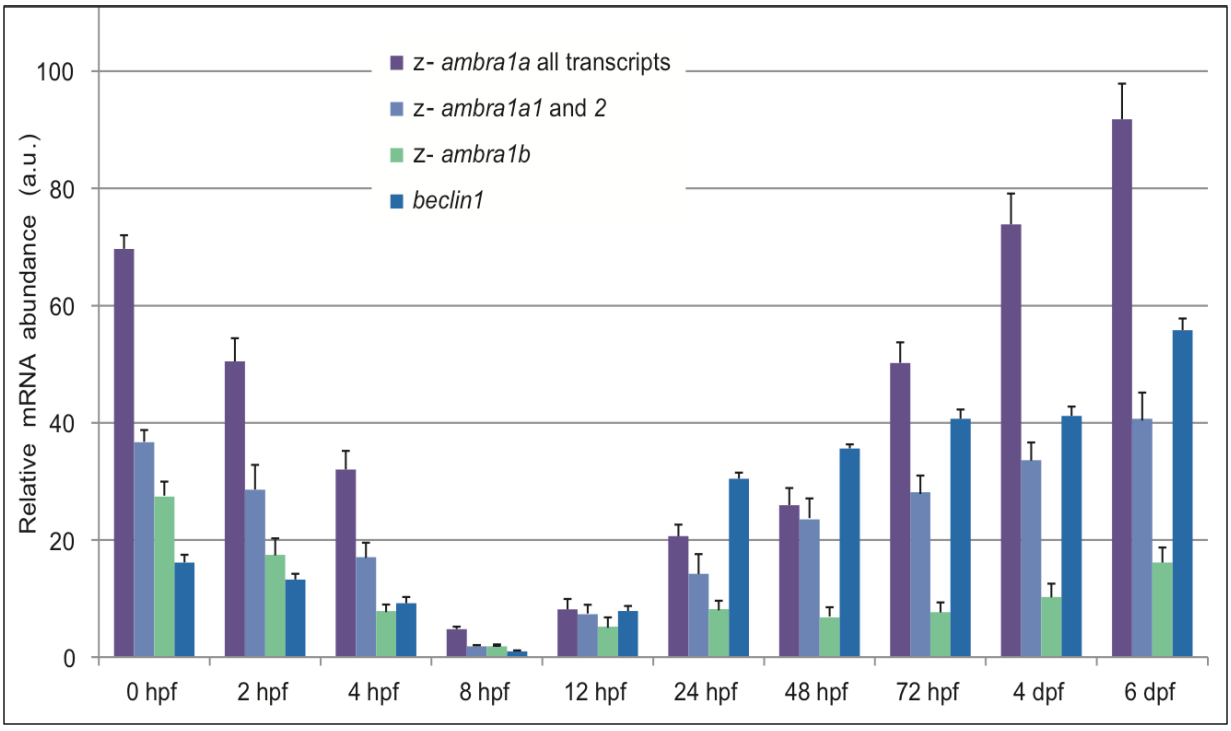

Figure 4. Temporal expression patterns of the duplicated zebrafish *ambra1* genes. The graph shows the relative mRNA transcript abundance of *ambra1a* (all transcript variants), *ambra1a1* and *2* and *ambra1b*, as well as *becn1* mRNAs in whole zebrafish embryos, from 0 to 6 dpf, as determined by qPCR. Error bars indicate S.E.M.

qPCR analysis revealed that *ambra1a* and *b* transcripts, as well as *becn1*, were maternally deposited into the embryo. These transcripts dramatically declined throughout the first 8 hpf, being replaced, thereafter, by the corresponding embryonic mRNAs up to a maximum at 6 dpf (days post-fertilization), the last stage examined. Transcripts of *ambra1a* present a higher expression level at 4 and 6 dpf with respect to initially deposited maternal mRNAs, whereas *ambra1b* expression was somewhat reduced. The contribution of the short forms *(ambra1a3* and *4*), deduced from the difference between all *ambra1a* transcripts and the two long forms, seems to increase during embryo and larval development. Similarly, embryonic and larval *becn1 mRNA* is much higher than the maternal messenger.

To further investigate the spatio-temporal expression of maternal and zygotic *ambra1a* and *b* mRNAs during zebrafish development, WMISH assays were performed on WT embryos and larvae from 0.2 hpf to 6 dpf using digoxigenin-labeled antisense *ambra1a* and *ambra1b* mRNA probes. In order to ensure specificity and to avoid cross-hybridizations, each probe covered fragments of the C-terminus and the 3'-UTR region.

Consistently with the qPCR results, *ambra1a1* and *b* mRNAs could be detected in one-cell stage embryos and distributed evenly in the blastodisc (Figure 5). No or a very low signal was found at 10 hpf (tail bud), in agreement with qPCR results showing a minimum concentration of both transcripts at 8 hpf during gastrulation. At 1 dpf, the maternal *ambra1a* mRNA was replaced by zygotic expression observed in the brain and otic vesicles. At 1 dpf, *ambra1b* mRNA was concentrated in the head and in the trunk, but its expression was less well defined with respect to *ambra1a*. At 4 and 6 dpf, both transcripts are localized in the otic vesicles, oral cavity, intestine, swim bladder and trunk. As shown by histological analysis, the signal for *ambra1b* is more evident in the apical border of the intestinal epithelium with respect to *ambra1a*.

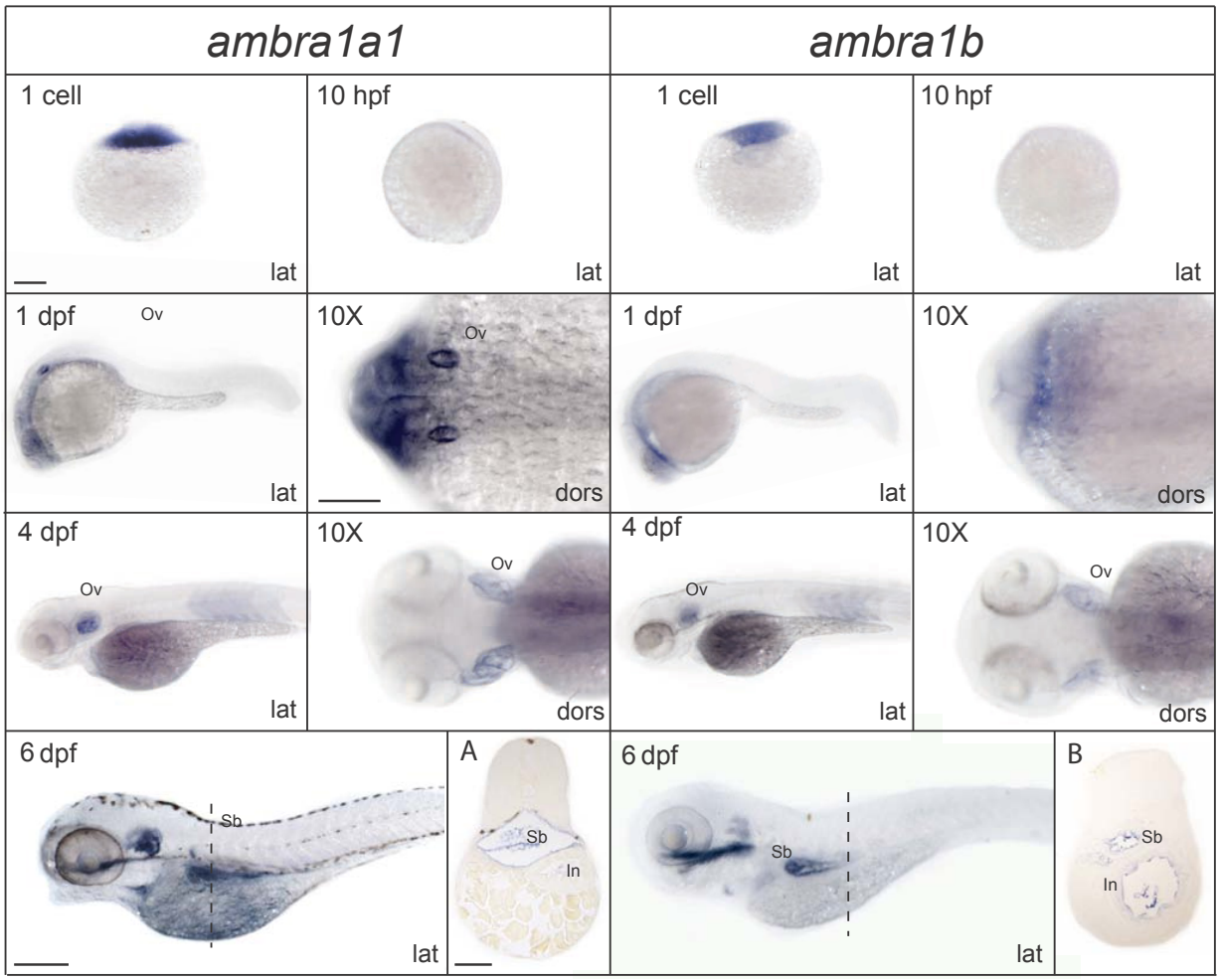

Figure 5. Spatio-temporal expression of *ambra1a1* and *ambra1b* mRNA during zebrafish development as evidenced by whole-mount *in situ* hybridization performed at the indicated stages. All embryos are lateral views with the animal pole up (1 cell and 10 hpf) and head pointing to the left (1, 4 and 6 dpf). 10X = magnification of the embryo (dorsal view) on the left. Bar = 200 µm. A and B: transverse histological sections 6 µm thick of the 6 dpf *ambra1a1* (A) and *ambra1b* (B) labelled embryos (the dashed lines in 6 dpf whole-mount embryos indicate the position of the section). Ov = otic vesicle, Sb = swim bladder, In = intestinal cavity.

Developmental consequences of Ambra1a and Ambra1b proteins depletion in zebrafish embryos and larvae

MOs effectiveness

To determine the functions of *ambra1a* and *b* during zebrafish development, gene-specific antisense MOs targeted to the ATG region (MO1-*ambra1a* and MO1-*ambra1b*) were injected into 1-cell embryos for translation knockdown. Five-nucleotide-mismatched MOs (MISMMO) (MO1-*ambra1a*-5m and MO1-*ambra1b*-5m) were used as negative controls.

Due to the lack of specific antibodies validated to detect zebrafish Ambra1a or Ambra1b proteins, the efficacy of MO1-*ambra1a* and MO1-*ambra1b* in targeting and blocking protein translation for each paralogous gene was analysed by an alternative approach. This was based on *in vitro* transcribed mRNAs encoding in-frame EGFP fusion constructs containing the MO-targeted sequence of each *ambra1* paralog. Coinjection of *ambra1a*- or *ambra1b*-*EGFP* fusion construct mRNAs with the corresponding 5-bp MISMMO, resulted in bright ubiquitous EGFP protein expression, thus demonstrating that the relative knockdown depends precisely on the complementary MO sequence (supplementary Figure 2, panel A). Coinjection of the EGFP fusion mRNAs for each paralog with the corresponding morpholino resulted in a drastic reduction in the EGFP expression, thus indicating that both MOs are able to efficiently inhibit protein translation (supplementary Figure 2, panel A). To confirm the absence of cross-target effects, each MO was coinjected with the EGFP fusion mRNA for the other paralog gene. In this case, no interference with EGFP expression was detected, indicating that it is unlikely that cross-targeting of MOs is occurring (supplementary Figure 2, panel A).

To discriminate between the contribution of maternal and zygotic *ambra1* transcripts, gene-specific antisense MOs targeted to the exon 3 - intron 3 junction of the predicted pre-mRNA of each gene were injected (MO2-*ambra1a* and MO2-*ambra1b*). These SPLICMOs caused the skipping of the exon 3 thus altering the translation reading frame of exon 4 with introduction of a premature stop codon and production of a truncated Ambra1a and Ambra1b proteins lacking all previously identified binding domains. The size of the mis-spliced product was consistent with the loss of the targeted exon 3, as confirmed by sequencing of both the mis-spliced RT-PCR products (supplementary Figure 2, panel B). Total RNAs extracted from 4, 6, 8, 12 and 24-hpf WT and MO2-ambra1a- and MO2-*ambra1b*-injected embryos were analysed by RT-PCR with two sets of specific primers flanking the splice site of each paralogous gene. Zygotic *ambra1b* expression takes place already at 6 hpf, although at very low level, as indicated by the predicted mis-spliced transcript detected as a lower band when embryos are injected with MO2-*ambra1b*. At 8 and 12 hpf, both *ambra1* zygotic RNAs become predominant and almost completely abolished by SPLICMOs. At 24 hpf, MO2-*ambra1a* still efficiently abrogates *ambra1a* splicing, while the effect of MO2-*ambra1b* started to decrease as shown by the reappearance of normally spliced band.

Optimization of MO injections

In order to optimize MO injections, 8.2, 10.3, 15.5, 20.6 and 25.8 ng of MO1-*ambra1a* or MO1-*ambra1b*, as well as of SPLICMOs (MO2-*ambra1a* or MO2-*ambra1b)* and MISMMOs (MO1-*ambra1a*-5m or MO1-*ambra1b*-5m) per embryo were injected in triplicates. Depending on the severity of defects compared to controls, morphant embryos from ATGMOs were classified into two graded phenotypes, less affected as Class I and more affected as Class II (Figure 6). As expected, the highest numbers of dead embryos was associated with the highest dose of both ATGMOs (25.8 ng). On the other hand, the lowest dose of both ATGMOs (8.2 ng) showed the least number of abnormal phenotypes (supplementary Table 2). Accordingly, 15.5 ng of MO1-*ambra1a* and 20.6 ng of MO1-*ambra1b* were chosen as optimal dosages to knockdown translation. At the same dosages, MO1-*ambra1a*-5m and MO1-*ambra1b*-5m had no or very low effects on zebrafish embryogenesis.

In the MO-coinjection experiment, just 5 ng of MO1-*ambra1a* plus 4 ng of MO1-*ambra1b* were selected as the best dosages for the simultaneous knockdown of the two paralogous genes. In this case, morphant embryos were classified into three graded phenotypes, with Class III corresponding to highly deformed morphants (Figure 6).

Moreover, accordingly to the optimization analysis, 18.5 ng of MO2-*ambra1a* and 15.5 ng of MO2-*ambra1b* were chosen as optimal dosages to knock down ambra1 splicing (supplementary Table 2). Injected embryos were analyzed by light microscopy and their morphology was recorded.

To further prove the specificity of the observed Ambra1 knockdown phenotypes, each ambra1 ATGMO was coinjected with *tp53/p53* MO. The rationale is based on a report that MOs can nonspecifically activate the tumor suppressor TP53-induced apoptosis, causing off-target phenotypic effects that are not caused by the specific MO used [19]. However, the *tp53* MO failed to eliminate the morphant phenotypes and showed that these were specifically target-related (Figure 6).

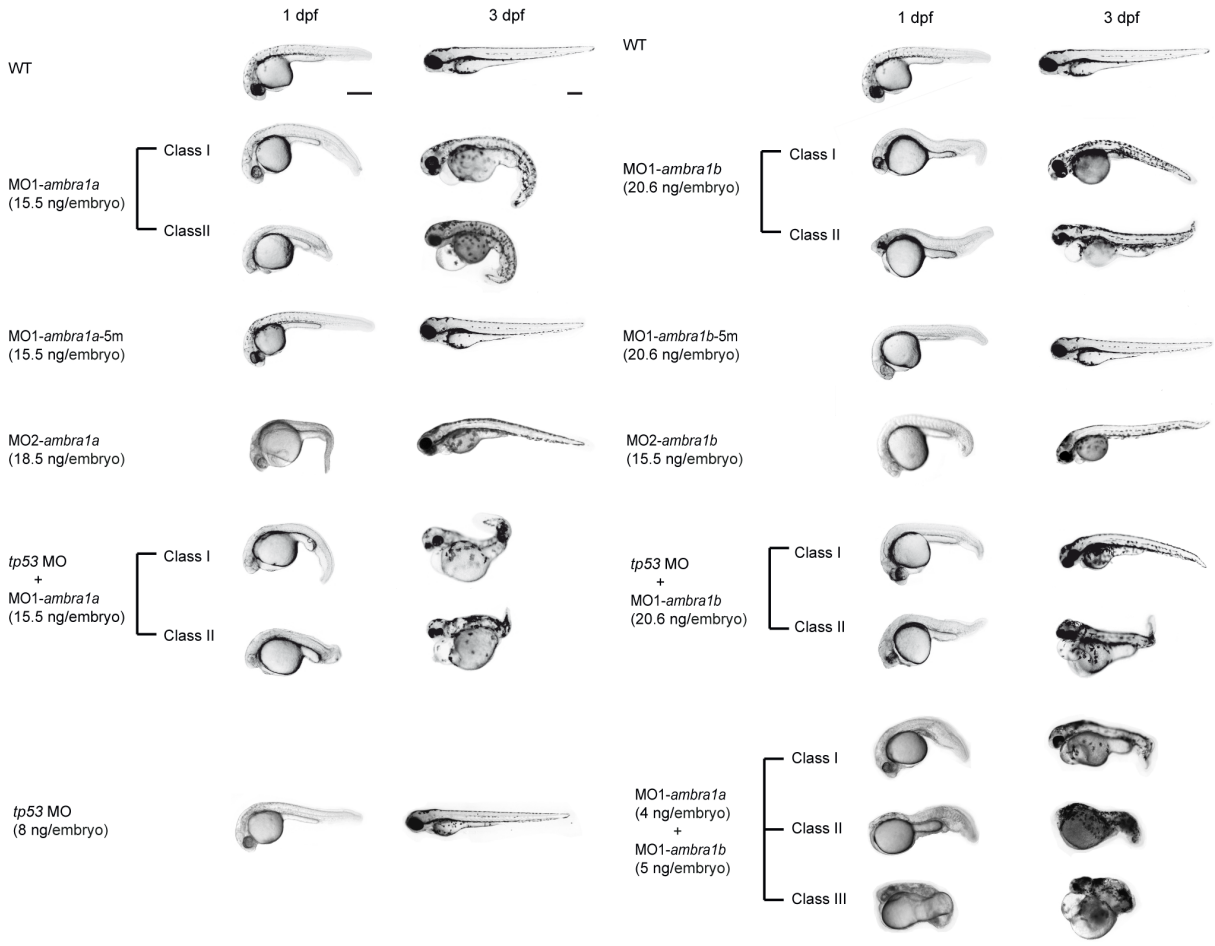

Figure 6. Phenotypes of embryos or larvae at 1 and 3 dpf after treatment with the different ambra1 ATGMOs alone or together with *tp53* MO or with SPLICMOs. Morphants phenotypes are compared to control groups (WT or MISMMOs). Phenotypes of *tp53* MO morphants are also reported. Animals are presented as lateral view, anterior to the left. Bar = 200 µm.

Analysis of morphant phenotypes

This analysis showed that treatment with *ambra1* ATGMOs causes severe embryonic malformations, because, at the selected MO dosages, ATGMOs morphants could survive for only 3 and 4 days, respectively.

During early development (cleavage period, 0-3 hpf), MO1-*ambra1a*- and MO1-*ambra1b*-injected embryos could not be morphologically distinguished from the controls (non-injected and MISMMO-embryos). However, by 4 hpf (sphere stage), both ATGMO-injected and coinjected embryos often exhibited a slight developmental delay, which was more evident in the MO1-ambra1a and coinjected morphants.

At 1 dpf, growth impairment was manifest, since both morphant embryos of Class II had smaller head, reduced eyes and trunk, curved or twisted tail and delayed pigmentation compared to controls. Otoliths were also smaller in size. Coinjection of both ATGMOs produced more extensive morphological alterations with a complete derangement of the body plan in Class III morphants (Figure 6).

At 2 dpf morphants were analysed by light microscopy analysis of morphology as well as by scanning electron microscopy (SEM) and toluidine blue stained semithin sections. As shown in Figure 7, morphants showed abnormal head development involving smaller eyes and pronounced hydrocephalus, that is present in both midbrain and hindbrain ventricles in MO1-*ambra1a* morphants compared with wild-type and control morphants (Figure 7, Panel B). This problem is instead present only in hindbrain ventricles in MO1-*ambra1b* morphants. In coinjected morphants hydrocephalus was present in both midbrain and hindbrain and was more severe, as shown by the corresponding semithin sections, where also the notochord appeared disorganized (Figure 7, Panel E).

At 3 dpf, these defects were further aggravated, as hatched MO1-*ambra1b* and in particular MO1-*ambra1a* larvae were very poorly developed (Figure 6). Abnormalities were more severe in MO1-*ambra1a* larvae (Figure 6), which displayed higher degrees of ventral curvature of the spine with misshapen tail (Figure 6). MO1-*ambra1a* larvae of class I show a slight ventralizated phenotype that is more evident in ambra1a and ambra1b morphants of class II as reported in supplementary Table 6.

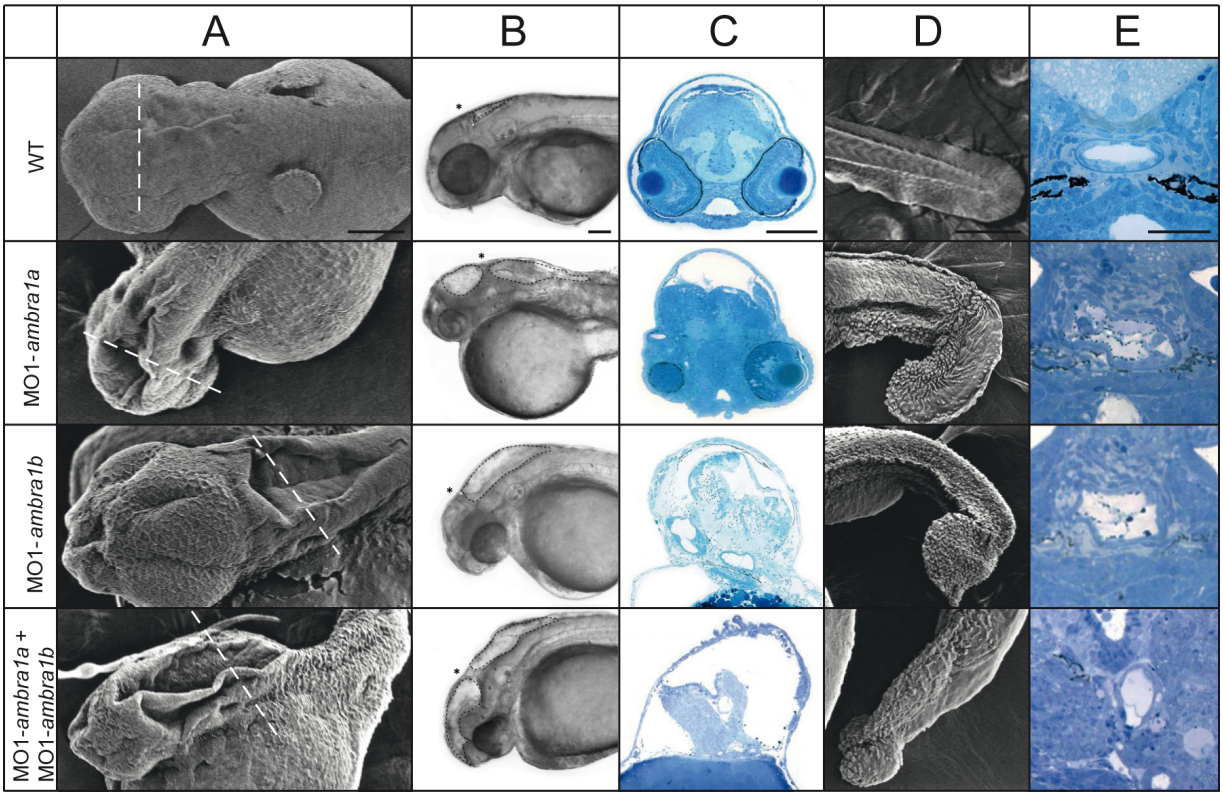

Figure 7. Two-dpf embryos treated with different ambra1 ATGMOs and compared to controls. (A) SEM (scanning electron microscope) images of dorsal view, anterior to the left. The white dashed lines indicate position of the section reported in (C). (B) Light microscope image showing hydrocephalus (dashed lines). Asterisks indicate midbrain-hindbrain boundary. Lateral view head to the left. (C) Toluidine blue staining of semithin transverse sections. (D) SEM images of lateral view tails showing the morphants deformities compared to controls. (E) Transversal semithin sections stained with toluidine blue displaying notochord malformations in different morphants. Bar = 100 µm.

At 3 dpf, light microscopy analysis of morphology of less deformed morphants showed that otic vesicles were much smaller in MO1-*ambra1a* and coinjected morphants (dashed lines in Figure 8). Eyes were smaller with both MOs, while MO1-*ambra1b* and coinjected morphants showed also mild cyclopia (close-set eyes, white arrowheads in Figure 8). Both morphants presented pericardial oedema (arrows in Figure 8) and persistent voluminous and oedematous yolk sac.

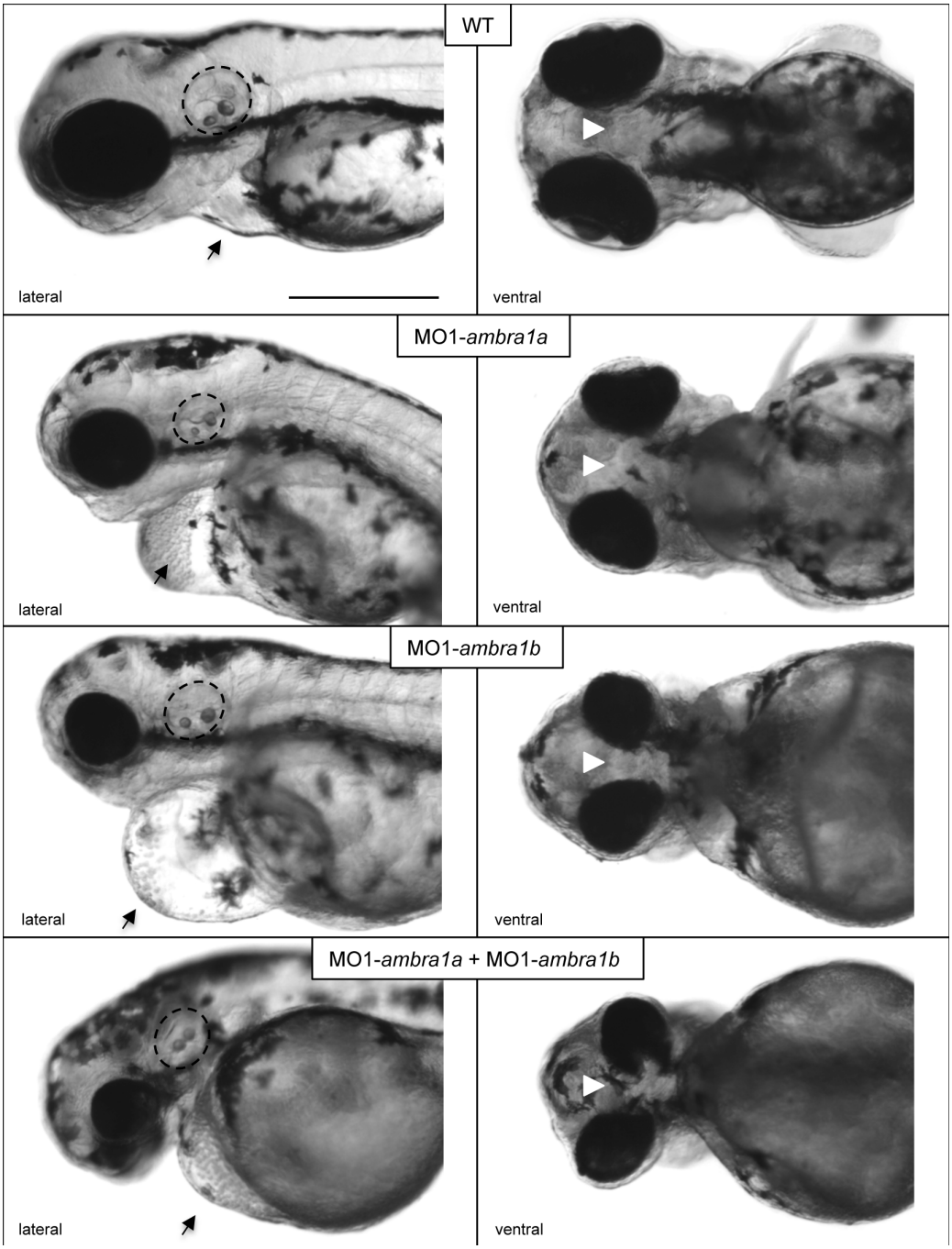

Figure 8. Close-up lateral and ventral light microscopy views of 3 dpf wild-type and ATGMOs-injected embryos. The genes targeted by ATGMOs are indicated for each image. Otic vesicles are smaller in MO1-*ambra1a* and ATGMO-coinjected morphants (dashed lines). White arrowheads indicate cyclopia in *ambra1b* and coinjected morphants. All morphants presented pericardial oedema (arrow). Bar = 200 µm

The network of sub-intestinal vessels at the yolk stalk, examined at 3 dpf, was devoid, in both morphants, of the 2 to 3 loop series observed in WT, following blood vessel visualization by endogenous alkaline phosphatase activity. The pattern of intersegmental vessels in the trunk and tail was also less defined (supplementary Figure 3). The lack of a properly established circulation could explain the large yolk sac still present in 48 and 72 hpf morphant embryos.

Knockdown of *ambra1a* and/or *ambra1b* indicates that both genes act in a synergistic fashion during development, as the gravity and number of abnormalities when both ATGMOs were injected was greater than the sum of those obtained following injection of each ATGMO separately (Figs. 6, 7, 8). With both MISMMOs, no morphological abnormalities were observed up to 7 dpf.

Moreover, the analysis of morphant phenotypes showed that MO2-*ambra1a*- and MO2-*ambra1b*-injected embryos (SPLICMOs) are comparable to controls during the first developmental period (0-24 hpf). By 1 to 3 dpf morphant obtained by SPLICMOs seem only slightly deformed with a lightly curved tail shape (Figure 6). SEM analyses, performed at 2 dpf, highlighted a pronounced hydrocephalus in the hindbrain area of both MO2-*ambra1a* and MO2-*ambra1b* morphants (Figure 9).

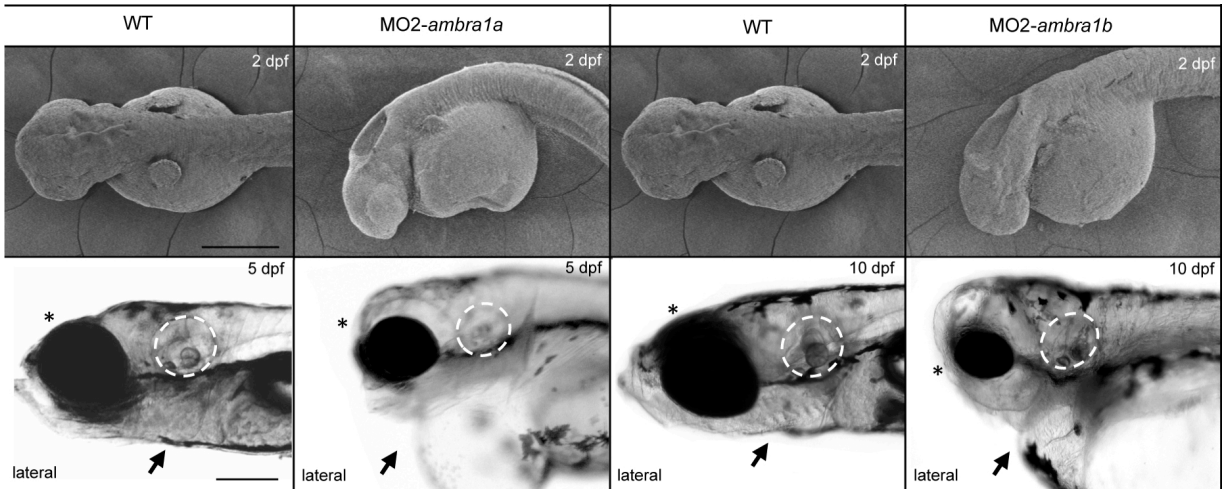

Figure 9. Lateral SEM and light microscopy views of wild-type and SPLICMOs-injected embryos. Top panel: Two-dpf embryos treated with ambra1a and b SPLICMOs and compared to controls. SEM images of dorsal view showing the morphant deformities compared to control. Botton panel: Close-up lateral and ventral light microscopy views of 5 and 10 dpf WT and SPLICMOs-injected embryos. The genes targeted by SPLICMOs are indicated for each image. Otic vesicles are smaller in MO2-*ambra1a* (dashed lines). Both SPLICMO morphants presented pericardial oedema (arrow) and reduced eyes (asterisks). Bar = 200 µm

Further abnormalities appeared later in development: by 5 dpf, MO2-*ambra1a*-injected embryos showed developmental defects, such as a pronounced pericardial oedema, highly reduced eyes and smaller otic vesicles compared to controls. The same abnormalities were evident in MO2-*ambra1b* embryos by 10 dpf (Figure 9) and were similar to those displayed by ATGMOs-injected embryos earlier in development (Figure 8). MO2-*ambra1a*- and MO2-*ambra1b*-injected embryos died within 12 dpf.

Rescuing of MO1-*ambra1b* or MO1-*ambra1a* knockdown with synthetic *ambra1a* and *b* mRNAs

To rescue the knockdown phenotype, the MO1-*ambra1a* was coinjected with *in vitro*-transcribed mutated zebrafish *ambra1a1* and *1a3* mRNAs encoding the full length of each transcript variant, but containing eight silent mutations in the region recognised by MO1-*ambra1a*. Similarly the MO1-*ambra1b* was coinjected with *in vitro*-transcribed mutated zebrafish *ambra1b* (Figure 10 and supplementary Table 3).

We found that coinjection, at the one-cell stage, of 15.5 ng MO1-*ambra1a* with either 200 pg of *ambra1a1* mRNA or 150 pg of *ambra1a3* mRNA was not able to fully rescue the ambra1a loss-of-function phenotype, proving that this phenotype derives from the loss of both long and short Ambra1a proteins. This was confirmed by coinjection of 15.5 ng of MO1-*ambra1a* with 200 pg of *ambra1a1* and 150 pg of *ambra1a3* mRNAs that led to highly efficient rescue of the loss-of-function phenotype. The same result was obtained with coinjection of 20.6 ng of MO1-*ambra1b* with 200 pg of *ambra1b* mRNA*,* verifying that this phenotype is a result of loss-of-function of *ambra1b.*

To test whether Ambra1a has equivalent functional capacities to Ambra1b, we attempted to rescue the *ambra1a* loss-of-function phenotype by coinjection with *ambra1b* mRNA and *vice versa*. In both cross-injection experiments (15.5 ng of MO1-*ambra1a* with 200 pg of *ambra1b* mRNA or 20.6 ng of MO1-*ambra1b* with 200 pg of *ambra1a1* and 150 pg of *ambra1a3* mRNAs) the phenotypes were not rescued. Moreover, in the MO1-*ambra1a* (4 ng) plus MO1-*ambra1b* (5 ng) loss of function, a complete rescue was obtained only with coinjection of *ambra1a1* (200 pg), *ambra1a3* (200 pg) and *ambra1b* (150 pg) mRNAs (Figure 10 and supplementary Table 3).

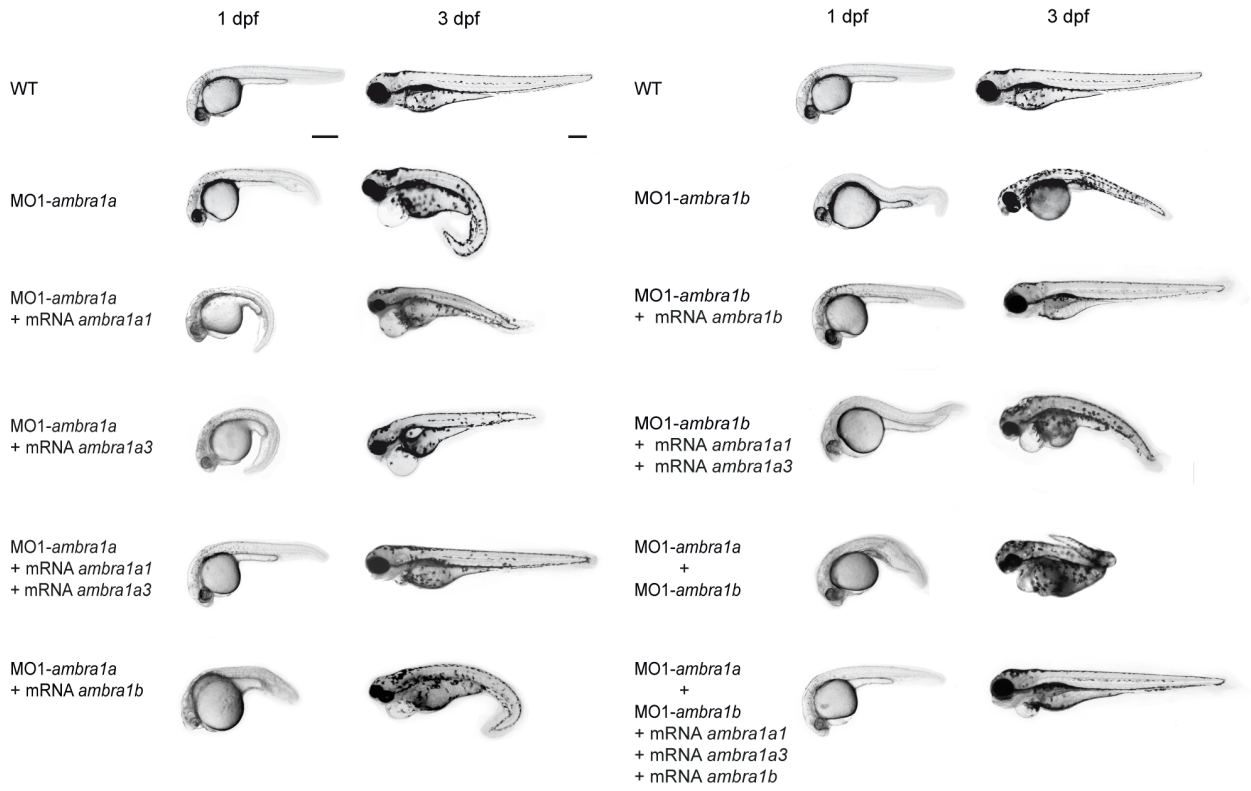

Figure 10. Phenotypes comparison among ATGMOs treated embryos and uninjected controls (WT) after the different rescue experiments. The genes targeted by ATGMOs and the mRNAs injected are indicated for each image. All the embryos are lateral view, anterior to the left. Bar = 200 µm.

Inhibition of *ambra1a* and *b* expression results in reduced autophagy and increased apoptosis during embryogenesis

In order to elucidate whether Ambra1 expression is required for autophagy induction during zebrafish development, LC3-II levels were examined in ATGMOs- and SPLICMOs-injected embryos by immunoblotting analysis at 48 hpf. The analysis was also performed in the presence of the lysosomal inhibitor bafilomycin A_1 (Baf A1) to prevent autophagosome degradation, thus making it possible to measure the whole amount of LC3-II produced at this stage. As shown in figure 11, high rate of autophagy was detected in control embryos (WT and MISMMOs) as revealed by the strong increase of LC3-II signal observed following bafilomycin A_1 treatment. In contrast, the inhibition of either *ambra1a* or *ambra1b* expression led to a reduced levels of LC3-II in the same experimental settings. In particular, *ambra1a* ATGMOs-injected embryos show the lowest amount of LC3-II, indicating a main contribution of this gene product at this stage, possibly because of its higher expression level when compared to *ambra1b* and zygotic *ambra1a* expression (Figure 4) or due to subfunction partitioning of the two *ambra1* paralogous genes.

Moreover, we analyzed whether the injection of MOs targeting the *ambra1a* or the *ambra1b* genes affects the expression of the proautophagic factor Becn1, a component of the class III phosphatidylinositol 3-kinase complex whose activity is regulated by its interaction with Ambra1[14]. Interestingly, Ambra1 downregulation led to increased levels of Becn1 protein, particularly evident with morpholinos targeting both zygotic and maternal transcripts (MO1-*ambra1a* and *ambra1b*) (Figure 11, panel C), which may be interpreted as an attempt of the system to counterbalance the absence of a positive regulator of the autophagic process.

To examine whether Ambra1a and b protein deficiency causes apoptosis, whole-mount TUNEL-staining was used to detect apoptotic cells in WT and morphant embryos analyzed at 24 hpf. Minimal evidence of apoptosis was found in WT (Figure 12), whereas a highly increased number of TUNEL-positive cells was detectable in the head region of both ATGMOs- and SPLICMOs-injected embryos (Figure 12), suggesting that the developmental defects may be partially caused by an increase of apoptosis.

The t-test showed significant differences in the apoptotic cell number between both ATGMOs- and SPLICMOs-injected embryos compared to the control embryos (WT and MISMMOs) (Graphic in Figure 12).

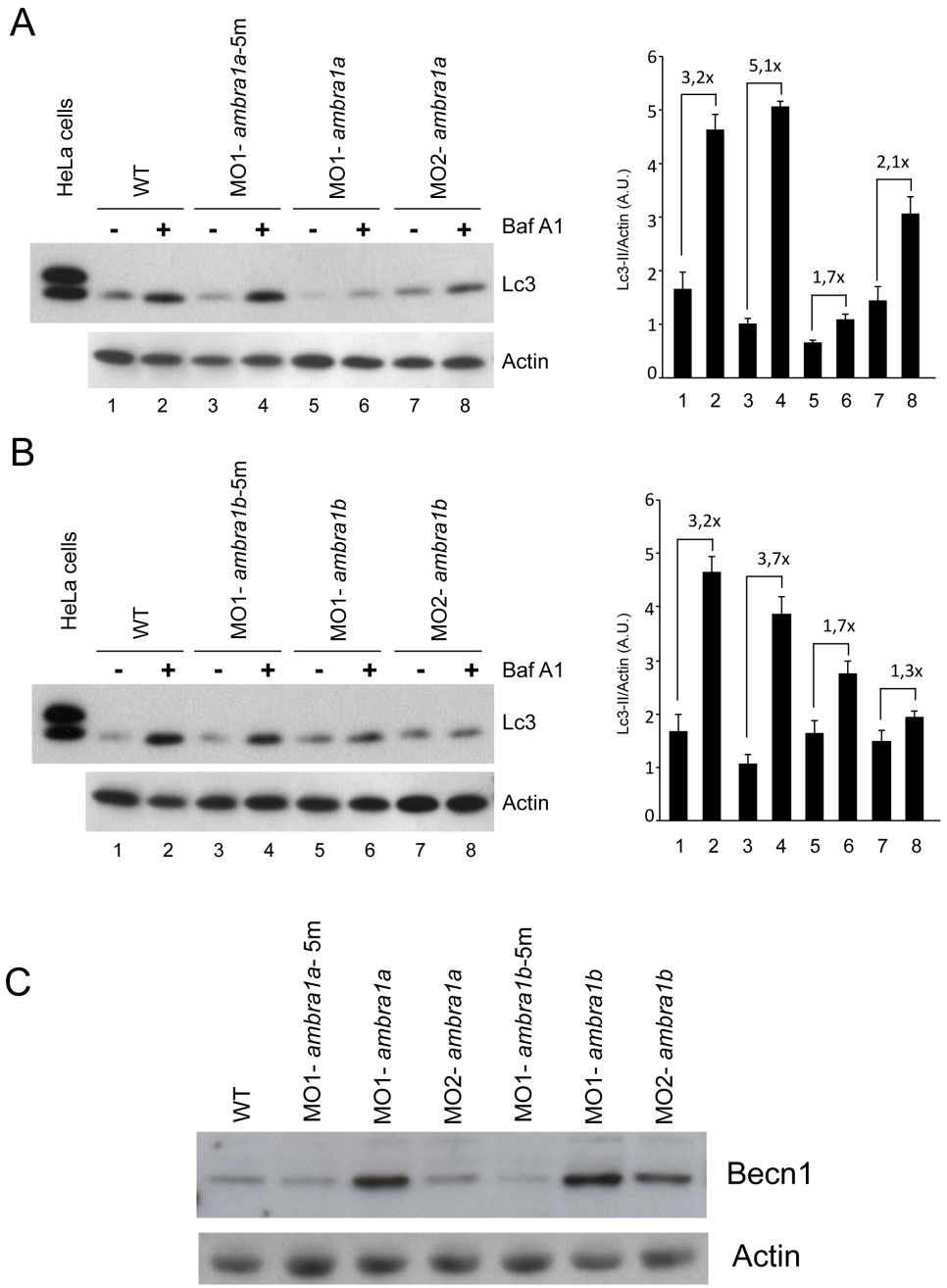

Figure 11. Analysis of autophagy and of BECN1 levels in *ambra1*-MOs injected embryos. (A and B) Analysis of autophagy in *ambra1*-MOs injected embryos. Protein extracts were prepared from WT and ambra1a (A) or ambra1b (B) MOs-injected embryos at 48 hpf and subjected to immunoblotting analysis using an anti-LC3 antibody. A parallel set of embryos were incubated with the lysosome inhibitor bafilomycin A_1 for 6 h before lysis, in order to assess the rate of autophagic flux upon Ambra1 downregulation. A graph reporting data from three independent experiments is shown together a representative immunoblot image. Values represent the densitometric measurement of LC3-II band intensities normalized to the signals of the loading control actin. A.U.: arbitrary units. Please note that this LC3 antibody shows a stronger reactivity for the zebrafish type II form of LC3 than the type I, which is detected only at longer exposure times. However, to ensure that the detected LC3 isoform was LC3-II, protein extracts from HeLa cells was run as reference marker. (C) Analysis of Becn1levels in *ambra1*-MOs injected embryos. Protein extracts were prepared from WT and *ambra1*-MOs-injected embryos at 48 hpf and subjected to immunoblotting analysis using an anti-BECN1 antibody. Actin expression was monitored as loading control.

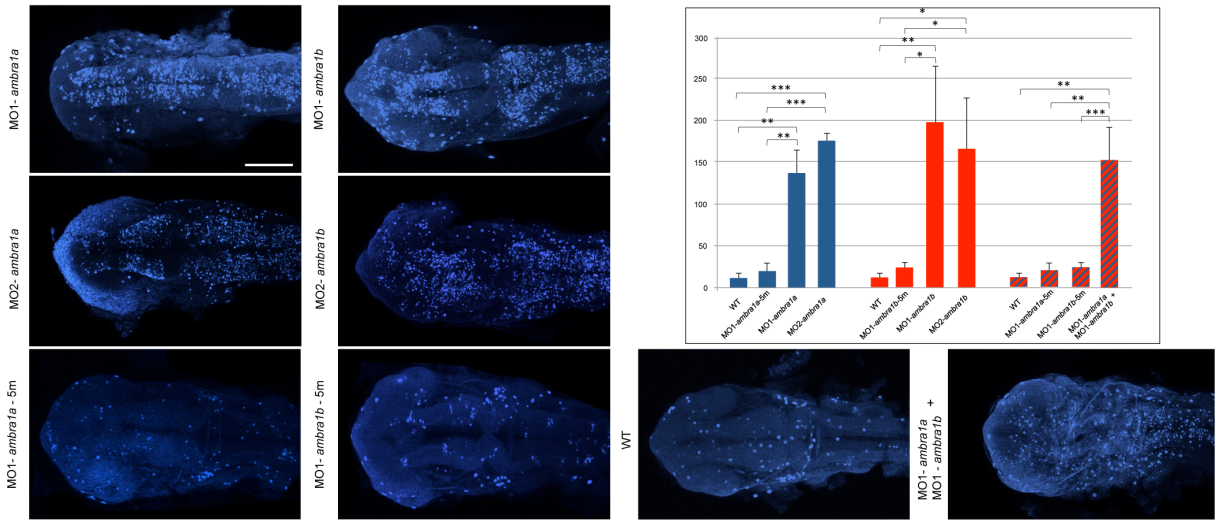

Figure 12. TUNEL analysis to detect apoptotic nuclei in WT embryos and ambra1 ATGMOs (MO1-*ambra1a* and MO1-*ambra1b*), SPLICMOs (MO2-*ambra1a* and MO2-*ambra1b*) and MISMMOs (MO1-*ambra1a*-5m and MO1-*ambra1b*-5m) embryos at 24 hpf. Minimal evidence of apoptosis was found in WT while a highly increased number of TUNEL-positive cells was detectable in the head region of ATGMOs- and SPLICMOs-injected embryos. Bar = 200 µm. Insert: differences in the TUNEL-positive cell number between both ATGMOs- and SPLICMOs-injected embryos compared to the control embryos (WT and MISMMOs). Values represent the mean ± S.D. (n = 5). * indicates that the difference in the expression levels are significantly different ($P < 0.05$); ** ($P < 0.01$); *** ($P < 0.001$).

Alteration of dorso-ventral patterning in Ambra1-deficient embryos

To further characterize the ATGMOs phenotypes, the expression of marker genes that are critical for dorso-ventral patterning and notochord formation was analysed by WMISH in morphants and compared to WT or MISMMOs embryos during different developmental stages. For each marker and each developmental stage, 15 embryos from three different microinjection experiments were used (Figure 13).

The *in situ* hybridization assay showed that MO1-*ambra1b* and coinjected morphants displayed a decrease in the expression of *gsc* and a reduction of *chd* staining in the dorsal axis. The modifications are less evident in MO1-ambra1a morphants and absent with SPLICMOs.

WMISH analysis of *sonic hedgehog* (*shha*), a marker for notochordal and floor plate cells, showed undulating notochord in both ATGMOs-injected embryos compared to control ones. This was not evident with SPLICMOs-injected embryos. SPLICMOs do not seem to interfere with the early developmental stages likely due to the presence of the *ambra1* maternal transcripts during the first developmental stages.

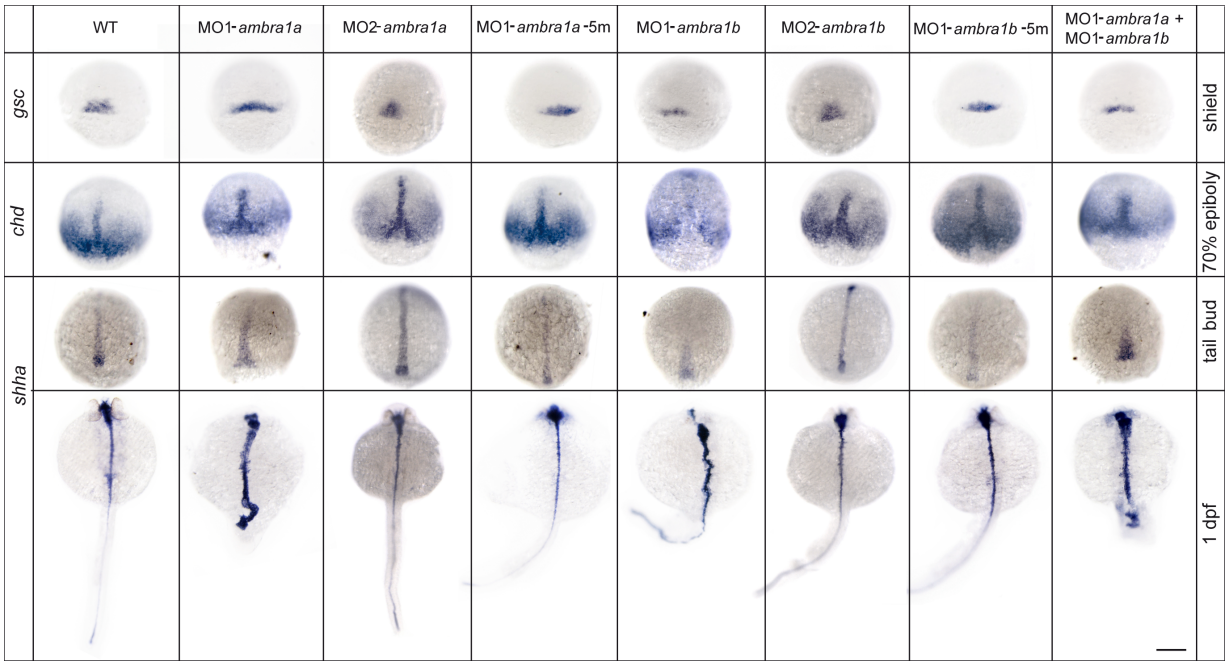

Figure 13. WMISH showing expression of the developmental markers, *gsc, chd* and *shha*, in *ambra1*-MOs-injected and control embryos. Dorsal views with the head pointing to the top in 1 dpf embryos. Bar= 200 µm.

DISCUSSION

In this study, we report the identification, through genome searches and targeted cloning, of two paralogous *ambra1* genes in the zebrafish genome. The conserved synteny with human *AMBRA1* gene located in chromosome 11, suggests that *ambra1a* and *ambra1b* genes, like other genes in chromosomes 7 and 25 they are linked to, arose as part of the fish-specific whole-genome duplication that occurred after divergence of the fish and tetrapod lineages.[20] Analysis performed on other available teleostean genomes shows that only *D. rerio* retained both *ambra1* paralogs, whereas the fate of the second *ambra1* gene in the other teleosts examined so far was likely nonfunctionalization and loss. Phylogenetic analysis showed that the *D. rerio ambra1b* gene is the orthologous form of the other sequenced teleostean *ambra1s*. Retention of initially redundant genes in teleost genomes is expected to be caused by either neofunctionalization or subfunction partitioning of the multiple roles of their mammalian ortholog, as the maintenance of functional redundancy over long times is unlikely. Thus, the study of paralogous gene function in zebrafish can help understanding the roles of the homologous human gene in health and disease [16].

Zebrafish *ambra1a* and *ambra1b* genes share the same genomic organization of mammalian *Ambra1* genes, but present some mutual differences: *ambra1a* is spliced as four alternative transcripts coding for proteins reduced in three ways in their C-terminal region, whereas only one transcript was identified for the *ambra1b* gene. Interestingly, Ambra1a3 and Ambra1a4 proteins lack the DYNLL1 binding domain, suggesting that these Ambra1 isoforms escape from the inhibitory interaction with the dynein complex. Moreover, the majority of *ambra1a* transcript variants lacked exon 8 that is instead always present in *ambra1b* mRNA. Exon 8 is located inside the region involved in the interaction with the BECN1 protein, suggesting a possible modulation of the BECN1 binding properties of AMBRA1 and of its autophagic potential. Although the exon 8 is located inside the region involved in the interaction with BECN1 protein, human AMBRA1 isoforms either containing or not exon 8 are able to bind BECN1 [14,21], suggesting the sequence encoding by this small exon may regulate other functions of the protein.

During embryogenesis, at all time points analysed through the first 6 days of development, the expression of *ambra1a* mRNA was greater than that of *ambra1b* messenger, suggesting that *ambra1a* may have more important functions during development. We find that the expression pattern of these two genes, analysed by WMISH, is partially overlapping, but the *ambra1a* probe was more specifically localized in the anterior brain and otic vesicles until 4 dpf. At 6 dpf the signal of both genes was weak and hardly detectable in the brain, but evident in the alimentary canal and in the swim bladder. Although this overlapping expression might suggest a potential for at least partially functional redundancy, this was not supported by the rescue experiments.

We selectively depleted the Ambra1 proteins both separately and together by MO-mediated translation and splicing blockages. The present work demonstrates that both the maternal and zygotic *ambra1a* and *b* mRNAs are required for normal embryogenesis and

larval development because the MO-induced deficiency of the corresponding proteins is associated with several developmental abnormalities and increased loss of viability at 3 to 4 days after fertilization in ATGMOs-injected embryos and at 12 days in SPLICMO-injected embryos. This conclusion is supported by the incorporation of several MO controls in the experimental design (see Results). However, the neural abnormalities observed in Ambra1a and b knockdowns are not due to activation of the TP53 pathway because they were still observed after coinjection with *tp53* MO. Embryos coinjected with both ATGMOs display even more severe malformations with a complete derangement of the body plan in Class III morphants. The increased mortality in zebrafish Ambra1s targeted loss-of-function is consistent with previous data obtained in a mouse model.[14] Rescue experiments show that the two genes could not compensate each other deficiencies, at least morphologically. Moreover, in the Ambra1a knockdown experiments, the normal phenotype was restored only after coinjection of short and long transcripts, suggesting specific functions also for Ambra1a3 and Ambra1a4 proteins that lack the DYNLL1 binding domain.

The phenotype that we observed with Ambra1a and b silencing with both ATGMOs occurred as early as 24 hpf, suggesting that both paralog genes may play a role in the early development of zebrafish and potentially during gastrulation. AMBRA1 deficiency in mice also results in neural abnormalities, including exencephaly due to failure in neural tube closure.[14]

Moreover, the two SPLICMOs (MO2-*ambra1a* and MO2-*ambra1b*) that target only zygotic *ambra1* transcripts, led to developmental defects only at a late stage, indicating the importance of maternally supplied *ambra1* transcripts and fundamental functions of the corresponding proteins in early embryonic development.

At the molecular level, the downregulation of Ambra1 expression leads to autophagy impairment associated with increased cell death, confirming the crucial role of Ambra1 in the crosstalk among these processes during embryogenesis and gametogenesis [22, 23]. In accordance with what observed in mice [14], an early increased rate of cell proliferation (manuscript in preparation) was observed in zebrafish, that is largely counterbalanced by an excess of cell death.

The comparative analysis of zebrafish morphant phenotypes of autophagy genes confirms a clear difference between the core members of the *BECN1* complex and the genes involved at later stages of the autophagic pathway, such as *ATG5* and *ATG7* [24,25], in the regulation of development, as previously reported in mammals. Indeed, the silencing of *AMBRA1* results in early embryonic lethality both in fishes and mice with similar defects in neural tube formation. Conversely, zebrafish *atg5* silencing causes a longer embryonic survival with respect to *ambra1* [26], similarly to mice in which death occurs only after birth[24]. The earlier appearance of Ambra1a and b morphant phenotypes suggests that Ambra1 may play multiple roles in early development, not all directly related to its positive regulation of the autophagic process. This conclusion is also supported by the observation that conversion to the LC3-II form is observed in zebrafish embryos starting from 32 hpf [27] (and data not shown), relatively late compared to the onset of the developmental defects.

Other interesting differences were also observed between Ambra1 and ATG5 morphant embryos when the expression profiles of patterning-regulating genes were analysed. Indeed, Ambra1 morphant embryos show a ventralized phenotype with reduced or modified expression of the dorsal *chd* and *gsc* genes, while ATG5 downregulation causes embryonic over-dorsalized deformities [25]. The *chd* and *gsc* are organizer-specific genes, expressed in the dorsal mesoderm, which induce the morphogenesis of dorsal structures, such as the notochord. Therefore, the pattern observed in the *in situ* hybridisation experiment with ATGMOs may explain the ventralized phenotype of morphants. Also *shha* pattern, a marker of the notochord, was differently shaped in morphants resulting in detectable undulations in the notochord with respect to WT, as previously observed in mouse by Fimia and colleagues [14].

Importantly, the inhibition of Ambra1 expression interferes with the regulation of cell proliferation and death during embryogenesis in both zebrafish and mice, while this effect was not detected for *atg5* gene. This is probably due to the fact that the upstream regulators of the autophagic process play a more complex role by interacting and regulating the activity of members of other cell pathways [28]. The functional link between proliferation, apoptosis and autophagy suggests that these processes are coordinately regulated in early development in order to limit uncontrolled cell demise and/or cell growth during the profound remodeling occurring in the course of organogenesis. Collectively, these findings confirm an important developmental role for Ambra1 in early vertebrate embryogenesis and provide compelling evidence for subfunctionalization of *ambra1* gene paralogs in zebrafish after ancestral duplication.

ACKNOWLEDGEMENTS

The authors wish to thank Dr. E. Negrisolo for help in phylogenetic analysis and comments and L. Pivotti for the valuable assistance in the fish facility. Research was supported by 60% funding from the Ministry of the University and Scientific and Technological Research of Italy (L.D.V. Padova, O.C. Ancona and M.P. Rome), FIRB “Accordi di programma” (M.P.), the Italian Ministry of Health (“Ricerca Corrente” M.P. and G.M.F.), “Ricerca Finalizzata” (RF08MDPINK M.P.)

REFERENCES

1. Ravikumar B, Futter M, Jahreiss L, Korolchuk VI, Lichtenberg M, Luo S, et al. 2009. Mammalian macroautophagy at a glance. J Cell Sci, 122:1707-1711.

2. Sharp ZD. 2011. Aging and TOR: interwoven in the fabric of life. Cell Mol Life Sci, 68:587-597.

3. García-Arencibia M, Hochfeld WE, Toh PP, Rubinsztein DC. 2010. Autophagy, a guardian against neurodegeneration. Semin Cell Dev Biol, 21:691-698.

4. Cecconi F, Levine B. 2008. The role of autophagy in mammalian development: cell makeover rather than cell death. Dev Cell, 15:344-357.

5. Rubinsztein DC, Gestwicki JE, Murphy LO, Klionsky DJ. Potential therapeutic applications of autophagy. 2007. Nat Rev Drug Discov, 6:304-312.

6. Williams A, Jahreiss L, Sarkar S, Saiki S, Menzies FM, Ravikumar B, et al. 2006. Aggregate-prone proteins are cleared from the cytosol by autophagy: therapeutic implications. Curr Top Dev Biol, 76:89-101.

7. Levine B, Kroemer G. 2008. Autophagy in the pathogenesis of disease. Cell, 132:27-42.

8. Mizushima N, Levine B, Cuervo AM, Klionsky DJ. 2008. Autophagy fights disease through cellular self-digestion. Nature, 451:1069-1075.

9. Grumati P, Coletto L, Sabatelli P, Cescon M, Angelin A, Bertaggia E, et al. 2010. Autophagy is defective in collagen VI muscular dystrophies, and its reactivation rescues myofiber degeneration. Nat Med, 16:1313-1320.

10. Di Bartolomeo S, Nazio F, Cecconi F. 2010. The role of autophagy during development in higher eukaryotes. Traffic, 11:1280-1289.

11. Huang WP, Klionsky DJ. 2002. Autophagy in yeast: a review of the molecular machinery. Cell Struct Funct, 27:409-420.

12. Matsunaga K, Saitoh T, Tabata K, Omori H, Satoh T, Kurotori N, et al. 2009. Two Beclin 1-binding proteins, Atg14L and Rubicon, reciprocally regulate autophagy at different stages. Nat Cell Biol, 11:385-396.

13. Zhong Y, Wang QJ, Yue Z. Atg14L and Rubicon: yin and yang of Beclin 1-mediated autophagy control. Autophagy 2009, 5:890-891.

14. Fimia GM, Stoykova A, Romagnoli A, Giunta L, Di Bartolomeo S, Nardacci R, et al. 2007. Ambra1 regulates autophagy and development of the nervous system. Nature, 447:1121-1125.

15. Di Bartolomeo S, Corazzari M, Nazio F, Oliverio S, Lisi G, Antonioli M, et al. 2010. The dynamic interaction of AMBRA1 with the dynein motor complex regulates mammalian autophagy. J Cell Biol, 191:155-168.

16. Postlethwait J, Amores A, Cresko W, Singer A, Yan YL. 2004. Subfunction partitioning, the teleost radiation and the annotation of the human genome. Trends Genet, 20:481-90.

17. Catchen JM, Conery JS, Postlethwait JH. 2009. Automated identification of conserved synteny after whole-genome duplication. Genome Res, 19:1497-1505.

18. Volff JN. 2005. Genome evolution and biodiversity in teleost fish. Heredity (Edinb), 94:280-294.

19. Robu ME, Larson JD, Nasevicius A, Beiraghi S, Brenner C, Farber SA, et al. 2007. p53 activation by knockdown technologies. PLoS Genet, 3:e78.

20. Meyer A, Van de Peer Y. 2005. From 2R to 3R: evidence for a fish specific genome duplication (FSGD). BioEssays, 27:937-945.

21. Behrends C, Sowa ME, Gygi SP, Harper JW. 2010. Network organization of the human autophagy system. Nature, 466: 68-76.

22. Pagliarini V, Wirawan E, Romagnoli A, Ciccosanti F, Lisi G, Lippens S, et al. 2012. Proteolysis of Ambra1 during apoptosis has a role in the inhibition of the autophagic pro-survival response. Cell Death Differ, doi: 10.1038/cdd.2012.27.

23. Gioacchini G, Dalla Valle L, Benato F, Fimia GM, Nardacci R, Ciccosanti F, et al. 2013. Interplay between autophagy and apoptosis in the development of Danio rerio follicles and the effects of a probiotic. Reproduction, Fertility and Development 25, 1115-1125.

24. Kuma A, Hatano M, Matsui M, Yamamoto A, Nakaya H, Yoshimori T, et al. 2004. The role of autophagy during the early neonatal starvation period. Nature, 432:1032-1036.

25. Komatsu M, Waguri S, Ueno T, Iwata J, Murata S, Tanida I, et al. 2005. Impairment of starvation-induced and constitutive autophagy in Atg7-deficient mice. J Cell Biol, 169:425-434.

26. Hu Z, Zhang J, Zhang Q. 2011. Expression pattern and functions of autophagy-related gene atg5 in zebrafish organogenesis. Autophagy, 7:1514-1527.

27. He C, Bartholomew CR, Zhou W, Klionsky DJ. 2009. Assaying autophagic activity in transgenic GFP-Lc3 and GFP-Gabarap zebrafish embryos. Autophagy, 5: 520–526.

28. Fimia GM, Piacentini M. 2010. Regulation of autophagy in mammals and its interplay with apoptosis. Cell Mol Life Sci, 67:1581-1588.

29. Westerfield, M. The Zebrafish Book. A Guide for the Laboratory Use of Zebrafish (Danio rerio), 3rd Edition. Eugene, OR, University of Oregon Press 1995.

30. Lawrence C. 2007. The husbandry of zebrafish (Danio rerio): a review. Aquaculture, 296:1-20.

31. Kimmel CB, Ballard WW, Kimmel SR, Ullmann B, Schilling TF. 1995. Stages of embryonic development of the zebrafish. Dev Dyn, 203:253-310.

32. Thompson JD, Higgins DG, Gibson TJ. 1994. CLUSTAL W: improving the sensitivity of progressive multiple sequence alignment through sequence weighting, position-specific gap penalties and weight matrix choice. Nucleic Acids Res, 22:4673-4680.

33. Felsenstein J. Inferring phylogenies. Sunderland (MA): Sinauer Associates. 2004.

34. Stamatakis A. 2006. RAxML-VI-HPC: maximum likelihood-based phylogenetic analyses with thousands of taxa and mixed models. Bioinformatics, 22:2688-2690.

35. Felsenstein J. 1985. Confidence limits on phylogenies: an approach using bootstrap. Evolution, 39:783-791.

36. Thisse C, Thisse B. 2008. High-resolution in situ hybridization to whole-mount zebrafish embryos. Nat Protoc, 3:59-69.

37. Serbedzija GN, Flynn E, Willett CE. 1999. Zebrafish angiogenesis: a new model for drug screening. Angiogenesis, 3:353-359.

38. Miller-Bertoglio VE, Fisher S, Sanchez A, Mullins MC, Halpern M. 1997. Differential regulation of chordin expression domains in mutant zebrafish. Dev Biol, 192:537-550.

39. Schulte-Merker S, Hammerschmidt M, Beuchle D, Cho KW, De Robertis EM, Nüsslein-Volhard C. 1994. Expression of zebrafish goosecoid and no tail gene products in wild-type and mutant no tail embryos. Development, 120:843-852.

40. Krauss S, Concordet JP, Ingham PW. 1993. A functionally conserved homolog of the Drosophila segment polarity gene hh is expressed in tissues with polarizing activity in zebrafish embryos. Cell, 75:1431-2444.

41. Jones DT, Taylor WR, Thornton JM. 1992. The rapid generation of mutation data matrices from protein sequences. Comput Appl Biosci, 8:275–282.

SUPPLEMENTARY MATERIAL

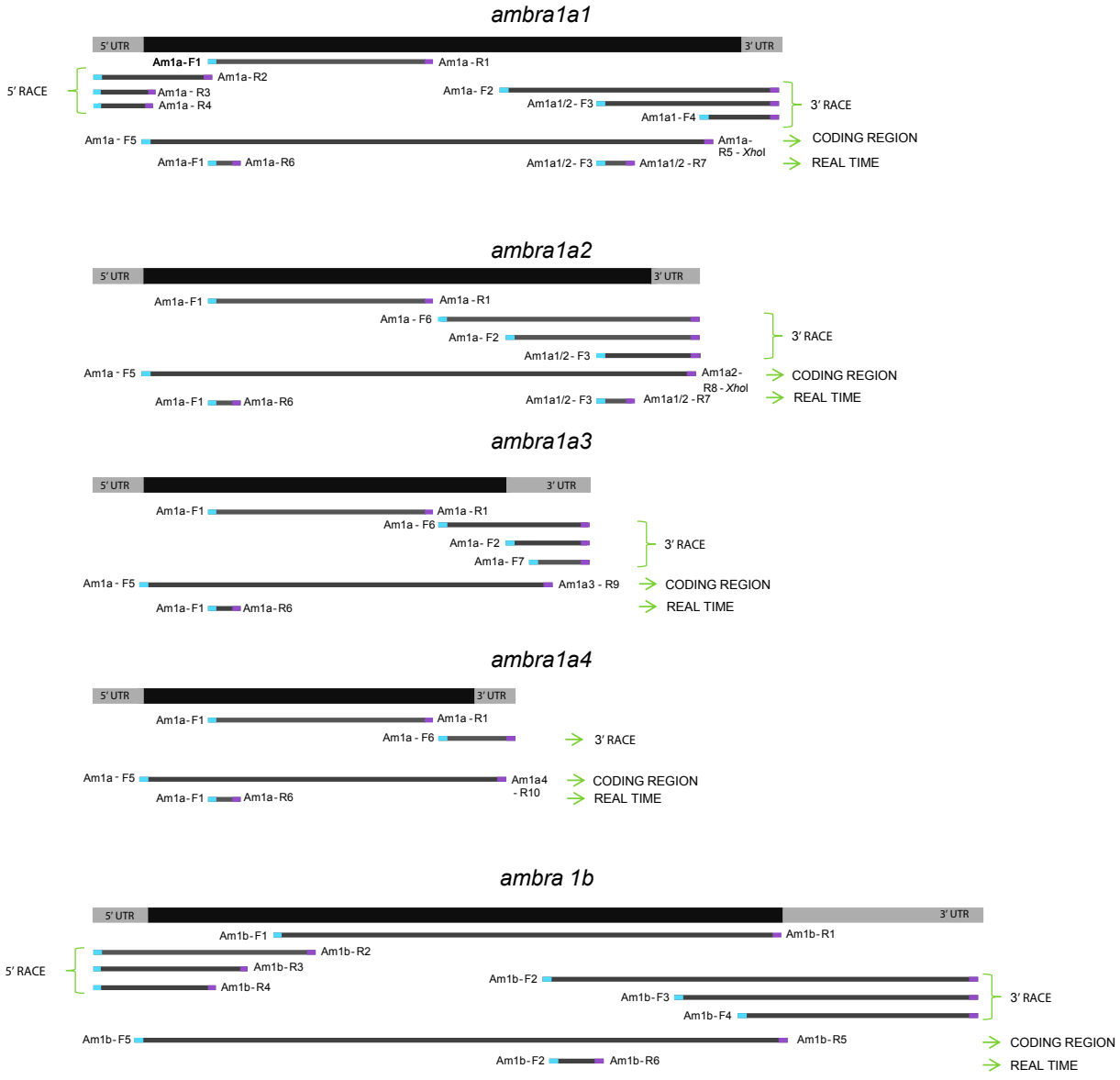

S-Figure 1. Schematic representation of the cloning strategy for *ambra1a1, a2, a3, a4* and *ambra1b* zebrafish cDNAs. Primers used are indicated.

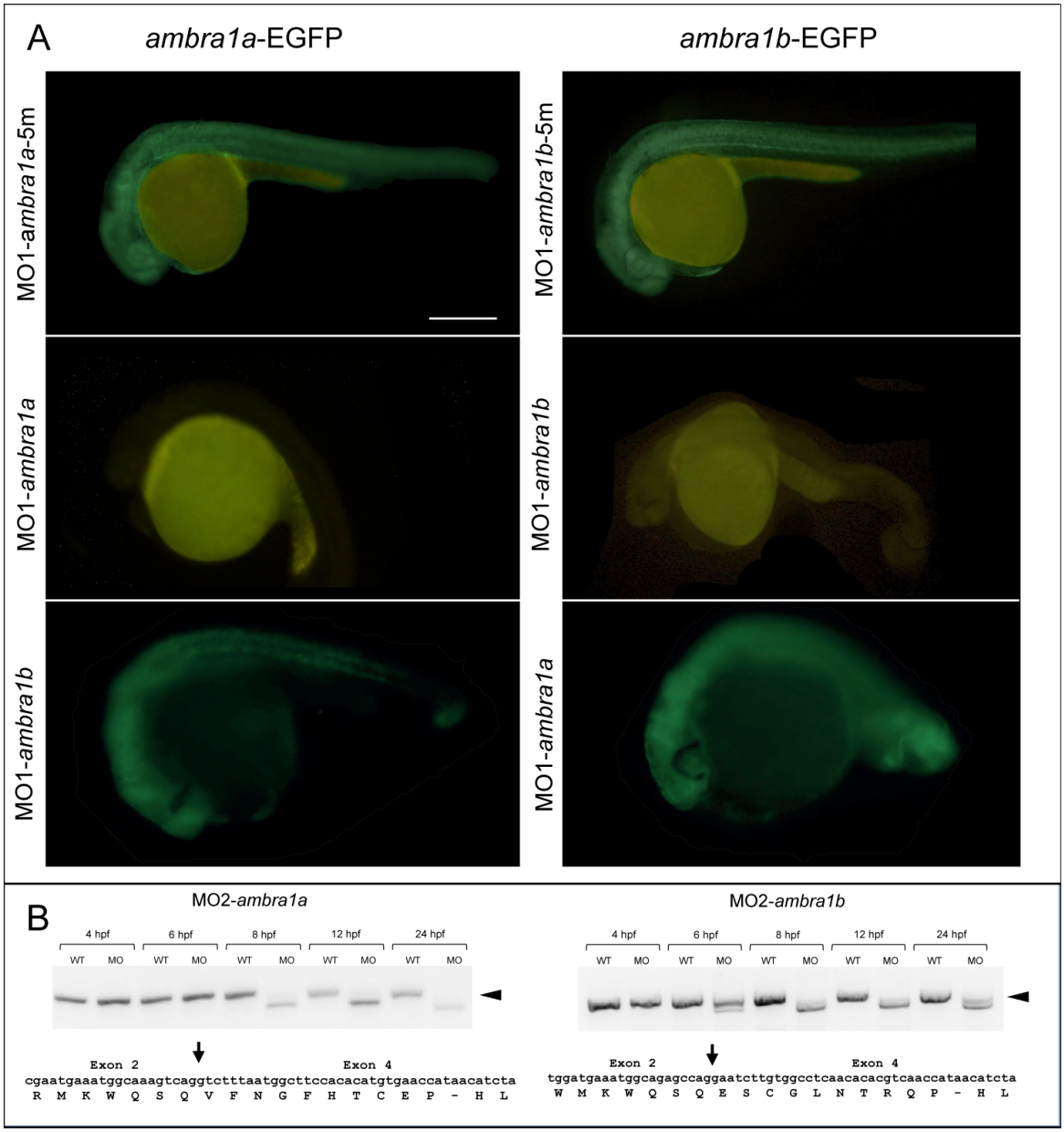

S-Figure 2. Validation of the ATGMOs and SPLICMOs mediated knockdown of *ambra1* genes. (A) Control experiments to verify the ATGMOs-mediated knockdown of *ambra1a* and *ambra1b*. *ambra1a*- and *ambra1b*-EGFP mRNAs were coinjected with ATGMOs as indicated inside each image, and embryos were examined for the presence of EGFP fluorescence at 24 hpf. All the embryos are lateral view, anterior to the left. Bar= 200 µm. (B) RT-PCR analysis with cDNA of 4, 6, 8, 12 and 24 hpf embryos (controls and SPLICMOs-injected) confirmed deletion of exons 3 in the *ambra1a* and *b* transcripts. The arrow-head indicates the residual wild-type transcripts at the different stages. Under the agarose gel, sequences of the misspliced *ambra1a* and *b* transcripts show the loss of exon 3 (arrow) and the introduction of a premature stop codon.

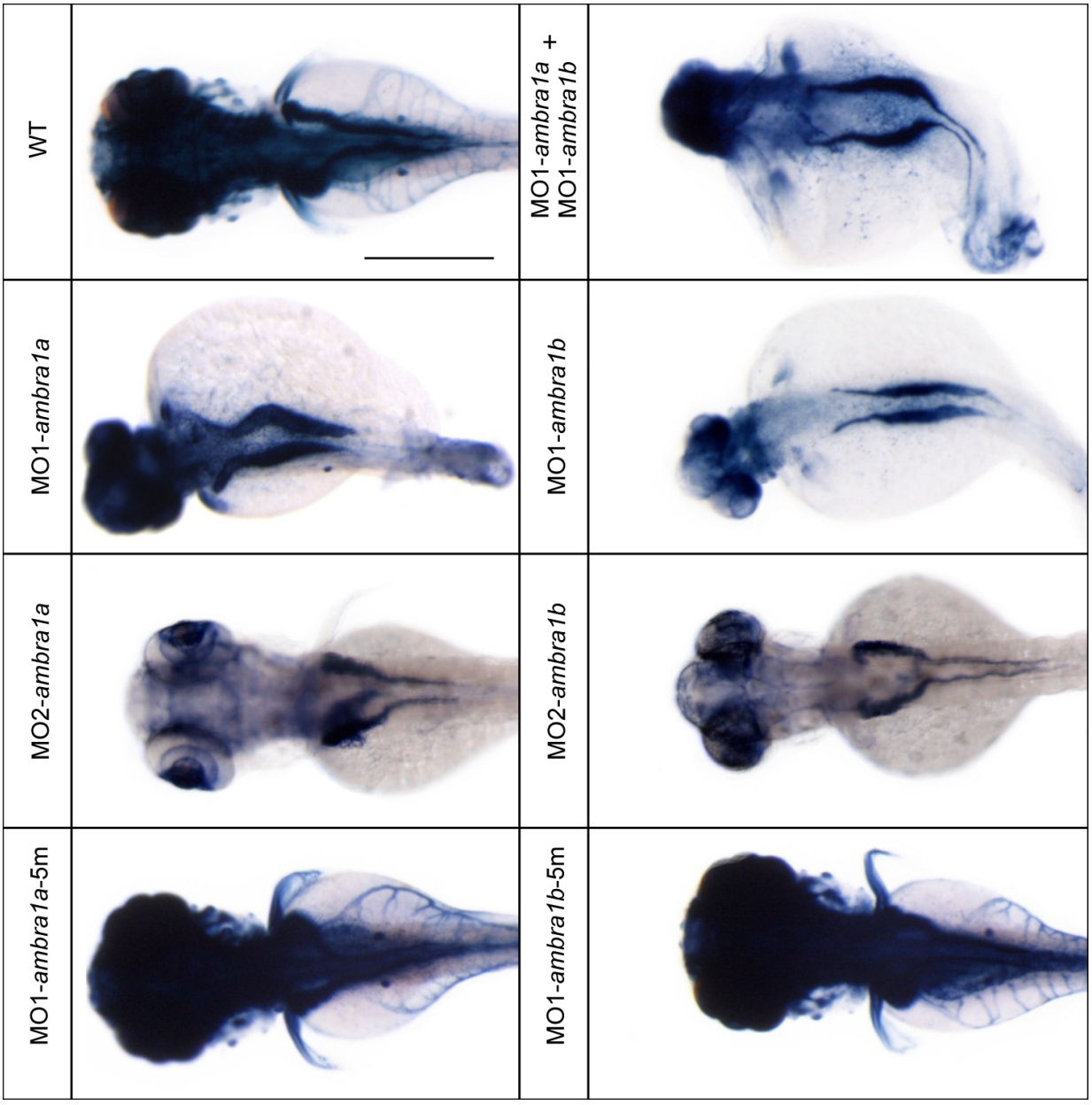

S-Figure 3. Alkaline phosphatase staining showing well-organized sub-intestinal vessels (SIVs) in WT larvae at 3 dpf. In *ambra1*-MOs-injected larvae SIVs are reduced or absent and pattern of intersegmental vessels in the trunk and tail are also less defined. Bar= 200 µm. Sv=sub-intestinal vessels.

	1° ex	1° intr	2° ex	2° intr	3° ex	3° intr	4° ex	4° intr	5° ex	5° intr	6° ex	6° intr	7° ex	7° intr	8° ex	8° intr	9° ex	9° intr	10° ex	10° intr
Mus musculus Ambra1	201	36070	254	350	59	570	178	1030	180	1820	65	1310	1459	31260	87	4920	182	14250	79	710
Danio rerio ambra1a1	206	3010	233	2168	59	167	184	113	173	986	67	97	1373	7293	87	4736	183	2268	78	917
Danio rerio ambra1a2	206	3010	233	2168	59	167	184	113	173	986	67	97	1373	7293	87	4736	183	2268	78	917
Danio rerio ambra1a3	206	3010	233	2168	59	167	184	113	173	986	67	97	1373	7293	87	4736	183	2268	78	917
Danio rerio ambra1a4	206	3010	233	2168	59	167	184	113	173	986	67	97	1373	7293	87	4736	548			
Danio rerio ambra1b	266	801	217	1462	59	104	184	233	173	437	67	115	1463	2937	87	275	183	163	81	2285

	11° ex	11° intr	12° ex	12° intr	13° ex	13° intr	14° ex	14° intr	15° ex	15° intr	16° ex	16° intr	17° ex	17° intr	18° ex	18° intr	19° ex
Mus musculus Ambra1	100	50360	113	9770	189	1030	155	13520	137	9710	92	1020	197	5720	878		
Danio rerio ambra1a1	101	19177	111	20026	189	3132	155	4999	140	3466	111	3226	209	21056	132	3025	733
Danio rerio ambra1a2	101	19177	111	20026	189	3132	155	4999	140	3466	111	3226	507				
Danio rerio ambra1a3	340																
Danio rerio ambra1a4																	
Danio rerio ambra1b	101	103	111	115	189	412	155	2050	140	4475	99	95	203	2009	123	3125	1802

Supplementary Table 1. Exons and introns size of *Mus musculus* and *Danio rerio ambra1* genes.

MO1-*ambra1a*	n.	Dead (%)	n. surviving	Normal (%)	Abnormal (%)
8.2 ng/embryo	161	12±6	141	50±3	50±3
10.3 ng/embryo	328	17±2	271	31±9	69±9
15.5 ng/embryo	354	24±12	269	30±6	70±6
20.6 ng/embryo	350	25±17	260	10±8	90±8
25.8 ng/embryo	278	47±6	147	4±8	96±8
MO2-*ambra1a*	n.	Dead (%)	n. surviving	Normal (%)	Abnormal (%)
8.2 ng/embryo	183	3±1	176	96±3	4±3
10.3 ng/embryo	152	3±4	147	89±2	11±2
15.5 ng/embryo	151	6±1	142	87±2	13±2
18.5 ng/embryo	269	19±7	218	64±6	36±6
20.6 ng/embryo	173	22±7	136	67±4	33±4
25.8 ng/embryo	185	47±6	99	71±5	29±5
MO1-*ambra1a*-5m	n.	Dead (%)	n. surviving	Normal (%)	Abnormal (%)
8.2 ng/embryo	164	1±2	162	99±0	1±0
10.3 ng/embryo	304	14±7	269	94±3	6±3
15.5 ng/embryo	321	11±12	277	93±5	7±5
20.6 ng/embryo	294	36±5	182	92±3	8±3
25.8 ng/embryo	245	30±5	164	82±9	18±9
MO1-*ambra1b*	n.	Dead (%)	n. surviving	Normal (%)	Abnormal (%)
8.2 ng/embryo	159	5±4	151	64±4	36±4
10.3 ng/embryo	195	2±2	189	61±7	39±7
15.5 ng/embryo	298	4±1	286	32±7	68±7
20.6 ng/embryo	317	29±9	226	16±8	84±8
25.8 ng/embryo	231	36±16	150	14±7	86±7
MO2-*ambra1b*	n.	Dead (%)	n. surviving	Normal (%)	Abnormal (%)
8.2 ng/embryo	163	7±1	153	87±2	13±2
10.3 ng/embryo	174	6±3	165	74±7	26±7
15.5 ng/embryo	271	7±1	253	45±3	55±3
20.6 ng/embryo	161	13±10	141	22±2	78±2
25.8 ng/embryo	180	30±7	127	38±3	62±3
MO1-*ambra1b*-5m	n.	Dead (%)	n. surviving	Normal (%)	Abnormal (%)
8.2 ng/embryo	161	1±1	160	98±1	2±1
10.3 ng/embryo	218	3±1	209	91±3	9±3
15.5 ng/embryo	286	7±5	267	92±3	8±3
20.6 ng/embryo	318	7±2	295	83±7	17±7
25.8 ng/embryo	287	13±6	249	77±8	23±8
MO1-*ambra1a* + MO1-*ambra1b*	n.	Dead (%)	n. surviving	Normal (%)	Abnormal (%)
1/2 ng/embryo	276	55±8	128	24±3	76±3
1/4 ng/embryo	283	23±4	215	26±4	74±4

Supplementary Table 2. Effects of different dosages of morpholinos on the percentages of dead fish and of normal and abnormal phenotypes calculated from the number of surviving prelarvae at 3 dpf.

	n.	Dead (%)	n. surviving	Normal (%)	Abnormal (%)
MO1-*ambra1a* + 20ng mRNA *ambra1a1*	164	46±9	90	39±7	61±7
MO1-*ambra1a* + 15ng mRNA *ambra1a3*	170	51±4	83	28±5	72±5
MO1-*ambra1a* + 20ng mRNA *ambra1a1* + 15ng mRNA *ambra1a3*	160	30±3	112	73±7	23±7
MO1-*ambra1a* + 20ng mRNA *ambra1b*	240	58±12	121	35±7	65±7
MO1-*ambra1b* + 20ng mRNA *ambra1b*	329	35±5	224	73±9	27±9
MO1-*ambra1b* + 20ng mRNA *ambra1a1*	152	24±6	105	31±6	69±6
MO1-*ambra1a* + MO1-*ambra1b* + 20ng mRNA *ambra1a1* + 15ng mRNA *ambra1a3* + 20ng mRNA *ambra1b*	177	39±10	110	65±10	35±10

Supplementary Table 3. Effects of different mRNAs coinjected with MOs on the percentages of dead embryos and of normal and abnormal phenotypes calculated from the number of surviving prelarvae at 3 dpf.

Primer	SEQUENCE 5'-3'
Am1a-F1	CTGCTGCTCATTGCCACC (18)
Am1a-F2	GCAACGCACTCATCCGTC (18)
Am1a1/2-F3	GTCGATGTGCATTCTGATGG (20)
Am1a1-F4	CGGAGTCTTTAGCTGCAGC (19)
Am1a-F5	GAGGAAGAGTGTTTGGAGATG (21)
Am1a-F6	ACAGTCTGCCTCCTCTCG (18)
Am1a-F7	AGGAGGACTCTCAGCTGG (18)
Am1a-M-F-*Cla*I	***CCATCGATGG***CTCAGCAACAGTCTTTCGTGATGAAGCTGG (40)
Am1a-5'-F-*Xba*I	***GCTCTAGAGC***GGTAGCAGCAGAGGTAG (27)
Am1a-R1	CTGCTCCTCATGCTGACC (18)
Am1a-R2	GTGGCAATGAGCAGCAGC (18)
Am1a-R3	ACAAGCTGCTGCAGAACC (18)
Am1a-R4	CGCTCTCGACTGGACAGG (18)
Am1a1-R5-*Xho*I	***CCGCTCGAGCGG***GATAACTACTATCGCTGTTGC (33)
Am1a-R6	CGCATCTCCACACTGTCC (18)
Am1a1/2-R7	GCTGGTTCTGTGTCTGCG (18)
Am1a2-R8-*Xho*I	***CCGCTCGAGCGG***CGGATGGACTTCACTCAC (30)
Am1a3-R9	CGTCCTACAGTAACTTTGCAC (21)
Am1a4-R10	CTCTGGTAGAATCGTTGGC (19)
Am1a-5'-R-*Kpn*I	***CGGGGTACCCCG***GTTCCTCTGTCCCAGC (28)
Am1b-F1	GCATACCACGTCAGACTCG (19)
Am1b-F2	AGGTGACGGACAGTCAGC (18)
Am1b-F3	GAACACACACACCACATCC (19)
Am1b-F4	GTAGACTCTCTAGAAGCTCC (20)
Am1b-F5	GCGTGCTGCTGAGTTAGTG (19)
Am1b-M-F-*Cla*I	***CCATCGATGG***GGTGCAGGACTTAACAGCATAAATGGC (37)
Am1b-F5-*Xba*I	***GCTCTAGAGC***GTGCTGCTGAGTTAGTG (27)
Am1b-R1	TCTGCCATACAGGTCGTC (18)
Am1b-R1-*Xho*I	***CCGCTCGAGCGG***GACTATCTGCCATACAGGTCG (33)
Am1b-R2	CTGAGTTCCCTGCAGTCC (18)
Am1b-R3	AAGCCATCTCCATACTATCC (20)
Am1b-R4	CGATGAGGAGAAGCTGAGC (19)
Am1b-R5	***CCGCTCGAGCGG***TCCAGCACCATGCAGACC (30)
Am1b-R6	CCTACCATCACATAGCAGC (19)
Am1b-5'-R-*Kpn*I	***CGGGGTACCCCG***TCTGTTCTGCACAGCCA (29)
LC3-F	GAGAAGTTTTTGCCGCCTCT (20)
LC3-R	ACCTGTGTCCGAACATCTCC (20)
BECLIN-F	GGACCACTTGGAACAACT (18)
BECLIN-R	CCGAAGTTCTTCAGTGTCCATC (21)
ARP-F	CTGAACATCTCGCCCTTCTC (19)
ARP-R	TAGCCGATCTGCAGACACAC (19)
18S-F	TCGAATGTCTGCCCTATCAACT (21)
18S-R	AGACTTGCCCTCCAATGGATC (20)

Supplementary Table 4. List of Primers used in this work. The recognition sequences for restriction enzymes are shown in bold italic letters.

Gene	Reference	GenBank cDNA reference	Vector	Endonuclease and RNA polymerase
chd	Miller-Bertoglio *et al*., 1997. [38]	AF034606	pBluescriptKS(+)	*Spe*I, T7
gsc	Schulte-Merker *et al*., 1994. [39]	NM_131017	pBS SK	*Bam*HI, T7
shha	Krauss et al., 1993. [40]	NM_131063	pCS2+	*Hind*III, T7
z-am1a1-3'-UTR	This work	XM_002667669	pGEM	*Apa*I, Sp6
z-am1b-3'-UTR	This work	XR_084457	pGEM	*Sal*I, T7

Supplementary Table 5. List of markers used in the whole-mount *in situ* hybridization analyses.

Deformity grade	MO1-*ambra1a*	MO1-*ambra1a* + *tp53*MO	MO2-*ambra1a*	MO1-*ambra1b*	MO1-*ambra1b* + *tp53*MO	MO2-*ambra1b*	MO1-*ambra1a* + MO1-*ambra1b*
N° of injected eggs	354	320	269	317	288	271	283
Dead (%)	24±12	21±9	19±7	29±9	13±11	7±1	23±4
N° surviving	269	250	218	226	253	253	215
Normal (%)	30±6	38±9	64±6	16±8	43±6	45±3	26±4
Tot. abnormal (%):	70 ±6	62±9	36±6	84±8	57±6	55±3	74±4
Abnormal class I - slight developmental delay - smaller eyes and otolithis - ventral curvature of the spine with misshapen tail - pericardial oedema and persistent voluminous and oedematous yolk sac - slight ventralization*	68±8*	53±14*	36±6	77±14	55±6	55±3	63±3*
Abnormal class II - smaller head, eyes and otoliths - curved or twisted tail - pericardial oedema and persistent voluminous and oedematous yolk sac - delayed pigmentation - ventralization	2±2	9±5	-	7±9	2±1	-	9±5
Abnormal class III - extensive morphological alterations with a complete derangement of the body plan	-	-	-	-	-	-	2±1

Supplementary Table 6. Summary of the ratio of abnormal phenotypes present in each class.

Zebrafish Ambra1a and Ambra1b are involved in control of cell proliferation

As reported in the General introduction of this PhD thesis, inactivation of Ambra1 in mouse embryos determines not only early embryonic lethality and severe abnormalities in the neural tube formation but also uncontrolled cell proliferation [1]. The increase of cell proliferation was associated to the onset of neurulation thus suggesting a role for Ambra1 in cell division, in particular during the nervous system development [1].

Starting from these data, we decided to analyze if, also in zebrafish, the two Ambra1 proteins we have characterized are involved in cell proliferation control and weather this property is controlled by cell autonomous or non-cell autonomous mechanism. If a gene acts in cell-autonomous manner, then morphant cells will exhibit the morphant phenotype when transplanted in a wild-type embryo. Conversely, if a gene acts in non cell-autonomous manner, morphant cells will exhibit wild-type phenotype when transplanted in wild-type embryo as they are influenced by surrounding environment.

The results of the experiments described in this chapter were performed in collaboration with the group of Prof. Francesco Cecconi (University of Rome 'Tor Vergata', IRCCS Fondazione Santa Lucia and Danish Cancer Society Research Center). The resulting paper, submitted for evaluation, shows that AMBRA1 is implicated in the control of cell proliferation by interfering with the C-MYC phosphorylation pathway.

Autophagy signalling controls C-MYC activity in cell proliferation and tumorigenesis

Valentina Cianfanelli[1,2], Claudia Fuoco[1,2], Mar Lorente[3,4], Maria Salazar[3,4,§] , Fabio Quondamatteo[5], Pier Federico Gherardini[1, §], Daniela De Zio[1,6], Francesca Nazio[1,2], Manuela Antonioli[7], Melania D'Orazio[1], **Tatjana Skobo**[8], Matteo Bordi[1,2], Mikkel Rohde[9], Luisa Dalla Valle[8], Manuela Helmer-Citterich[1],Gian Maria Fimia[7], Mauro Piacentini[1,7], Sabrina Di Bartolomeo[1,2], Guillermo Velasco[3], and Francesco Cecconi[1,2,6*]

[1]Department of Biology, University of Rome 'Tor Vergata', 00133 Rome, Italy,
[2]Laboratory of Molecular Neuroembryology, IRCCS Fondazione Santa Lucia, 00143 Rome, Italy
[3]Department of Biochemistry and Molecular Biology I, School of Biology, Complutense University, 28040 Madrid, Spain
[4]Instituto de Investigaciones Sanitarias San Carlos (IdISSC), 28040 Madrid, Spain
[5]Skin and Extracellular Matrix Research Group, Anatomy NUI Galway
[6]Unit of Cell stress and survival, Danish Cancer Society Research Center, 2100 Copenhagen, Denmark
[7]National Institute for Infectious Diseases IRCCS 'L. Spallanzani', 00149 Rome, Italy
[8]Department of Biology, University of Padua, Padua, Italy
[9]Unit of Cell death and metabolism, Danish Cancer Society Research Center, 2100 Copenhagen, Denmark
*Correspondence to: Francesco Cecconi, e-mail: cecconi@cancer.dk.

Submitted

Chapter II

INTRODUCTION

A great number of evidence suggests a possible involvement of the autophagic process in cell cycle regulation. The increase of proliferation in the neuroepithelium of the Ambra1 mutant mice during development has been previously described in the general introduction [1]. However, Ambra1 has been demonstrated to influence cell proliferation rate also *in vitro* as shown by downregulation and overexpression experiments with 2F cells [1].

As dysregulation of cellular proliferation is present also in other adult mouse model of autophagy genes knockout [2], the involvement of the autophagic process in cell cycle regulation seems to be a more general feature. Actually, deletion or downregulation of genes such as Beclin 1, UVRAG, Bif-1 and Atg4C result in an increase of tumor occurrence [3-6]. Moreover, the autophagic activity has shown to be reduced in tumor cells [7].

Autophagy, and the genes related with this process, can protect the cells from tumors by elimination of damaged mitochondria and peroxisomes. This activity could prevent the accumulation of toxic oxygen radicals that may cause genome instability and mutagenesis [8].

However, it is important to underline that autophagy could also provide cancer cells with a survival strategy under unsuitable conditions [8].

METHODS

Zebrafish maintenance and embryo production

Zebrafish maintenance, breeding, and staging were performed according to standard procedures ([9, 10].

Morpholino and microinjection

Morpholino antisense oligonucleotides (MO) were obtained from Gene Tools, LLC. ATG-morpholinos, MO1-ambra1a^{ATG} (5'- CTC CAA ACA CTC TTC CTC ACT CCC T -3') and MO1-ambra1b^{ATG} (5'-TTT TCC TCT TTA GTG CTC CAC GGC C- 3'), were used in order to knockdown both the maternal and the zygotic *ambra1a* and *ambra1b* zebrafish transcripts [11](Benato et al., 2013). As control, five-nucleotide-mismatched MOs, MO1-ambra1a^{5M} (5'-CTC gAA AgA CTg TTC CTg AgT CCC T-3') and MO1-ambra1b^{5M} (5'-TTa TgC TgT TTA GTc CTC CAC cGC C-3') were used (lowercase bold letters indicate the mismatch changes). Morpholinos were diluted in Danieau solution and microinjected as in Nasevicius and Ekker [12].

Transplantation

For the creation of genetic chimeras, embryos were injected, at one-cell stage, with a mixture containing 200 pg EGFP mRNA and 10 ng Biotin-dextran Lysine Fixable (10.000 Mw, Sigma) alone (control donors), or in combination with designated MOs: I) 10 ng MO1-ambra1a^{ATG}, II) 20 ng MO1-ambra1b^{ATG}, III) 2.5 ng MO1-ambra1a^{ATG} + 5 ng MO1-ambra1b^{ATG} mixture. At blastula stage (4 hpf), donor and wild-type host embryos were manually dechorionated and mounted side by side in 1,2 % agarose low melting chambers (Figure 1. A).

The transplantation apparatus is constituted by a 10 µl Hamilton syringe connected to a mineral oil reservoir through polyethylene tubes and connected at the end to a glass capillary needle (Figure 1. B). The use of mineral oil provides control of the suction and pressure required to pick up and expel cells (ZFIN: Zebrafish Book: Cellular Methods, http://zfin.org/zf_info/zfbook/chapt5/5.7.html).

Approximately 30 cells from donor embryos were then transplanted into host embryos (Figure 1. C). At 90% epiboly (9 hpf), transplanted embryos were fixed in paraformaldehyde 4% in phosphate buffered saline, for 2 h at RT (Figure 1. D). Biotin injected transplanted cells were detected in hosts using an avidin-biotinylated complex (ABC Kit, Vectastain) and the DAB substrate.

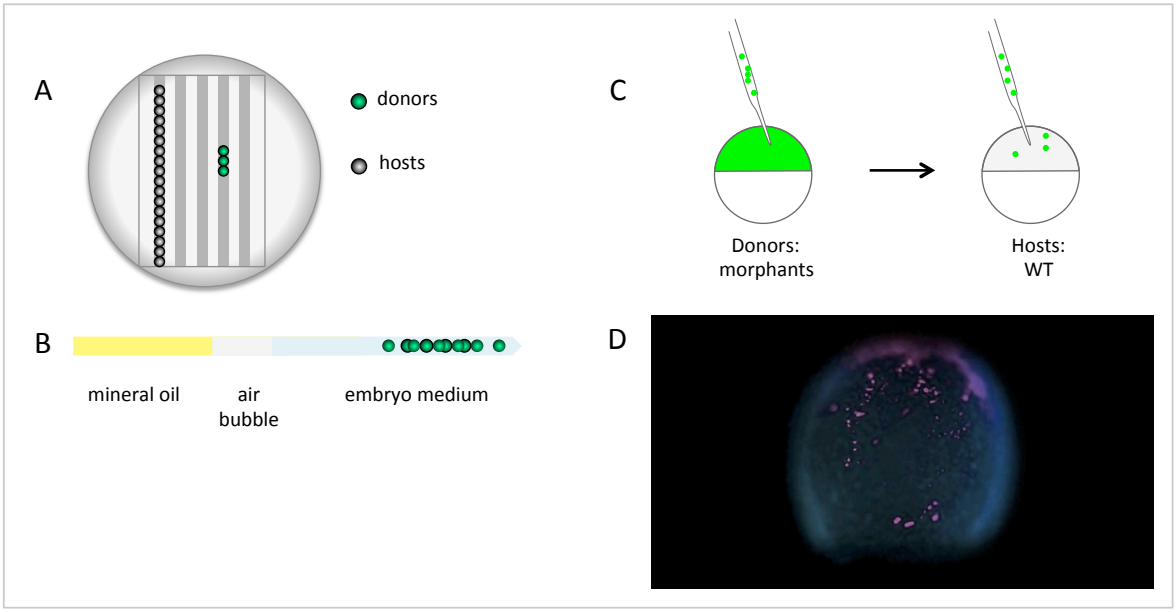

Figure 1. A) Petri dish with agarose low melting, holding host and donor embryos in different rows. B) Transplantation needle. C) Schematic representation of cell transplantation experiment: about 30 cells were transplanted from donor morphants to the host embryos. D) Image of transplanted zebrafish embryo at 9 hpf. Population of transplanted cells is labeled in purple.

Proliferation analysis

Proliferation was analyzed both directly in morphant embryos as well as in the genetic chimeras above described. To analyze proliferation, whole mount immunohistochemistry was performed with anti-phosphohistone H3 antibody (polyclonal rabbit Millipore) according to the manufacturer instructions and revealed with NBT/BCIP solution (Roche) or FAST BLUE (Sigma). For imaging stereomicroscope Leica DMR and confocal microscope Leica SP5 were used.

Statistical analysis

Quantitative data are expressed as mean ± SEM. Statistical significance of transplantation experiment was determined by chi-squared test using the Primer statistical software. Statistical significance of proliferation assay was determined by Kruskal-Wallis one-way analysis of variance (Anova) and differences between groups were assessed with the Mann–Whitney *U*-test using the statistical software Statistic 10. p-value of less than 0.05 was considered statistically significant.

RESULTS

Proliferation analysis

Embryos injected with I) MO1-ambra1a^{ATG}, II) MO1-ambra1b^{ATG}, III) MO1-ambra1a + MO1-ambra1b and their controls (wild-type and injected with MO1-ambra1a-5m or with MO1-ambra1b-5m) were analysed, at 9 hpf, by means of whole-mount immunohistochemistry with anti-phosphohistone H3. The number of phosphohistone H3 positive cells, quantified within an equal area in each embryo, is significantly higher in all ATG morphant embryos (MO1-ambra1a^{ATG}, MO1-ambra1b^{ATG} and coinjection of both MOs) compared with the three control samples with the exception of coinjection of both MOs when compared with MO1-ambra1b-5m morphant control embryos. In particular, as shown in Figure 2, the number of cells in proliferation was similar in all the three control samples (WT and MO1-ambra1a^{5M} or MO1-ambra1b^{5M} morphant embryos). Moreover, proliferation of MO1-ambra1b embryos was higher than MO1-ambra1a and co-injection of both MOs even if not significantly.

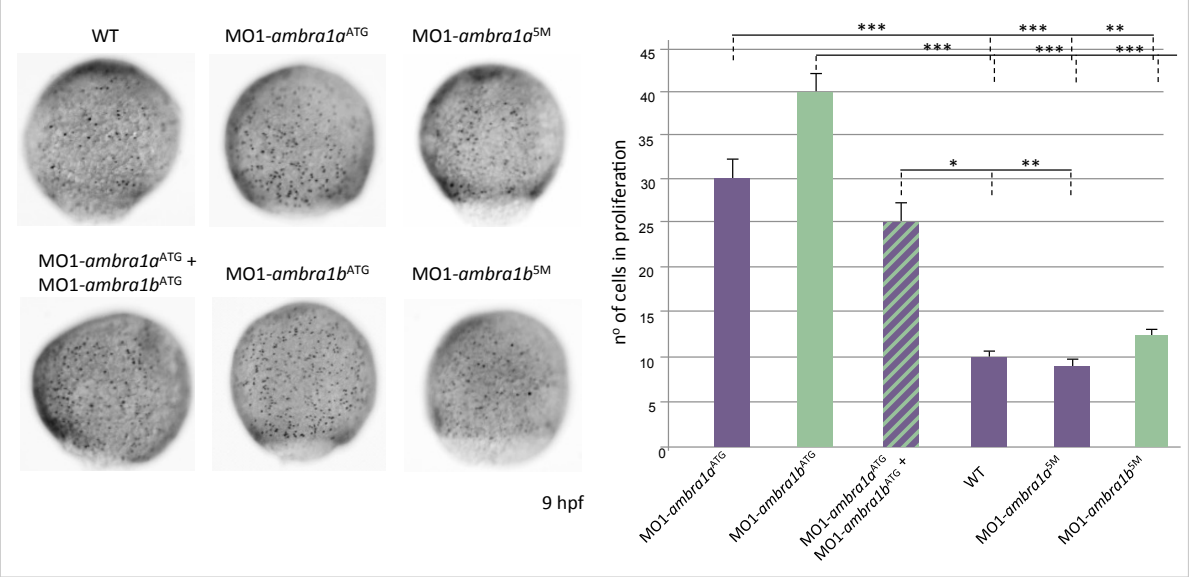

Figure 2. Proliferation analysis: embryos were injected with MO1-ambra1a^{ATG} and MO1-ambra1b^{ATG} (alone or together), and stained, by immunohistochemistry, with anti-phosphohistone H3 antibodies at 9 hpf. The number of pH3 positive cells is represented in bar graphs (mean ± standard error of the mean). The results are the average of three independent experiments with at least 7 embryos for each treatment. * indicates that the differences in the number of cell in proliferation are significantly different ($P < 0.05$); ** ($P < 0.01$); *** ($P < 0.001$).

Transplantation

To determine whether the cellular higher proliferation rate observed in embryos injected with MO1-ambra1a^{ATG} and MO1-ambra1b^{ATG} is cell-autonomous or non cell-autonomous, we transplanted a small population of MO-microinjected cells into wild type embryos and analyzed their proliferation rate. Donor embryos were injected with a mixture containing EGFP mRNA and biotin-dextran (to trace the cells before and after transplantation) and I) MO1-*ambra1a*^{ATG}, II) MO1-*ambra1b*^{ATG}, III) MO1-*ambra1a*^{ATG} + MO1-*ambra1b*^{ATG}.

Cell proliferation rate and biotin-dextran injected transplanted cells were visualized by whole mount immunohistochemistry at 9 hpf. The percentage of proliferating cells (dark cells) that co-localized with transplanted cells (blue cells) was evaluated in relation to the whole number of transplanted cells (%).

Proliferation of transplanted cells deriving from embryos injected with MO1-ambra1a, MO1-ambra1b, or co-injected with both MOs was significantly higher with respect to WT donors. Moreover, also in this experiment, proliferation of MO1-ambra1b transplanted cells was higher then MO1-ambra1a alone or after coinjection with MO1-ambra1b, even if not significantly.

These data suggest that the proliferation is regulated by a cell-autonomous mechanism.

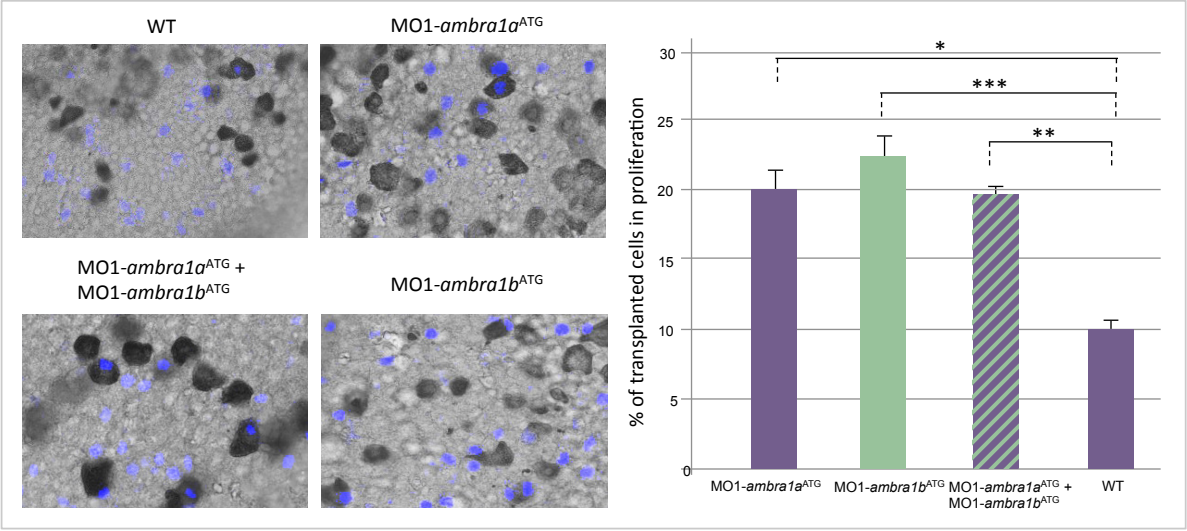

Figure 3. Transplantation and proliferation analysis: a small population of MO-treated cell where transplanted into wild type embryos. Biotin present in transplanted cells was detected by using an avidin-biotinylated complex and the DAB substrate (dark cells). Transplanted cells in proliferation were stained with anti-phosphohistone H3 antibodies (blue cells). The results are the average of three independent experiments with at least 7 embryos for each treatment. * indicates that the differences in the % of transplanted cells in proliferation are significantly different ($P < 0.05$); ** ($P < 0.01$); *** ($P < 0.001$).

REFERENCES

1. Fimia GM, Stoykova A, Romagnoli A, Giunta L, Di Bartolomeo S, Nardacci R, Corazzi M, Fuoco C, Ucar A, Schwartz P, Gruss P, Piacentini M, Chowdhury K, Cecconi F. 2007. Ambra1 regulates autophagy and development of the nervous system. Nature 447, 1121-1125.

2. Cecconi F, Levine B. 2008. The role of autophagy in mammalian development: cell makeover rather than cell death. Dev Cell 15, 344-57.

3. Yue Z, Jin S, Yang C, Levine AJ, Heintz N. 2003. Beclin 1, an autophagy gene essential for early embryonic development, is a haploinsufficient tumor suppressor. Proc. Natl. Acad. Sci. USA 100, 15077–15082.

4. Liang C, Feng P, Ku B, Dotan I, Canaani D, Oh BH, Jung JU. 2006. Autophagic and tumour suppressor activity of a novel Beclin1-binding protein UVRAG. Nat. Cell Biol. 8, 688–699

5. Marino G, Salvador-Montoliu N, Fueyo A, Knecht E, Mizushima N, Lopez-Otin C. 2007. Tissue-specific autophagy alterations and increased tumorigenesis in mice deficient in Atg4C/autophagin-3. J. Biol. Chem. 282, 18573–18583.

6. Takahashi Y, Coppola D, Matsushita N, Cualing HD, Sun M, Sato Y, Liang C, Jung JU, Cheng JQ, Mul JJ, et al., 2007. Bif-1 interacts with Beclin 1 throughUVRAGand regulates autophagy and tumorigenesis. Nature Cell Biology, 9, 1142–1151.

7. Kisen GO, Tessitore L, Costelli P, Gordon PB, Schwarze PE, Baccino FM, Seglen PO. 1993. Reduced autophagic activity in primary rat hepatocellular carcinoma and ascites hepatoma cells. Carcinogenesis 14, 2501–2505

8. Brech A, Ahlquist T, Lothe RA, Stenmark H. 2009. Autophagy in tumour suppression and promotion. Mol Oncol, 3, 366-375.

9. Westerfield M. 1995. The zebrafish book: a guide for the laboratory use of zebrafish (Danio rerio), Ed. 3. edn ([Eugene, OR], M. Westerfield).

10. Kimmel CB, Ballard WW, Kimmel SR, Ullmann B, Schilling TF. 1995. Stages of embryonic development of the zebrafish. Dev. Dyn. 203(3), 253-310.

11. Benato F, Skobo T, Gioacchini G, Moro I, Ciccosanti F, Piacentini M, Fimia GM, Carnevali O, Dalla Valle L. 2013. Ambra1 knockdown in zebrafish leads to incomplete development due to severe defects in organogenesis. Autophagy 9, 476-495.

12. Nasevicius A, Ekker SC. 2000. Effective targeted gene 'knockdown' in zebrafish. Nat. Gen. *26*, 216-220.

Zebrafish *ambra1a* and *ambra1b* knockdown impairs skeletal muscle development

Tatjana Skobo[1], Francesca Benato[1], Paolo Grumati[2], Valentina Cianfanelli[3], Silvia Castagnaro[2], Martina Chrisam[2], Sabrina Di Bartolomeo[3], Paolo Bonaldo[2], Francesco Cecconi[3,4,5], Luisa Dalla Valle[1]

[1] Department of Biology, University of Padova, 35131 Padova, Italy
[2] Department of Molecular Medicine, University of Padova, 35131 Padova, Italy
[3] Department of Biology, University of Tor Vergata, Rome 00133, Italy
[4] Department of Neuroscience, IRCCS Santa Lucia Foundation, Rome 00179, Italy
[5] Unit of Cell Stress and Survival, Danish Cancer Society Research Center, 2100 Copenhagen, Denmark

Submitted

Chapter III

ABSTRACT

The essential role of autophagy in muscle homeostasis has been clearly demonstrated by phenotype analysis of mice with muscle-specific inactivation of genes encoding autophagy-related proteins. Ambra1 is a key component of the Beclin 1 complex and, in zebrafish, it is encoded by two paralogous genes, both required for normal embryogenesis and larval development. In this study we focused on the function of Ambra1, a positive regulator of the autophagic process, during skeletal muscle development by means of morpholino (MO)-mediated knockdown and compared the phenotype of zebrafish ambra1-depleted embryos with that of Ambra1$^{gt/gt}$ mouse embryos.

Morphological analysis of zebrafish morphant embryos revealed that silencing of ambra1 impairs locomotor activity and muscle development, as well as *myoD1* expression. Skeletal muscles in ATG-morphant embryos displayed severe histopathological changes and contained only small areas of organized myofibrils that are widely dispersed throughout the cell. Double knockdown of *ambra1a* and *ambra1b* resulted in a more severe phenotype whereas defects were much less evident in splice-morphants. Together, these results indicate that *ambra1a* and *ambra1b* are required for the correct development and morphogenesis of skeletal muscle.

INTRODUCTION

Autophagy is an evolutionarily conserved catabolic process in which cells, through the lysosomal machinery, degrade and recycle, long-lived proteins and dismantle organelles in order to maintain a homeostatic intracellular environment. This process is tightly regulated and plays several important roles in normal physiology, differentiation, embryo development, and cell survival during starvation [1]. Defects of this degradative system play a role in various diseases, such as neurodegenerative and lysosomal storage disorders and in oncogenesis and cancer progression [2]. However, little is known about autophagy in muscular pathology.

In skeletal muscle, the role of autophagy was initially demonstrated in Atg5 and Atg7 muscle-specific knockout mice [3,4]. In both models, the muscle showed abnormal mitochondria and disorganized sarcomeres, confirming a homeostatic role of autophagy in this tissue. A direct connection between autophagy deregulation and muscular dystrophy was initially found in collagen VI null mice, where accumulation of abnormal organelles and spontaneous apoptosis, was shown to strictly depend on defective autophagy regulation [5]. In agreement with this, reactivation of autophagy restored myofiber survival and ameliorated the dystrophic phenotype of collagen VI null mice. More recently, deregulation of the autophagic process was also demonstrated in other dystrophic mouse models [6-9] as well as in the Vici syndrome, a human genetic disease caused by recessive mutations of the *EPG5* gene, which codes for a key autophagy regulator involved in the formation of autolysosomes [10].

Ambra1, originally identified in a gene trap screening for mutations in mice, is a positive regulator of the Beclin 1 dependent programme of autophagy [11]. Ambra1 is an intrinsically disordered protein, whose capability of binding a number of other regulatory partners involved in many cell processes highlights its crucial role as a “relay” molecule for autophagy [12]. In mammalian cells, Ambra1 is normally docked at a specific cytoskeletal site, corresponding to the dynein light chain, where it is unleashed upon autophagy induction to translocate at the autophagosome origin sites on the endoplasmic reticulum [13]. Ablation of Ambra1, as demonstrated by loss-of-function in mice, leads to embryonic lethality and causes neural defects, suggesting a role for autophagy in nervous system development [11]. Results obtained with the zebrafish model confirmed the involvement of this protein in embryonic development and demonstrated that the duplicated fish *ambra1* paralogue genes are required for normal embryogenesis and larval development. Indeed, MO-induced ablation of the corresponding proteins was found to be associated with several developmental abnormalities and decreased viability [14].

The rapid development and transparency of zebrafish embryos, together with the high fecundity and amenability to genetic manipulation of this vertebrate model, as well as with the feature that skeletal muscles represent a large portion of the body and are easily accessible for analysis, have made this organism attractive for investigating muscle development and fiber-type specification [reviewed by 15] as well as myopathies and muscular dystrophies [reviewed by 16]. In this study, we investigated the role of Ambra1 in

skeletal muscle development by means of knockdown of *ambra1* paralogue genes in zebrafish. Depletion of zebrafish ambra1 proteins results in abnormal locomotor activity and a severe myopathy characterized by irregular myofiber orientation and highly disorganized sarcomeres, suggesting a role for ambra1 in muscle development. In agreement with this, histological analysis of Ambra1 gene trap mutant (*Ambra1*$^{gt/gt}$) mouse embryos showed a disorganized three-dimensional structure of developing muscles and an increased proliferation of muscle cells.

METHODS

Animal maintenance and handling

Zebrafish were raised, staged and maintained according to standard protocols [17,18]. Embryos were obtained by natural spawning and cultured in zebrafish fish water solution (50x: 25 g Instant Ocean, 39.25 g $CaSO_4$, 5 g $NaHCO_3$ for 1 l) at 28.5°C with a photoperiod of 14 h light/10 h dark. For *in vivo* imaging, embryos were anesthetized with 0.04% tricaine [18]. *Ambra1*$^{gt/+}$ mice (CD1 strain) breed in order to obtain *Ambra1*$^{gt/gt}$ embryos [11]. Data were obtained in E13.5 embryos by comparing *Ambra1*$^{gt/gt}$ and wild-type animals. Mice were housed in individual cages in an environmentally controlled room (23 °C, 12 h light/12 h dark cycle) and provided food and water *ad libitum*. All animal procedures were approved by the Ethics Committee of the University of Padova.

MO microinjection

MO (Gene Tools, Philomath, OR) treatment was performed with MOs against the ATG translation initiation sites of either *ambra1a* or *ambra1b* transcripts (MO-*ambra1a*-ATG and MO-*ambra1b*-ATG) and with splice-blocking MOs designed for both genes at the exon 3-intron 3 junction sequence (MO-*ambra1a*-splice and MO-*ambra1b*-splice). As controls, we used five-nucleotide-mismatched control MOs (MO-*ambra1a*-5m and MO-*ambra1b*-5m). All MOs were previously described and validated [14], however lower MO dosages were used in this work in order to reduce embryo mortality. Specifically, for each MO, 10.3 ng were injected in the yolk of 1-cell stage embryos, whereas the dosage was halved in the co-injection experiments. Injections were performed under a dissecting microscope using a microinjector attached to a micromanipulator (Leica Microsystems, Milan, Italy). MO-injected embryos were then incubated in 1x fish water solution at 28.5 °C up to the desired stages of development.

Birefringence assay

Muscle birefringence was analysed by placing anesthetized embryos on a glass polarizing filter and covering with a second polarizing filter on a Leica DMR microscope (Leica Microsystems Srl). Embryos were photographed with a Leica DC500 digital camera (Leica Microsystems Srl). The top filter was twisted until it was possible to see the light refracting through the striated muscle.

Whole mount in situ hybridization (WMISH)

Zebrafish embryos were fixed overnight in 4% paraformaldehyde (PFA, Sigma) in phosphate-buffered saline (PBS) at the required stages of development. WMISH was performed as previously described [19]. DIG-labeled *myoD1* riboprobe was synthesized by *in vitro* transcription with T7 RNA polymerases (Roche), following the manufacturer's instructions and after plasmid linearization with *Bam*HI restriction enzyme.

Imaging

For confocal microscopy, fixed embryos were embedded in 0.8% low-melting agarose and placed on a depression slide, and a Nikon C2 confocal system was used to record images. WMISH-stained embryos were mounted in 87% glycerol in PBT (Phosphate-buffered saline plus 0.1% Tween20) or cleared and mounted in 2:1 benzyl benzoate/benzyl alcohol, observed under a Leica DMR microscope, and photographed with a Leica DC500 digital camera.

Histology and immunofluorescence

Zebrafish embryos were fixed overnight in 4% paraformaldehyde in PBS at 4 °C. For histology, 5 mm thin paraffin sections were cut and stained with haematoxylin and eosin. Embryos were fixed for antibody staining with 4% PFA and whole-mount immunohistochemistry was performed according to Dolez et al., [20], using the following primary antibodies: rabbit polyclonal anti-PH3 (1:100; Millipore, USA); mouse monoclonal anti-Pax7 (1:20; Hybridoma Bank, USA), mouse monoclonal anti-F59 (1:100; Hybridoma Bank); mouse monoclonal anti-F59 (1:100, Hybridoma Bank). The following secondary antibodies were used: Alexa Fluor 488 goat anti-mouse IgG1(y1) (A-21121, Invitrogen); Alexa Fluor 594 goat anti-rabbit IgG (H+L) (A-11012, Invitrogen). E13.5 mouse embryos were fixed in 4% paraformaldehyde, de-hydrated and included in paraffin. Haematoxylin-eosin staining was performed following standard protocols. Images were detected using a Zeiss Axioplan microscope equipped with a digital camera.

Transmission electron microscopy

Samples were fixed in 6% glutaraldehyde in 0.1 M cacodylate buffer (pH 6.9) overnight at 4°C. After washing in cacodylate buffer, the specimens were post-fixed in 1% OsO_4 in the same buffer for 2 h and dehydrated in a graded ethanol series followed by propylene oxide. The specimens were embedded in EPON 812 resin. Thick sections (1 µm) were cut with an Ultracut S, Reichert ultramicrotome (New York, USA), counterstained with toluidine blue and examined with a light microscope. Thin sections (100 nm) were stained with uranyl acetate and lead citrate. Micrographs were taken with a FEI Tecnai G12 electron microscope operating at 100 kV.

Microinjection of the hsp 70l:lamp1-RFP plasmid into fertilized eggs

A total of 25 ng/µl of hsp70l:lamp1-RFP [21] plasmid was co-injected with each ambra1-MO into zebrafish embryos at one-cell stage. Microinjected embryos were raised to 3 dpf stage and heat shocked by replacing the embryo medium with fish water preheated at 41 °C and then incubated in an air incubator at 38 °C for 30 min to induce hsp70 expression. In parallel, microinjected embryos were incubated with the lysosome inhibitor bafilomycin A1 (1 µM; Sigma) for 6 h prior to the heat shock. Lamp1-RFP labeled punctae were analysed by confocal microscopy.

RESULTS

Knockdown of *ambra1a* and *ambra1b* interferes with embryo motility and muscle integrity

To investigate the effects of *ambra1a* and *ambra1b* ablation during muscle development, we injected validated antisense MOs [14] into the yolk mass of 1-cell embryos to suppress translation of both maternal and zygotic mRNA (ATG MOs) or to silence zygotic transcription of the two genes (splice-blocking MOs). In agreement with previous work [14], ATG-morphant embryos displayed severe abnormalities in their overall appearance and that mainly consisted in body growth delay, curved shape, hemorrhagic pericardial cavity, as well as neural tube defects. Almost all ATG-morphant embryos had to be manually dechorionated. The delay in hatching could be due to an overall developmental delay [14], but also to a reduction of the muscle activity that contributes to the exit of the embryos from their protective outer chorion. Moreover, after hatching, both *ambra1a* and *ambra1b* ATG-morphants, as well as co-injected morphant embryos, showed impaired or totally absent locomotor activity and did not respond to touch with the escape response normally observed in control embryos injected with mismatch MOs. Less severe aspects of the phenotypes included uncoordinated movements in response to tactile stimuli and often swim in a circular fashion. In agreement with the impaired locomotor activity, ATG-morphants exhibited a clear reduction of birefringence of the skeletal musculature when compared with control embryos, which is indicative of decreased striated muscle formation or loss of myofiber organization. Double morphants zebrafish muscle showed a higher reduction of birefringence compared with single morphants. Birefringence and motility were almost normal in both *ambra1a* and *ambra1b* splice-morphants (Figure 1).

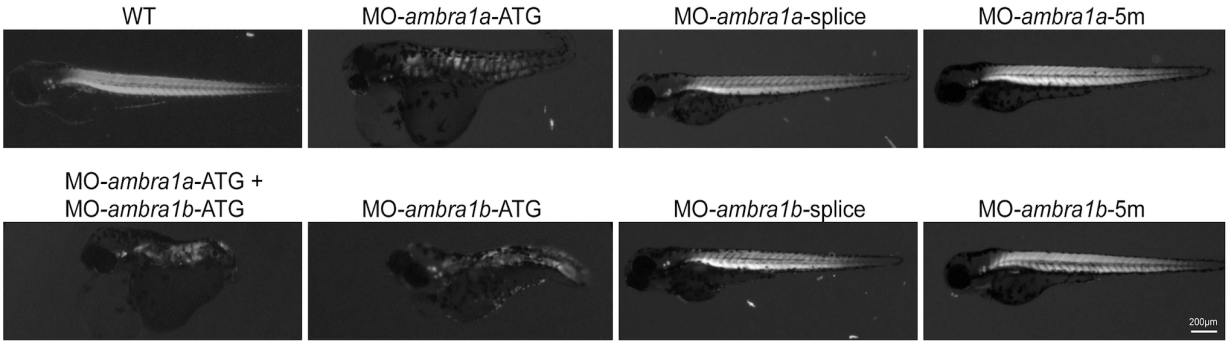

Figure 1. *Ambra1* silencing results in a reduced birefringence. Polarized light microscopy of 3 dpf live embryos shows that birefringence of trunk muscles is severely reduced in *ambra1* ATG-morphants and in co-injected morphants. The birefringence is weakly reduced in *ambra1* splice-morphants whereas wild-type (WT) and 5m-control embryos display highly birefringent skeletal muscles.

ambra1 downregulation interferes with *myoD1* expression during myogenesis

To assess the requirement for *ambra1a* and *ambra1b* during embryonic myogenesis, we performed WMISH analysis with the somite-specific marker *myoD1*. At the bud stage (10 hpf), expression of *myoD1* in the adaxial cells was reduced in ATG-morphants, while the width between them was increased, particularly at the posterior end (Figure 2). This was more evident in *ambra1a* ATG-morphants and in co-injected morphants. Expression of *myoD1* appeared normal in splice-morphants for both genes as well as in 5m-control morphants. At 20 hpf, ambra1 ablation resulted in broad shaped and less definite somites, suggesting impaired somite organization, undulated notochord, and shortened anterior/posterior axes. All defects were more evident in *ambra1a* ATG-morphants and in co-injected embryos. Segmentation pattern appeared normal in splice-morphants and in 5m-control morphants (Figure 2).

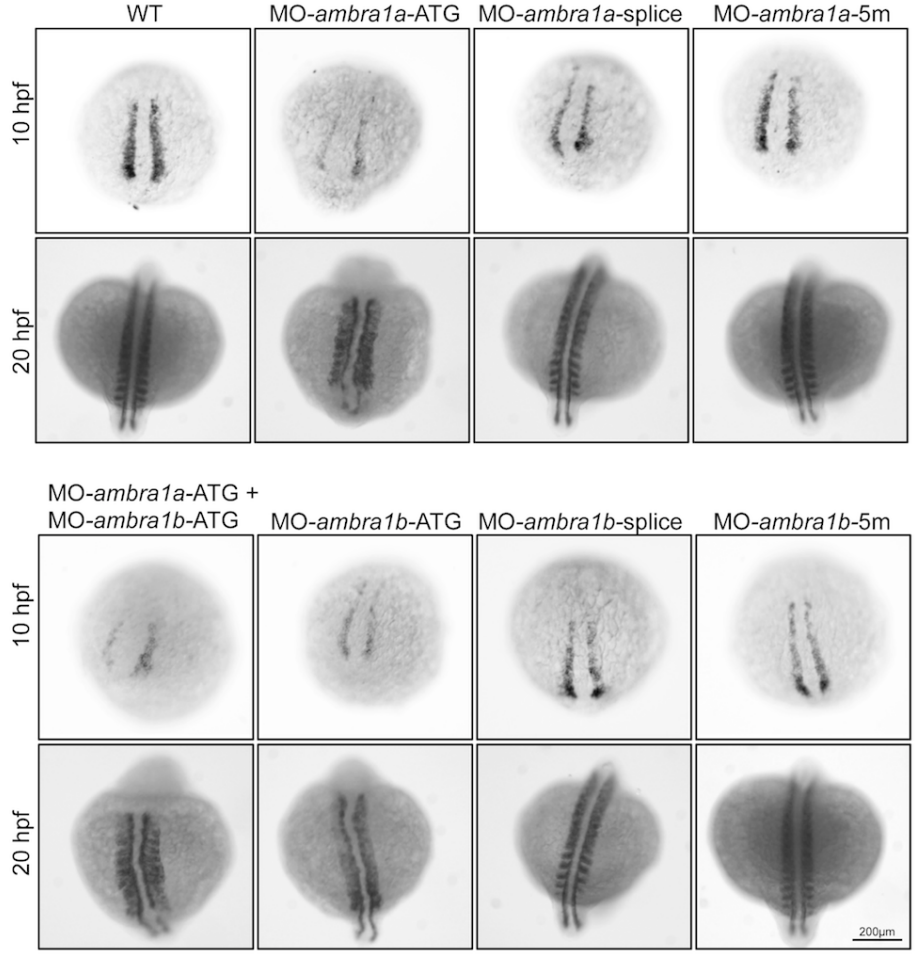

Figure 2. *In situ* hybridization analysis of *myoD1* expression in ambra1 knockdown embryos. Expression of *myoD1*, analyzed in embryos injected with the indicated MOs at 10 and 20 hpf, is affected in *ambra1* ATG-morphants and in co-injected morphants. No differences are evident in *ambra1* splice-morphants when compared to wild-type (WT) and 5m-control embryos. Embryos are shown in dorsal view, anterior toward the top.

ambra1 deficiency generates pathological changes of muscle morphology

To fully appreciate at a microscopic level the phenotype shown in Figure 1, we performed a histological analysis of haematoxylin/eosin stained longitudinal sections of muscles from 3 dpf embryos. This showed well-organized myofibers with elongated nuclei in wild-type and 5m-control muscles. In ATG-morphants, myosepta were not clearly evident, particularly in *ambra1a* ATG-morphants and co-injected embryos, and myofibers appeared misaligned with markedly disorganized shape and orientation. Moreover, ATG-morphants displayed an apparently increased number of myonuclei (Figure 3). Morphological changes were much less evident in splice-morphants, although the myosepta were thinner with respect to controls and myofibers appeared less organized.

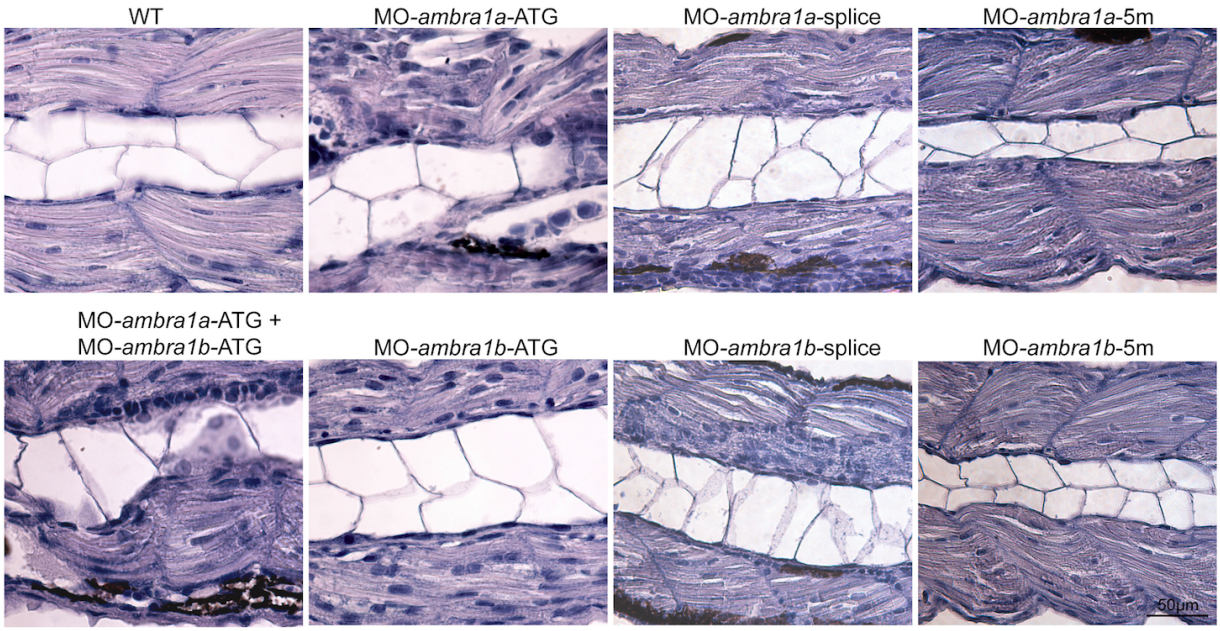

Figure 3. Abnormal morphology of *ambra1* knockdown embryos, as revealed by haematoxylin/eosin staining. Representative longitudinal sections of 3 dpf control and *ambra1* morphant embryos. Images show that myofibers of ATG- and co-injected morphant muscles are highly disorganized and present irregular myosepta boundaries. The phenotype of splice-morphants is much less severe when compared to wild-type (WT) and 5m-control embryos.

The irregular arrangement of muscle fibers was confirmed by toluidine blue stained semithin longitudinal sections of muscle fibers running between the vertical myosepta (Figure. 4). In both *ambra1a* and *ambra1b* ATG-morphants, the myoseptum was difficult to distinguish and in some places it seemed interrupted. Multiple areas devoid of staining were present within myofibers of both ATG-morphants and amorphous opaque material replaced lost myofibers. In *ambra1a* ATG-morphants and in co-injected morphants many fibers appeared detached. Skeletal muscles of splice-morphants displayed only minor modifications. Cross sections of the trunk region analysed by toluidine blue staining showed extensive disruption of muscle fiber structure and organization, with empty spaces and region filled with amorphous opaque material. Several myonuclei appeared large, abnormally rounded, and centrally localized (Figure 4).

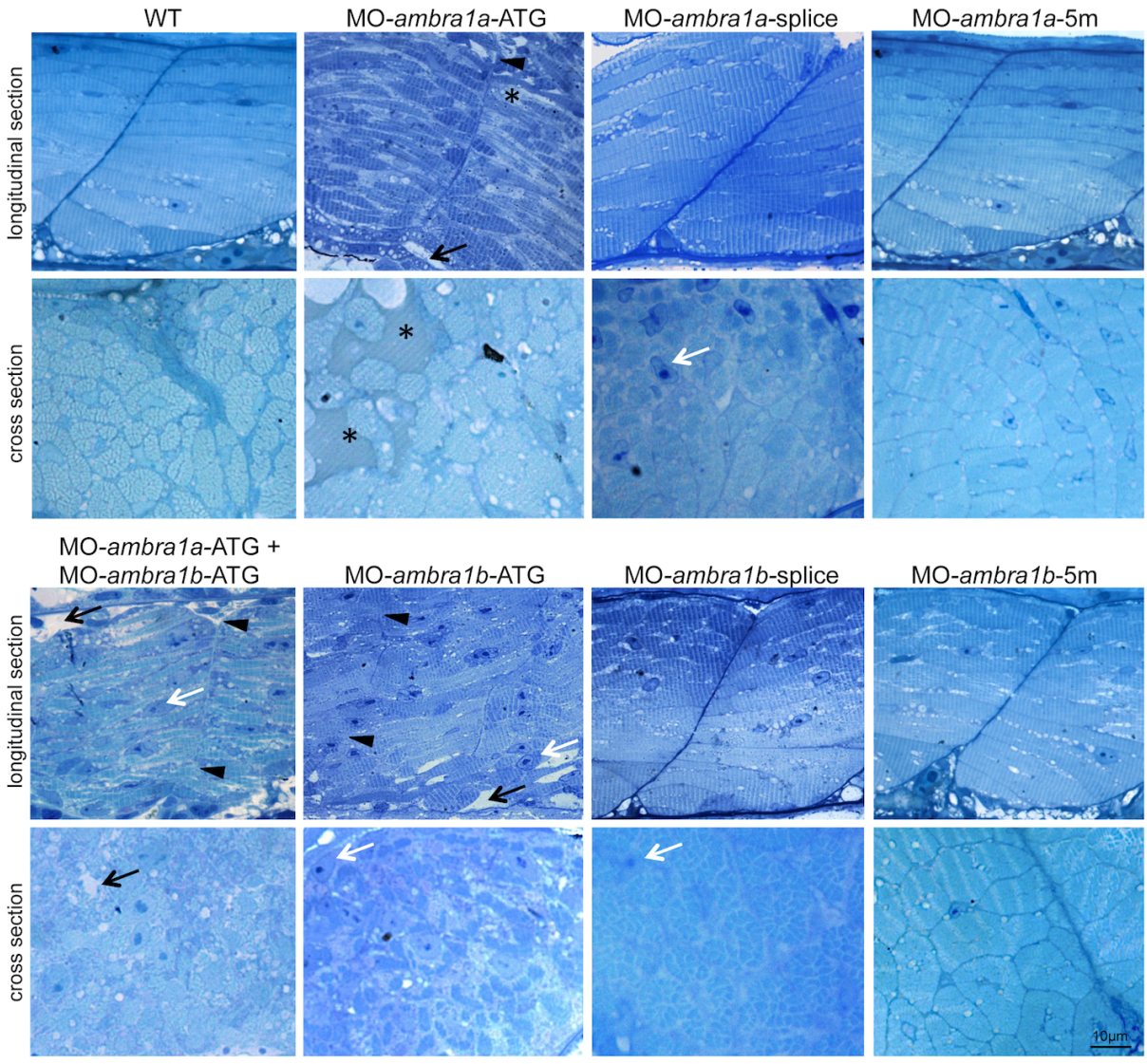

Figure 4. Abnormal morphology of *ambra1* knockdown embryos, as revealed by toluidine blue staining. Representative longitudinal and cross sections of 3 dpf control and *ambra1* morphant embryos. Muscles of *ambra1* ATG-morphants show a severe phenotype, with misaligned myofibers and scattered in the somitic compartment. Black arrows: areas devoid of staining; white arrows: large myonuclei with condensed chromatin; black arrowhead: interruption of myoseptum; asterisks: opaque material replacing fibers lost.

Immunostaining of 3 dpf embryos for phospho-histone H3, a mitotic marker, showed a higher proliferation rate in ATG-morphant embryos, while the number of phospho-histone H3 positive nuclei in splice-morphants was intermediate compared to controls (Figure 5).

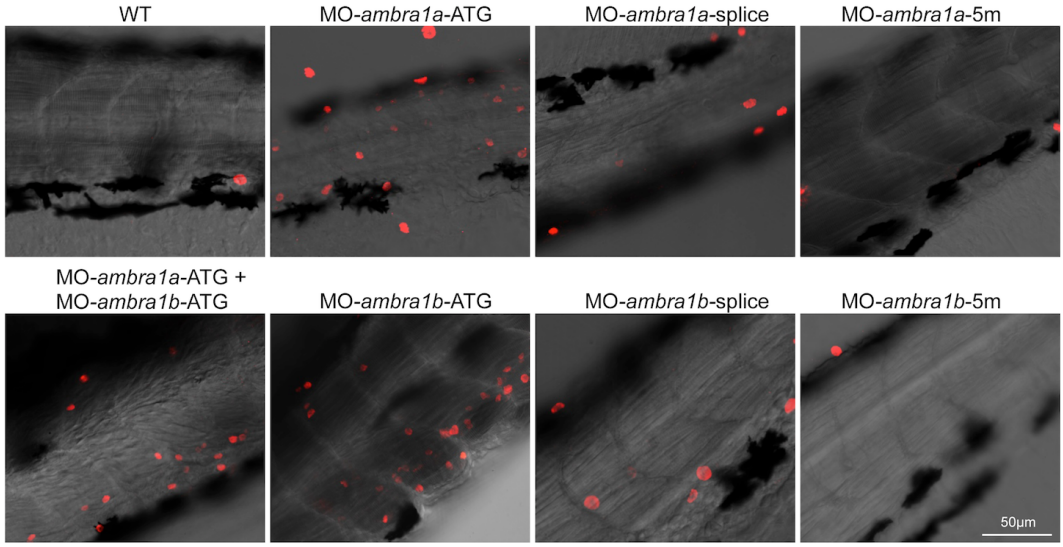

Figure 5. Cell proliferation in muscles of 3 dpf control and *ambra1* morphant embryos. Mitotic cells, analyzed by immunostaining for phospho-histone H3 in longitudinal sections, are more abundant in ATG-morphant embryos with respect to wild-type (WT) and 5m-control embryos. Anterior is to the left and dorsal up.

Immunofluorescence at 2 dpf for Pax7, a key regulator of muscle progenitor cells [22], showed that both ATG- and splice-morphants had a higher incidence of Pax7-positive cells in the spaces between myosepta, instead of being regularly localized to the edges of the somites as in wild-type and 5m-control embryos (Figure 6).

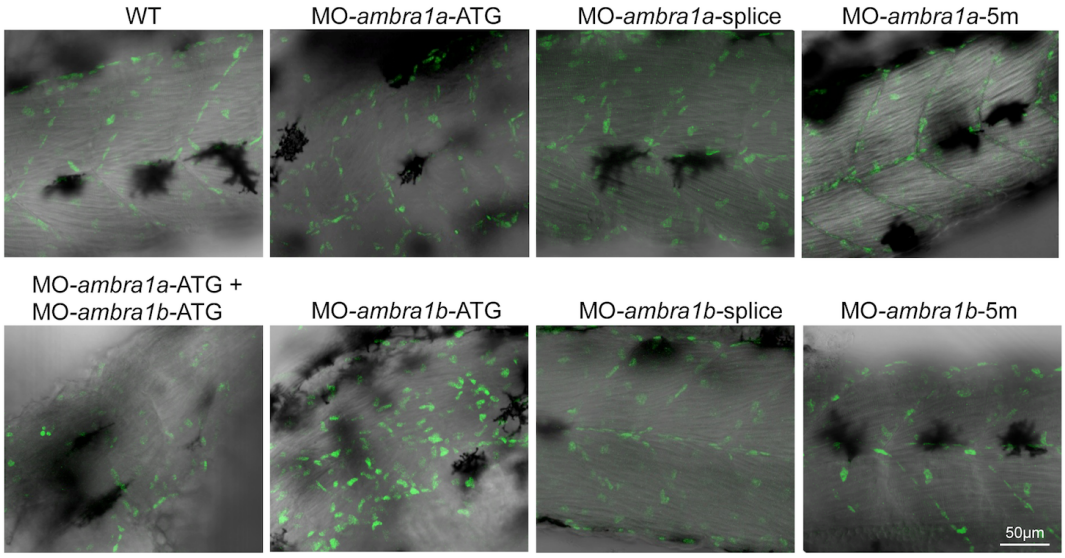

Figure 6. Pax7 expression in control and *ambra1* morphant embryos. Lateral views of 2 dpf muscles analyzed by immunofluorescence for Pax7. In wild-type (WT) and 5m-control embryos Pax7-positive cells are localized at the edge of somites, whereas in *ambra1* morphants many Pax7-positive cells are misplaced in the spaces between myosepta. Anterior is to the left and dorsal up.

Ablation of *ambra1* causes ultrastructural defects of myofibers

To better understand the subcellular alterations responsible of the observed fiber disturbances, we performed an electron microscopy analysis of longitudinal and cross sections. Zebrafish embryos at 3 dpf showed that wild-type and 5m-control embryos (not shown) had well-defined muscle fiber structure with normally developed sarcoplasmic reticulum encircling myofibrils and intermyofibrillar mitochondria. In control embryos, sarcomeres were clearly visible and formed regular repeating units with alignment of well-defined Z-lines, mitochondria were aligned in rows and had tightly packed cristae, and myofibers were surrounded by very small areas of amorphous material (Figure 7, panels A1-A4). In contrast, muscle fibers of ATG-morphants and of co-injected embryos contained only small areas of organized filaments, widely dispersed throughout the cells and surrounded by enlarged areas of disorganized cytoplasm devoid of normally appearing organelles. Remnants of degenerating myofibers were also seen in these regions (Figure 7, panels B1-B4, D1-D4, F1-F4). Although ATG-morphants muscle fibers contained sarcomeres, they were substantially reduced in number, torn, not correctly aligned and dispersed within amorphous material. Areas with myofibrils showing orthogonal arrangement to each other were also visible (Figure 7). The ultrastructural muscle defects were less severe in splice-morphants, where only small regions devoid of myofibrils were present together with a milder disorganization of sarcomeres (Figure 7).

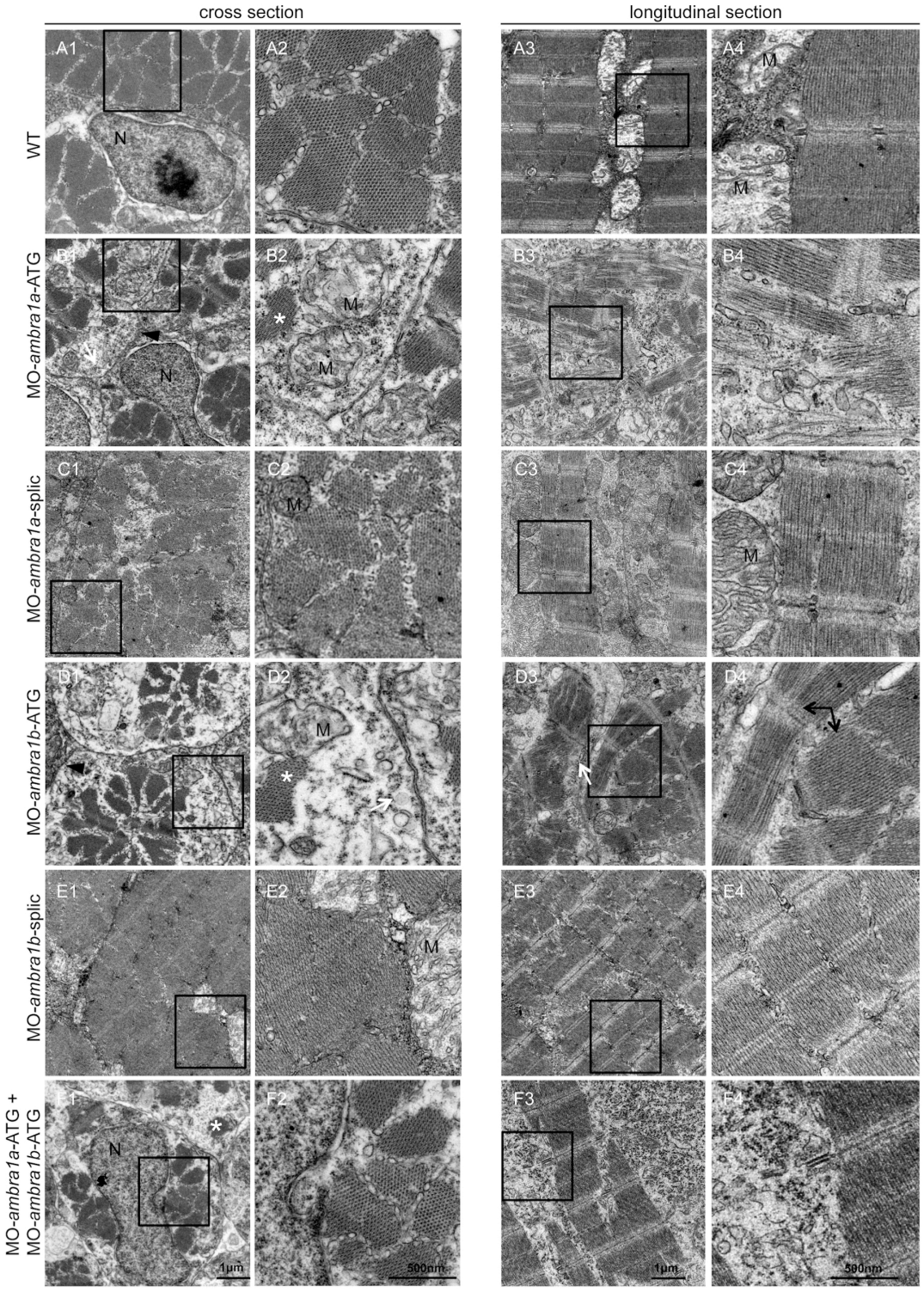

Figure 7. Ultrastructural analysis of *ambra1* morphants reveals disorganized sarcomeres. Representative electron micrographs of cross and longitudinal sections of 3 dpf wild-type (WT, panels A1-A4), *ambra1a* ATG-morphant (panels B1-B4), *ambra1a* splice-morphant (panels C1-C4), *ambra1b* ATG-morphant (panels D1-D4), *ambra1b* splice-morphant (panels E1-E4), and co-injected morphant (panels F1-F4) zebrafish embryos. Columns 2 and 4 show higher magnification views of the boxed areas in column 1 and 3, respectively. Muscles of WT and 5m-control (not shown) embryos display well-organized myofibers, showing densely packed sarcomeres with regular organization of thin and thick myofilaments. *ambra1*-depleted muscles show a large number of defects, with small patches of disorganized myofibers and mitochondria scattered throughout the cytoplasm. *, fragments of torn myofibers; white arrow, dilated sarcoplasmic reticulum not in contact with myofibers; black arrow, area with myofibers having different orientations; M, mitochondria; N, nucleus.

Patterning of internal membranes was also affected in ATG-morphants and in co-injected embryos, as the sarcoplasmic reticulum appeared dilated and often not closely associated with myofibrils (Figure 8, row E). Ambra1 morphant embryos showed several ultrastructural abnormalities of T-tubules and sarcoplasmic reticulum, ranging from mild changes in splice-morphants to unrecognizable triad areas in co-injected morphants, whereas wild-type embryos and 5m-control embryos displayed a normal pattern of T-tubules and sarcoplasmic reticulum resulting in regularly spaced triads (Figure 8, row C). In *ambra1* morphant embryos, mitochondria were scattered throughout the cytoplasm and their morphology was also markedly affected, as they were often swollen and devoid of cristae or, when present, these were disorganized or abnormal (Figure 7, panel B2 and Figure 8, row A). Ultrastructural analysis also confirmed that myonuclei were often larger in morphant embryos, with an irregular shape and more numerous when compared to control embryos (Figure 8, row B). The abnormal myofiber ultrastructure of ambra1 depleted embryos was particularly evident in cross sections, where myofibers of control embryos showed a regular hexagonal arrays of thick and thin filaments while in ambra1 morphants the hexagonal arrays were irregular, with areas in which thick filaments were not associated with thin filaments (Figure 8, row D).

Taken together, our results highlight a severe disorganization of muscle tissue and cells upon ambra1 disruption. Also, alteration of mitochondria and ER structure seem to be causative of the phenotype.

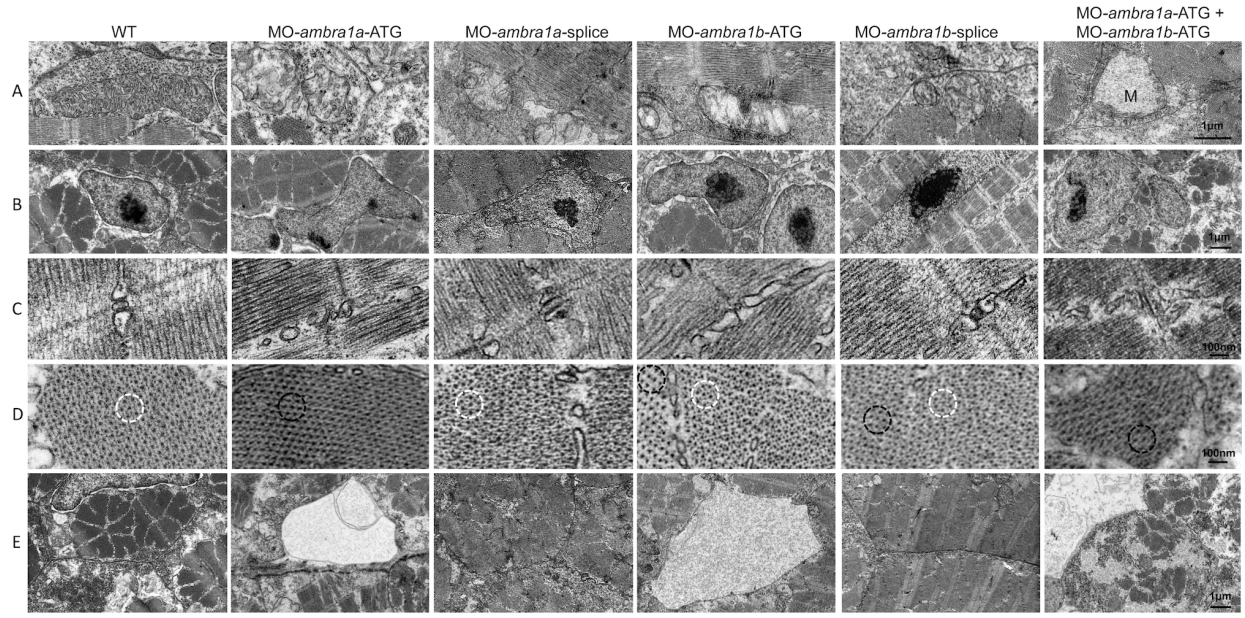

Figure 8. Ultrastructural analysis of *ambra1* morphants reveals disorganized subcellular structures. When compared to wild-type (WT) and 5m-control (not shown) embryos, *ambra1* morphant embryos display abnormal features of mitochondria (row A), nuclei (row B), triads (row C), hexagonal arrangement of thick and thin filaments (row D), and dilations of the endoplasmic reticulum (row E). Morphant embryos display the presence of areas with reduced thin filaments (black circles in row D) adjacent to more normal-appearing hexagonal structures (white circles in row D). Co-injected double morphant embryos show exacerbated defects of these structures, whereas defects in splice-morphants are barely evident.

Ablation of *ambra1* affects both fast and slow muscle fibers

Next, to assess whether knockdown of *ambra1a* and *ambra1b* expression results in defective specification and patterning of slow and/or fast muscle fibers, we examined myosin thick filaments in ambra1 knockdown embryos by immunostaining with the F59 and F310 antibodies, which label slow and fast myosin isoform, respectively. Slow muscle fibers were still present after ambra1 knockdown, although myofiber density appeared lower in *ambra1a* ATG-morphants and in co-injected embryos (Figure 9). However, whereas in control embryos the thick filaments were nicely organized and the myotomal segments were V-shaped and regularly spaced, thick filaments in slow muscles of ATG-morphant embryos appeared highly disorganized, with wavy and twisted myofibrils. Moreover, the characteristic V-shaped appearance of the vertical myoseptum was almost completely absent. Some muscle fibers were missing or detached from the myosepta generating cell-free spaces in ATG-morphants. Combined injection of both ATG-MOs exacerbated the phenotype. The phenotype was almost normal in ambra1 splice-morphants, where myofibrils presented only a slightly wavy morphology (Figure 9). A similar disruption in myofiber organization was also evident in fast muscles. In wild-type and 5m-control embryos, the fast muscle fibers appeared relatively uniform in size and were regularly arranged in parallel rows. Conversely, in ATG-morphants fast muscle fibers displayed variable shapes and were highly disorganized, showing a dystrophic appearance with detachment and retraction of myofibers from the vertical myosepta forming the somite boundaries and with irregular and wavy myofiber morphology (Figure 9). Interestingly, splice-morphants displayed a more evident phenotype in fast muscle fibers than in low muscle fibers. These data indicated that although slow and fast muscle fibers were still present and in the correct positions within the somites, myofiber organization was disrupted.

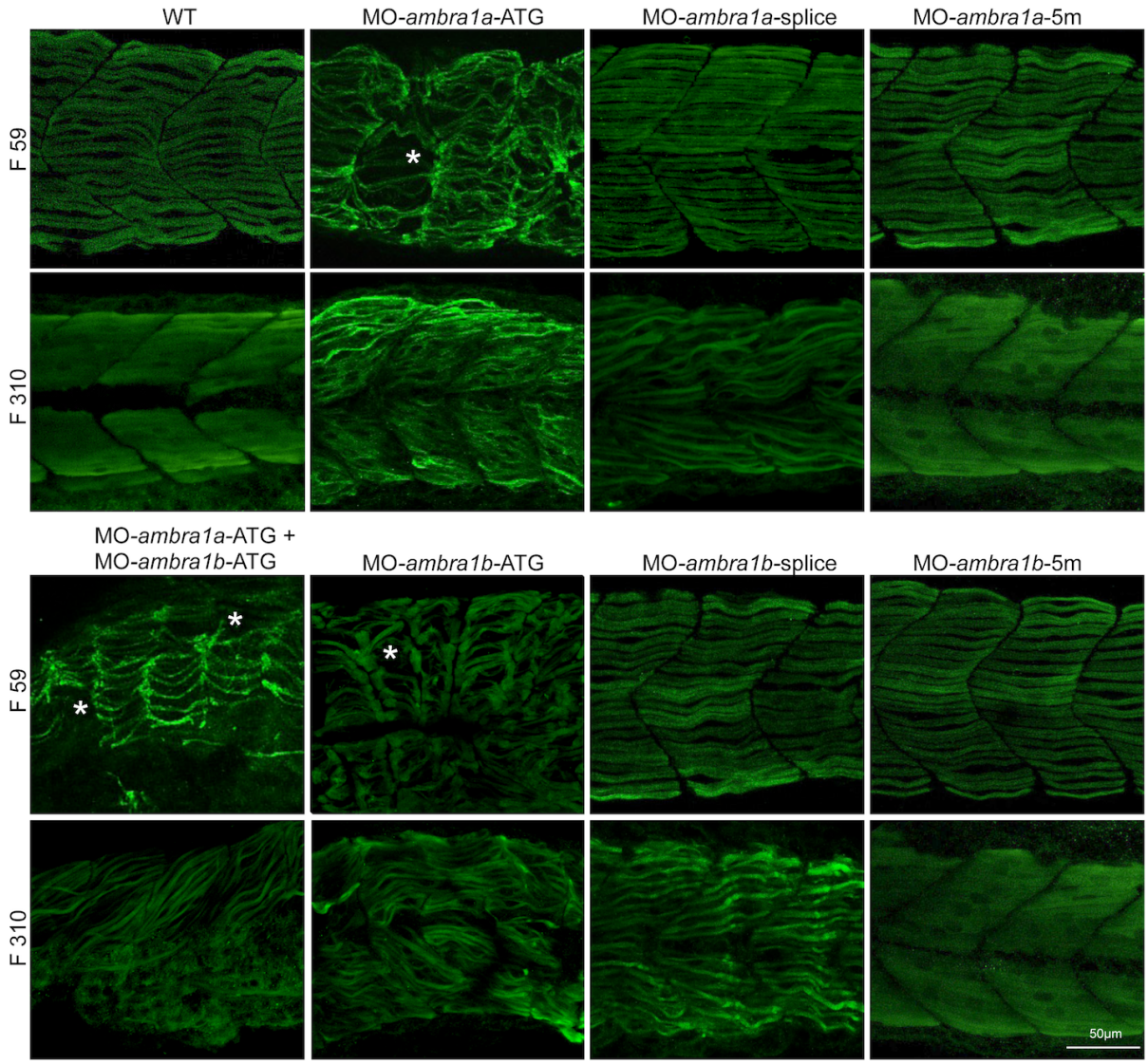

Figure 9. Knockdown of *ambra1* interferes with myosin heavy chain organization in slow and fast muscles. Lateral views of 3 dpf muscles labeled with the F59 antibody (slow muscle fibers) and with the F310 antibody (fast muscle fibers), showing abnormally organized myofilaments in ATG-morphant embryos when compared to wild-type (WT) and and 5m-control embryos. Slow fibers are thinner in ATG-morphant embryos, whereas fast fibers of splice-morphant embryos display a wavy phenotype, visibly different from controls. The asterisks indicate broken or missing muscle fibers. Anterior is to the left and dorsal up.

Muscle fibers from *ambra1* morphants display abnormal autophagy

To evaluate the effect of zebrafish *ambra1a* and *ambra1b* knockdown on the autophagic process, we analysed autophagy in muscle fibers where transient expression of the lysosomal lamp1-RFP reporter protein was obtained by microinjection of zebrafish embryos with hsp70l:lamp1-RFP reporter construct, in which the zebrafish lamp1 gene is driven by the hsp70l promoter and thus induced by heat-shock treatment [21]. Muscle fibers were analysed at 3 dpf in the absence or presence of the lysosomal inhibitor bafilomycin A1, in order to prevent the fusion between lysomes and autophagosomes and allow accumulation of lysosomes, which appear as punctate structures at the confocal microscope (Figure 10). This analysis showed that several lamp1-RFP puncta were present in myofibers from wild-type and 5m-control embryos, with a noticeable increase following bafilomycin treatment. In contrast, knockdown of either *ambra1a* or *ambra1b* led to an almost complete lack of lamp1-RFP puncta in muscle fibers and to a very low increase after bafilomycin treatment.

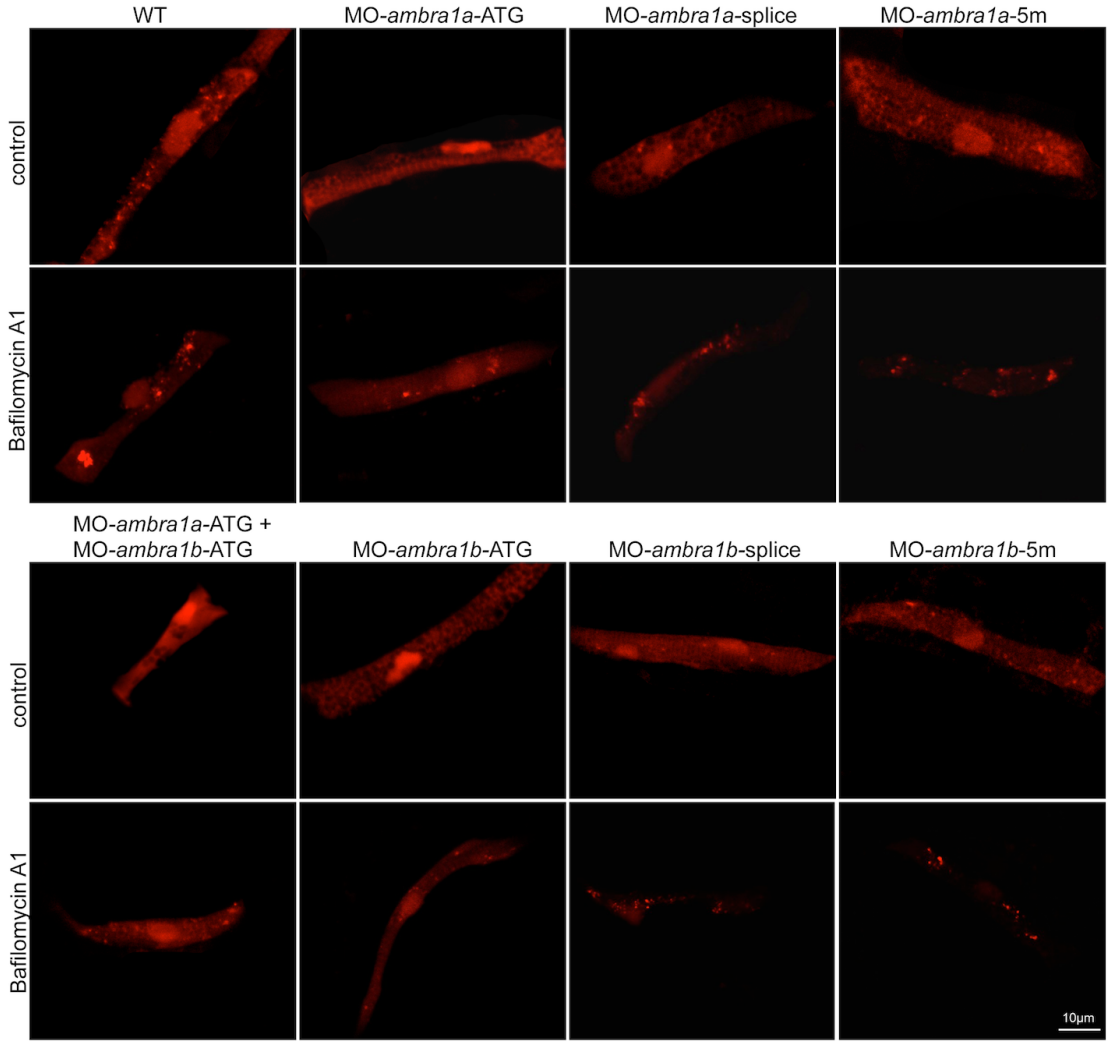

Figure 10. Fluorescence detection in muscle fibers of control and *ambra1* morphant embryos following transfection with a lamp1-RFP reporter construct. Fluorescent puncta are detected in muscle fibers isolated from wild-type (WT) and 5m-morphant embryos, both under control conditions and following bafilomycin treatment, whereas only few puncta are visibile in ATG-morphant embryos after bafilomycin treatment.

Skeletal muscles in *Ambra1*$^{gt/gt}$ mouse embryos display morphological defects

To further get insight into the role of Ambra1 during muscle development, we investigated skeletal muscles from *Ambra1*$^{gt/gt}$ mutant mice, which bear a gene trap insertion in the *Ambra1* gene [11]. We first analyzed muscle morphology by haematoxylin-eosin staining in E13.5 mouse embryos, when differentiation of muscles is not yet complete and myogenic cells are undergoing fusion to form myofibers and organize the architecture of muscle tissue. In wild-type E13.5 mouse embryos, the structure of the developing muscles appeared normal. Myofibers were well organized and aligned to generate the ordered structure of the muscle, with many nuclei already localized at the periphery (Figure 11A, upper panels). In *Ambra1*$^{gt/gt}$ E13.5 mouse embryos, skeletal muscles were present but the three-dimensional organization of the tissue was less organized (Figure 11A, lower panels). The abnormal structure of developing muscles in *Ambra1*$^{gt/gt}$ embryos may be due to a failure in completing muscle development or to a delay in myofiber maturation. This was also supported by the presence of many immature myofibers displaying centrally located nuclei in *Ambra1*$^{gt/gt}$ embryos (Figure 11A, lower panels). These features, which we detected in all muscles of *Ambra1*$^{gt/gt}$ embryos that were analyzed, are clearly exemplified by the developing tongue. In wild-type E13.5 embryos, the tongue showed a well-defined array of parallel myofibers distinctly organized in the three different planes of the developing intrinsic tongue muscles (Figure 11B, upper panels). Conversely, in *Ambra1*$^{gt/gt}$ E13.5 embryos, the tongue displayed a general disorganization of the developing muscles and myofibers were less defined. In addition, there was a marked increase of cell density in the whole muscle tissue of *Ambra1*$^{gt/gt}$ embryos (Figure 11B, lower panels). Similar morphological and cellular alterations were also detected in the developing dorsal and limb muscles of *Ambra1*$^{gt/gt}$ embryos, which also showed a noticeable increase of the interstitial connective tissue (Figure 11C,D).

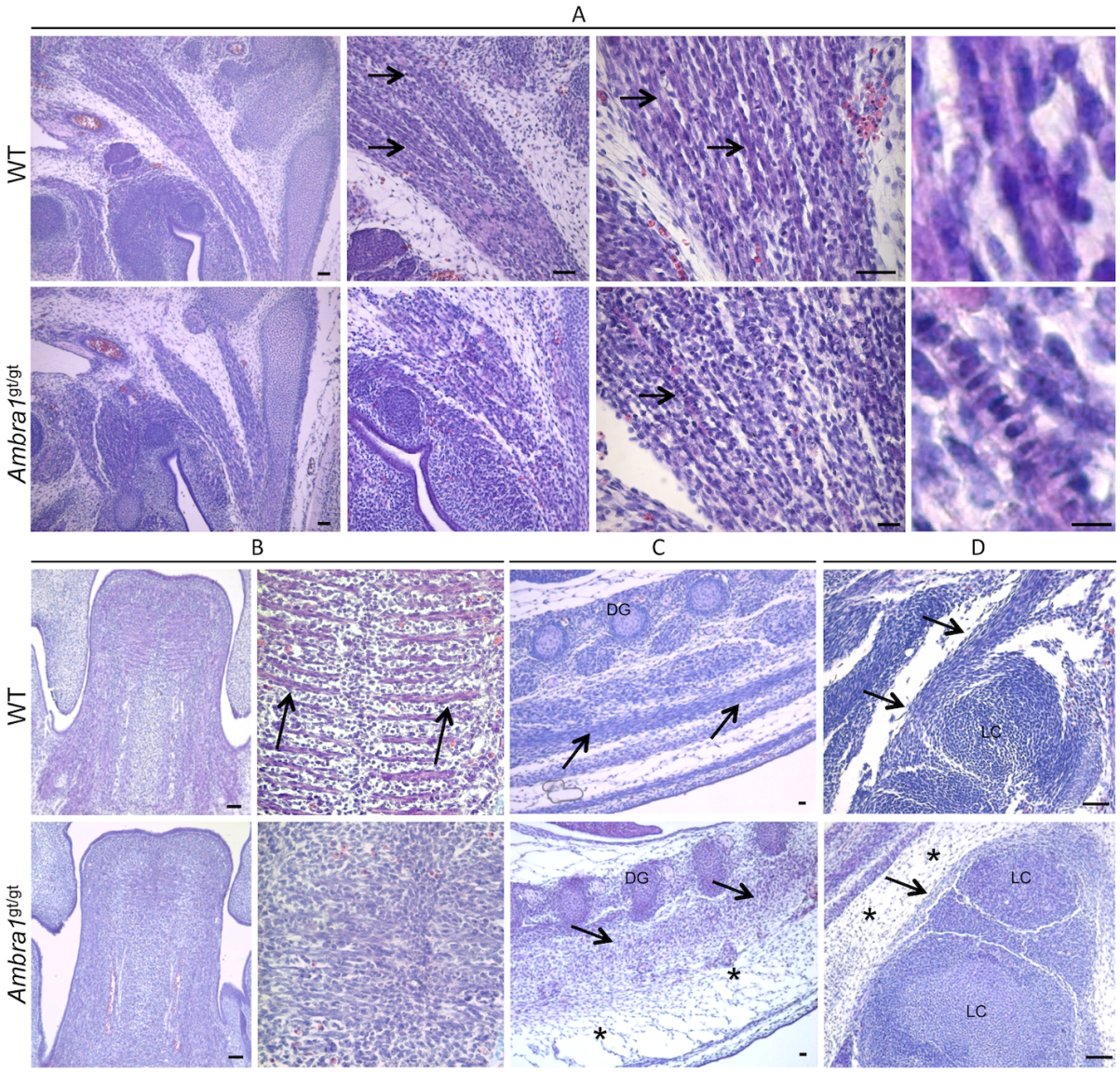

Figure 11. Morphological alteration of skeletal muscles in *Ambra*$^{gt/gt}$ mouse embryos. Representative pictures of skeletal muscles following haematoxylin-eosin staining of wild-type and *Ambra1*$^{gt/gt}$ E13.5 mouse embryos. (A) Details of neck muscle. Wild-type embryos display several well-organized and mature myofibers (black arrows), which have myonuclei already localized at the edge of the cell (right panel). In *Ambra1*$^{gt/gt}$ embryos, the muscle is much more immature, with poorly organized myofibers displaying centrally located nuclei (black arrows). (B) Details of the tongue. In wild-type embryos, myofiber are formed and well-organized (arrows), whereas in *Ambra1*$^{gt/gt}$ embryos there is a general disorganization of muscle architecture. (C, D) Representative pictures of dorsal (C) and limb (D) muscles (black arrows). In *Ambra1*$^{gt/gt}$ embryos, besides the general alteration of muscle organization, there is a marked thickening of the connective tissue (black asterisks). All the skeletal muscles analyzed display a noticeable increase of cell density in *Ambra1*$^{gt/gt}$ embryos. Scale bar, 50 µm. WT, wild-type.

DISCUSSION

In this work, we used a targeted protein depletion approach to investigate the involvement of ambra1 proteins in zebrafish muscle development. The severe phenotype of zebrafish *ambra1a* and *ambra1b* morphant embryos suggests a function of these proteins in myogenesis. Our analysis on muscles of *ambra1a* and *ambra1b* zebrafish morphants was mainly focused on 3 dpf embryos, as the muscle structure at this stage is mature. Our data show a severe myopathy characterized by a marked reduction of myofiber density associated with an abnormal orientation and decreased alignment of muscle fibers, with altered myofibrils and disorganization of sarcomeres, and with defects of the tubulo-reticular network and mitochondria morphology. Although a role for Ambra1 in skeletal muscle was never proposed before now, our findings are in agreement with other recent studies indicating that autophagy plays a key role in skeletal muscles, as shown by the myopathic phenotype of Atg5 and Atg7 muscle-specific knockout mice [3,4] and by the connection between autophagy deregulation and muscular dystrophies [5-9].

In zebrafish, transcripts for both *ambra1* genes are present as maternal RNAs in the eggs and display a gradual decline until 8 hpf, being replaced by zygotic mRNAs from 12 hpf onwards [14]. To verify a possible role of these proteins in the early stages of skeletal muscle development, the commitment to the myogenic fate was analysed by WMISH for *myoD1*, whose expression normally begin, prior to somite formation, in the adaxial cell [23,24]. These cells, after migrating laterally through the somites, forms the slow muscle cells [25], whereas those remaining near to the notochord form the muscle pioneer cells [26]. Later, *myoD1* expression takes place in the posterior half of each newly formed somite, giving raise to the fast muscle fibers [25]. Knockdown of zebrafish *ambra1* genes led to marked changes of *myoD1* expression, resulting in a reduced *myoD1* signal and a widening of the space between the bilateral adaxial cells of ATG-morphant embryos. Later, somites present a broad-shaped and non-homogeneous *myoD1* expression. Moreover, somite shape is not well defined. Interestingly, also expression of *shh*, a gene coding for a secreted signalling protein implicated in the commitment of muscle precursors [reviewed in 15,26], was found to be differently shaped in mouse [11], as well as in zebrafish *ambra1* ATG-morphant embryos resulting in notochord waving [14]. Depletion of ambra1 proteins in zebrafish did not prevent the specification and differentiation of slow and fast muscle fibers, but clearly interfered with myofibrillogenesis leading to an anomalous pattern of both fiber types. As different levels, along with range and timing, of Shh signalling specify different muscle subtypes [27,28], the displaced expression of this morphogen could explain the disorganization of the ambra1-morphant muscle fibers.

The changes in *myoD1* and *shh* expression, together with the reduced locomotor activity, observed in *ambra1* morphant embryos occur at very early developmental stages, when embryonic cells are likely not yet competent for autophagy, the biological process in which ambra1 is clearly involved. Actually, this process can be observed in zebrafish embryos starting from 32 hpf [29], and thus relatively late compared with the onset of the muscle developmental defects. Interestingly, depletion of Ambra1 seems to interfere with the gene

expression program responsible for correct muscle development, as suggested by the displaced expression of *shh* [14] and of *myoD1* and it is still unclear whether this regulation is related to ambra1 pro-autophagic roles. On the other side, ambra1 morphant embryos were also found to display reduced autophagy, as measured by immunoblot analysis for lipidated LC3 at 2 dpf [14]. A weakening of the autophagic process was also suggested by the lower incidence of puncta in muscle fibers isolated from zebrafish embryos expressing a hsp:lamp1-RFP reporter plasmid.

Pax7, a key regulator for myogenic progenitor cell in all vertebrates [30], was analysed at 2 dpf, when the Pax7-positive cells are generally aligned along the vertical and horizontal myosepta. In *ambra1* morphants embryos, the regular arrangement of Pax7-positive was disturbed and these cells also occurred in the spaces between myosepta, thus confirming the disorganization of somites. This morphological analysis did not reveal any obvious difference in the number of Pax7-positive cells between control and *ambra1* morphant embryos, although a significant increase of these cells has been measured in zebrafish with dystrophic phenotypes [30,31]. This result seems to contrast with the apparently higher proliferation rate seen in *ambra1* morphants both by haematoxylin/eosin staining and by immunofluorescence for phosphorylated histone H3. However, this discrepance may be explained by a higher proliferation of fibroblasts, as also suggested by muscles of *Ambra1*$^{gt/gt}$ mouse embryos that show a thickening of the interstitial connective tissue.

Although the muscle pathological defects of *ambra1a* and *ambra1b* ATG-morphant embryos are similar, the phenotype of co-injected embryos deficient for both ambra1 paralogue genes is more severe. This suggests the possibility that the two proteins not only work in similar biological process but also play roles in other process, thus justifying the retention of both genes as functional in the zebrafish genome after the fish-specific whole-genome duplication [32]. This was also indicated by rescue experiments in our previous study, which showed that the two genes couldn't fully compensate each other deficiencies, at least morphologically [14]. Moreover, knockdown of only zygotic *ambra1a* and *ambra1b* transcripts by means of splice-MOs resulted in less severe muscle developmental defects, indicating the importance of maternally supplied ambra1 transcripts and of the corresponding proteins in early embryonic development. Interestingly, and at difference from other parameters, splice-morphants showed a remarkably stronger phenotype than ATG-morphants with regard to fast fiber development, a finding that is in agreement with the different timing of slow and fast fiber differentiation [33]. Since fast fibers differentiate after slow fibers, the process in this case could be more affected by the silencing of zygotic transcripts because, at that stage, maternal transcript would be no longer available.

The physiological and pathological role of autophagy in mature skeletal muscle, although not completely understood, has been recently described [reviewed in 34,35]. Our data obtained from *ambra1a* and *ambra1b* zebrafish morphant embryos and from *Ambra1*$^{gt/gt}$ mouse embryos indicate that this autophagy related-protein plays a critical function during skeletal muscle development. In both animal models, ablation of Ambra1 leads to abnormal muscle morphogenesis. Ambra1 is critical not only for the correct architecture and maturation of myofibers, but it seems also implicated in cell proliferation

control. Our data suggest a new function of Ambra1 in muscle biogenesis. While the presence of abnormal organelles are likely be associated to the well-known role of Ambra1 in autophagy regulation, the altered morphology and the hypercellularity of the developing skeletal muscles may be due to a different function of Ambra1. Further studies will be necessary to fully elucidate the functional role of Ambra1 in the developing and postnatal skeletal muscles, in order to understand the role of this protein in muscle homeostasis and identify possible human muscle pathologies linked to Ambra1 mutations.

ACKNOWLEDGMENTS

The authors wish to acknowledge Prof. Michel Bagnat (Department of Cell Biology, Duke University Medical Center, Durham, NC 27710) for providing hsp70l:Lamp1-RFP plasmid, Prof. Gianfranco Bellipanni (Department of Biology, College of Science and Technology, Temple University, Philadelphia, PA) for providing *myoD1* plasmid and L. Pivotti and Dr. M. Milanetto for their valuable assistance in the fish facility.

REFERENCES

1. Levine B, Kroemer G. 2008. Autophagy in the pathogenesis of disease. Cell 132: 27-42.

2. Mizushima N, Komatsu M. 2011. Autophagy: renovation of cells and tissues. Cell 147:728–741.

3. Raben NV, Hill L, Shea S, Takikita R, Baum N, et al. 2008. Suppression of autophagy in skeletal muscle uncovers the accumulation of ubiquitinated proteins and their potential role in muscle damage in Pompe disease. Hum Mol Genet 17: 3897–3908.

4. Masiero E, Agatea L, Mammucari C, Blaauw B, Loro E, et al. 2009. Autophagy Is Required to Maintain Muscle Mass. Cell Metab 10: 507-515.

5. Grumati P, Coletto L, Sabatelli P, Cescon M, Angelin A, et al. 2010. Autophagy is defective in collagen VI muscular dystrophies, and its reactivation rescues myofiber degeneration. Nat Med 16: 1313-1320.

6. Carmignac V, Svensson M, Körner Z, Elowsson L, Matsumura C, et al. 2011. Autophagy is increased in laminin α2 chain-deficient muscle and its inhibition improves muscle morphology in a mouse model of MDC1A. Hum Mol Genet 20: 4891-4902.

7. De Palma C, Morisi F, Cheli S, Pambianco S, Cappello V, et al. 2012. Autophagy as a new therapeutic target in Duchenne muscular dystrophy. Cell Death Dis 15: e418.

8. Choi JC, Muchir A, Wu W, Iwata S, Homma S, et al. 2012. Temsirolimus activates autophagy and ameliorates cardiomyopathy caused by lamin A/C gene mutation. Sci Transl Med 4: 144ra102.

9. Ramos FJ, Chen SC, Garelick MG, Dai DF, Liao CY, et al. 2012. Rapamycin reverses elevated mTORC1 signaling in lamin A/C-deficient mice, rescues cardiac and skeletal muscle function, and extends survival. Sci Transl Med 4: 144ra103.

10. Cullup T, Kho AL, Dionisi-Vici C, Brandmeier B, Smith F, et al. 2012. Recessive mutations in EPG5 cause Vici syndrome, a multisystem disorder with defective autophagy. Nat Genet 45: 83-87.

11. Fimia GM, Stoykova A, Romagnoli A, Giunta L, Di Bartolomeo S, et al. 2007. Ambra1 regulates autophagy and development of the nervous system. Nature 447: 1121-1125.

12. Fimia GM, Corazzari M, Antonioli M, Piacentini M 2013. Ambra1 at the crossroad between autophagy and cell death. Oncogene 32:3311-3318.

13. Di Bartolomeo S, Corazzari M, Oliverio S, Nazio F, Lisi G, et al. 2010. The dynamic interaction of Ambra1 with the dynein motor complex regulates mammalian autophagy. J Cell Biol 191: 155-168.

14. Benato F, Skobo T, Gioacchini G, Moro I, Ciccosanti F, et al. 2013. Ambra1 knockdown in zebrafish leads to incomplete development due to severe defects in organogenesis. Autophagy 9: 476-495.

15. Jackson HE, Ingham PW. 2013. Control of muscle fibre-type diversity during embryonic development: the zebrafish paradigm. Mech Dev 130: 447-457.

16. Gibbs EM, Horstick EJ, Dowling JJ. 2013. Swimming into prominence: the zebrafish as a valuable tool for studying human myopathies and muscular dystrophies. FEBS J 280: 4187-4197.

17. Kimmel CB, Ballard WW, Kimmel SR, Ullmann B, Schilling TF. 1995. Stages of embryonic development of the zebrafish. Dev Dyn 203: 253-310.

18. Westerfield, M. 1995. The Zebrafish Book. A Guide for the Laboratory Use of Zebrafish (Danio rerio), 3rd Edition. Eugene, OR, University of Oregon Press.

19. Thisse C, Thisse B. 2008. High-resolution in situ hybridization to whole-mount zebrafish embryos. Nat Protoc 3: 59-69.

20. Dolez M, Nicolas JF, Hirsinger E. 2011. Laminins, via heparan sulfate proteoglycans, participate in zebrafish myotome morphogenesis by modulating the pattern of Bmp responsiveness. Development 138: 97-106.

21. Ellis K, Bagwell J, Bagnat M. 2013. Notochord vacuoles are lysosome-related organelles that function in axis and spine morphogenesis. J Cell Biol 200: 667-679.

22. Nord H, Nygård Skalman L, von Hofsten J. 2013. Six1 regulates proliferation of Pax7-positive muscle progenitors in zebrafish. J Cell Sci 126: 1868-1880.

23. Coutelle O, Blagden CS, Hampson R, Halai C, Rigby PW, et al. 2001. Hedgehog signalling is required for maintenance of myf5 and myoD expression and timely terminal differentiation in zebrafish adaxial myogenesis. Dev Biol 236: 136-150.

24. Weinberg ES, Allende ML, Kelly CS, Abdelhamid A, Murakami T, et al. 1996. Developmental regulation of zebrafish MyoD in wild-type, no tail and spadetail embryos. Development 122: 271-280.

25. Devoto SH, Melançon E, Eisen JS, Westerfield M. 1996. Identification of separate slow and fast muscle precursor cells in vivo, prior to somite formation. Development 122: 3371-3380.

26. Ochi H, Westerfield M. 2007. Signaling networks that regulate muscle development: lessons from zebrafish. Dev Growth Differ 49: 1-11.

27. Du SJ, Devoto SH, Westerfield M, Moon RT. 1997. Positive and negative regulation of muscle cell identity by members of the hedgehog and TGF-beta gene families. J Cell Biol 139: 145-156.

28. Wolff C, Roy S, Ingham PW. 2003. Multiple muscle cell identities induced by distinct levels and timing of hedgehog activity in zebrafish embryos. Curr Biol 13: 1169–1181.

29. He C, Bartholomew CR, Zhou W, Klionsky DJ. 2009. Assaying autophagic activity in transgenic GFP-Lc3 and GFP-Gabarap zebrafish embryos. Autophagy 5: 520–526.

30. Seger C, Hargrave M, Wang X, Chai RJ, Elworthy S, et al. 2011. Analysis of Pax7 expressing myogenic cells in zebrafish muscle development, injury, and models of disease. Dev Dyn 240: 2440–2451.

31. Berger J, Berger S, Hall TE, Lieschke GJ, Currie PD. 2010. Dystrophin-deficient zebrafish feature aspects of the Duchenne muscular dystrophy pathology. Neuromuscul Disord 20: 826-832.

32. Postlethwait J, Amores A, Cresko W, Singer A, Yan YL. 2004. Subfunction partitioning, the teleost radiation and the annotation of the human genome. Trends Genet 20: 481-490.

33. Blagden CS, Currie PD, Ingham PW, Hughes SM. 1997. Notochord induction of zebrafish slow muscle mediated by Sonic hedgehog. Genes Dev 11: 2163–2175.

34. Sandri M, Coletto L, Grumati P, Bonaldo P 2013. Misregulation of autophagy and protein degradation systems in myopathies and muscular dystrophies. J Cell Sci 126: 5325-5333.

35. Vainshtein A, Grumati P, Sandri M, Bonaldo P 2013. Skeletal muscle, autophagy, and physical activity: the ménage a trois of metabolic regulation in health and disease. J Mol Med DOI 10.1007/s00109-013-1096-z.

Cloning and characterization of ambra1 in a non vertebrate chordate: the colonial *Botryllus schlosseri*

Tatjana Skobo[1], Fabio Gasparini[1], Francesca Benato[1], Federico Caicci[1], Oliana Carnevali[2], Lucia Manni[1], Luisa Dalla Valle[1]

[1]Department of Biology, University of Padova, Padova, Italy
[2] Department of Life Science and Environment, Marche Polytechnic University, Ancona, Italy.

In preparation

ABSTRACT

Ambra1 is a key component of the autophagic process that plays several important roles in normal physiology, differentiation, embryo development, and survival during starvation, but is also implicate in pathophysiological processes. The *ambra1* gene has been previously characterized only in mammals and in zebrafish. In this study, we report the identification, through genome bioinformatics searches and targeted cloning, of the first complete *ambra1* transcript in a non-vertebrate chordate, the tunicate *Botryllus schlosseri*. This is a marine colonial species, which couples sexual reproduction to budding (blastogenesis). Usually, three blastogenic generations are present in the colony: filtering adults, their buds and budlets produced by the latter. Colony life-cycle is characterized by a cyclical change of generation (take-over), in which adults are resorbed by apoptosis, buds become adults and a new generation of budles is produced. In *B. schlosseri*, Ambra 1 deduced amino acid sequence is shorter than vertebrate Ambra1 proteins but still contains the WD40 domain, a marker of this protein. Moreover, not all conserved regions are present in the experimentally determined *B. schlosseri* and in the predicted *C. intestinalis* Ambra1 proteins: both of them lack of the DLC1-binding consensus motifs (TQT) that blocks the protein at its specific cytoskeletal site. RT-PCR analysis revealed that *ambra1* transcripts are expressed both in take-over and in blastogenic phases distant to takeover (mid-cycle). Typical autophagosomes, bounded by a double membrane, where also recognized at transmission electron microscopy in cells of colonies in take-over. Our data allows consideration on relationships between autophagy and apoptosis and the role of these cellular processes in the homeostasis of the organism. Moreover, they open to evolutionary considerations on the role and control of autophagy in chordates.

INTRODUCTION

Autophagy is a catabolic process that cells use to degrade and recycle, through the lysosomal machinery, long-lived proteins and dismantle organelles in order to maintain a homeostatic environment within the cells. It is a tightly regulated process that plays several important roles in normal physiology, differentiation, embryo development, and survival during starvation [1, 2]. Since clearance of unnecessary or injured components is critical for cell life, dysfunction of the autophagic process is implicated in several pathophysiological processes, including cancer, myopathies and neurodegenerative disorders [3].

Due to its essential role in cell survival and viability, the autophagic process is conserved throughout the eukaryotes [4]. In particular, the molecular mechanism of this process has been preserved during evolution, as demonstrated by expression in different organisms of a basic set of key AuTophaGy-related genes (ATGs). These genes were initially identified in yeast [5], and then found also in higher eukaryotic organisms including mammal, insect, worm and plant [6]. However, some differences in the autophagic machinery exist between yeast and higher eukaryotes [4, 6]. In the latters, the Beclin1/Vps34 complex is regulated by additional key proteins such as UVRAG, Ambra1 and Bif-1 [7].

Among these genes, the activating molecule in Beclin 1-regulated autophagy (Ambra1) was identified only few years ago in mice [8]. It was found to be a central regulator of the autophagic process thanks to its ability to bind Beclin 1 upon autophagic stimuli, thus promoting the interaction between Beclin 1 and its target kinase Vps34 [9]. Since its initial characterization, Ambra1 was found to be involved not only in autophagy, a catabolic process used by the cells to maintain a homeostatic intracellular environment, but also in other key processes such as apoptosis, cell proliferation and nervous system development [8]. The surprisingly varied roles of this protein likely derive from its ability to bind different proteins (such as Beclin1, Bcl-2, DLC1 and E3-ligase), depending on the specific process under examination [10]. Ambra1 genes have been cloned and characterized in human, mouse and finally in zebrafish. In the latter, due to genome duplication during teleost evolution, two paralogous genes were found, both required for a correct embryonic development [11].

In the tunicate, *Ciona intestinalis ambra1* gene has been identified by genome search together with other genes involved in the autophagic process. Moreover, presence of these genes has been compared with their occurrence in *S. cerevisiae, C. elegans, D. melanogaster* and *H. sapiens* [12]. This analysis showed that all the non-yeast genes involved in autophagy are present in the genome of this organism that has an autophagic machinery comparable to the vertebrate one.

Tunicates are marine invertebrate animals, considered to form the sister group of vertebrates. Together with vertebrates and cephalochordates, they belong to the phylum Chordata. For their phylogenetic position, these animals are strategic to study the evolution of autophagic proteins in chordates. Ascidians, the main class of tunicates, are characterized by a bi-phasic cycle, with a swimming tadpole larva which metamorphoses in a sessile zooid. The larva possesses the body plan specific of chordates. However, they lose this organization

at metamorphosis, becoming sessile filter-feeding zooids, solitary or colonial. The last species couple to sexual reproduction also the asexual one: the zooid derived from larva metamorphoses begins a lifelong, recurring asexual reproduction (called also blastogenesis or budding) which eventually gives rise to genetically identical individuals, the blastozooids.

Among colonial ascidians, *Botryllus schlosseri* is considered a model species for several reasons: it is cosmopolitan, easy to rear in laboratory, its genome has been recently sequenced, its biological cycle is well known and a recognized staging method is available for asexual reproduction [13, 14] (Figure 1).

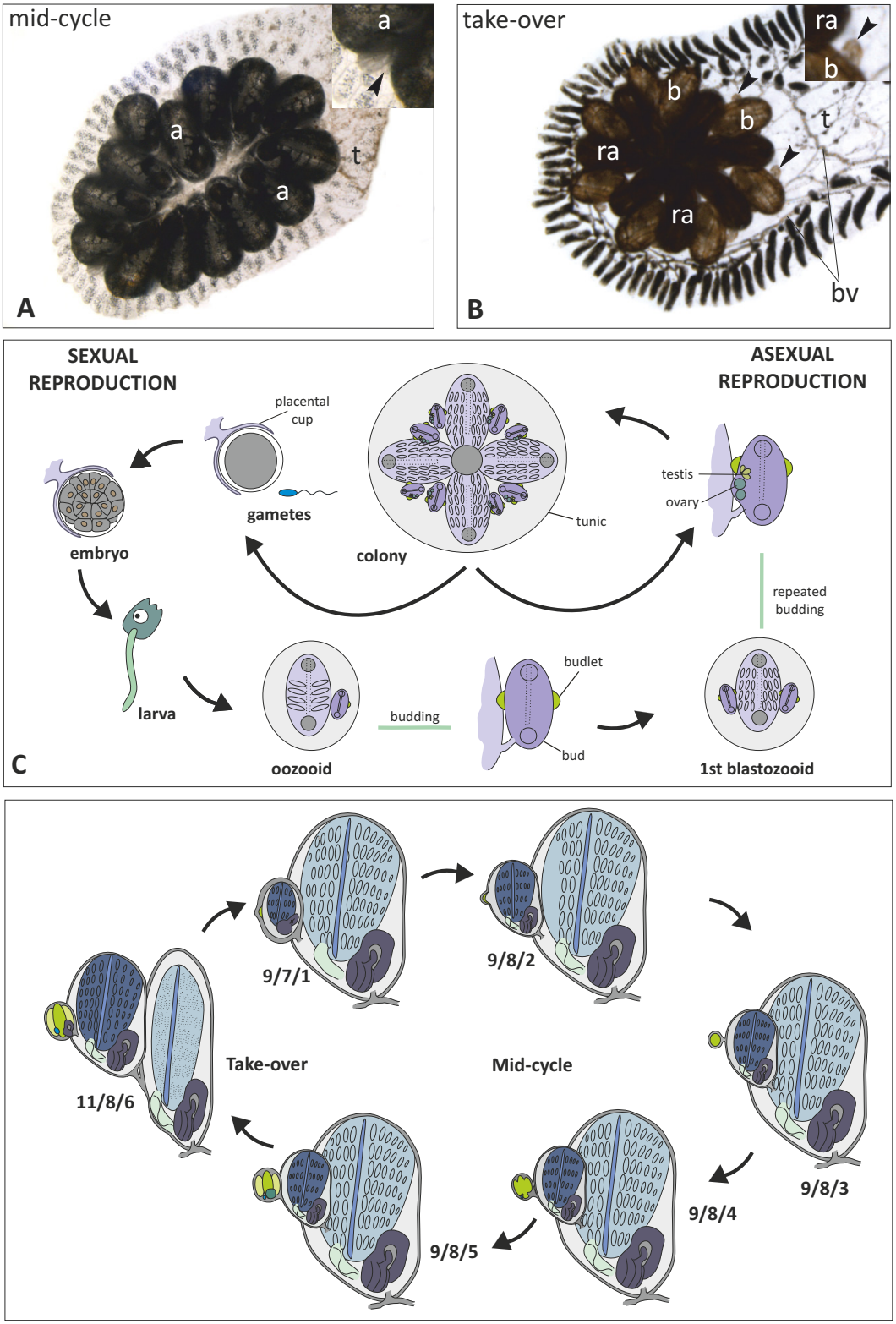

Figure 1. A-B. Colony of *B. schlosseri* in mid-cycle (stage 9/8/3) and in take-over (stage 11/8/6). Dorsal view. Squared areas are enlarged in insets to show details of buds (b) and budlets (arrowheads). a: adult; bv: blood vessels; ra: regressing adults; t: tunic. C. Life-cycle of *B. schlosseri*. Oozooid and blastozooids are shown in ventral view (modified from [34]). D. Colonial cycle of *B. schlosseri*. The coexisting three generations of blastozooids are visible. The change of generation occurs at take-over (stage 11/8/6), when adults undergo regression. In blastozooids, anterior at top and posterior at bottom (modified from [40]).

In *B. schlosseri*, each adult blastozooid carries one to several buds that bear a generation of young budlets. In laboratory condition, budding follows weekly-synchronized waves of cycles accompanied by regression and reabsorption of the filtering adults (a process called take-over). In the course of this process resorbed zooids are replaced by their buds, which develop into mature filtering zooids. After several blastogenetic cycles, the colony gets organized in a star-shaped system of a dozen of clonal blastozooids, arranged around a common cloacal, excurrent siphon. The whole colony is embedded in a common tunic, where all blastozooids are linked by a complex extrazooidic vascular system.

During the regression phase of adults, main organs undergo shrinkage and collapse, circulating phagocytes massively infiltrate senescent tissues and rapidly ingest effete cells [15, 16]. Within 24–36 h, cells undergo apoptosis and zooids are completely resorbed [16-19]. Since a colony is virtually immortal, many cyclical apoptotic events occur during its life span: these features renders *B. schlosseri* a useful and uncommon model to study on large scale and in natural conditions this modality of programmed cell death.

The role of autophagy in ascidian life cycle has not been studied in detail yet. In the solitary ascidian *Ciona intestinalis*, possible autophagic vacuoles, encircled by a single membrane and containing degenerating mitochondria were described in the cytoplasm of embryonic mesenchymal cells [20]. Similar vacuoles, bounded by a single membrane, and typical autophagosomes, bounded by a double membrane, were also signaled in *B. schlosseri* in different ontogenetic phases [15, 21, 22].

In the present study, we describe the molecular cloning and characterization of *ambra1* gene in *B. schlosseri* and compare its deduced amino acid sequence with those from *C. intestinalis* and mammals. We evidence, by RT-PCR analysis, that the gene is expressed both in mid-cycle and in take-over, and shows by transmission electron microscopy that autophagy and apoptosis concur together to regulate the crosstalk between generations, optimizing colony survival.

METHODS

Animals sampling

Colonies of *Botryllus schlosseri* (Styelidae, Stolidobranchia) were collected in the Lagoon of Venice and then cultured in laboratory according to Sabbadin's technique [23, 24] and fed with Liquifry Marine (Liquifry Co., Dorking, England).

The transparency of the colonies allowed us to follow the daily development *in vivo* of buds under the stereomicroscope, thereby permitting the selection of appropriate stages.

Three colony stages were utilized, carefully resolved *in vivo* following the recently revised Sabbadin stadiation [13, 19]: colony stage 11/8/6, that identifies the take-over, when adult zooids are absorbed and replaced by new ones, and colony stages 9/8/3 and 9/8/4, which are in the mid-cycle phase, when buds and zooids coexist together and no generation change occurs. Colonies at the appropriate developmental stages were immersed in RNAlater (Qiagen, Milan, Italy) and kept frozen at -20°C until use.

RNA isolation and RT-PCR

Pools of colonies, not genetically homogeneous, were used in all the experiments. Each set of colonies, averaging 100 mg, was minced for 2 min with a frosted glass pestle in 15 ml tubes filled with 2 ml of a heated (65°C) extraction buffer composed of CTAB Lysis buffer (Applichem, VWR International, Milan, Italy) and 2% β-mercaptoethanol. Samples were then maintained for 1,5 h at 65°C in a waterbath, shaking strongly for few seconds every 20 min, and cooled for 2 min in ice. Then, 3 volumes of a solution of chloroform-isoamyl Alcohol (24:1) was added, and the sample was thoroughly mixed shaking the tube with hands to get an emulsion. After a centrifugation step at 1600 *g* for 15 min at 4°C, the aqueous phase was collected into a new tube. An equal volume of 95% ethanol was then added and the total RNA was purified using the SV Total RNA Isolation Kit (Promega, Milan, Italy). A sample of RNA extracted form a mixed colony pool was enriched in polyadenylated mRNA utilizing the NucleoTrap mRNA Kit (M-Medical, Florence, Italy).

The cDNA was synthesized using the M-MLV Reverse Transcriptase (Promega) according to the manufacturer's instructions. Analysis of *ambra1* expression in colonies at different stages was performed by means of PCR analysis with the set of primers Bs-AM-F1 and Bs-AM-R1 and using the Biotherm Taq DNA polymerase (Società Italiana Chimici, Rome, Italy). The amplification procedure consisted of 2 min at 95°C followed by 30, 35 and 40 PCR cycles with 95°C for 30 s, 60°C for 30 s, and 72°C for 20 s. The extension phase of the last cycle was prolonged by 10 min. A negative control was prepared by replacing the cDNA solution with sterile water. The amplified products were analyzed for purity and size by electrophoresis in 2 % agarose gel.

Cloning of *B. schlosseri* ambra1 cDNA

To obtain *B. schlosseri* ambra1 cDNA, the 5'- and 3'-RNA ligase-mediated rapid amplification of cDNA ends (5'- and 3'-RLM-RACE) was performed with FirstChoice RLM-RACE Kit (Ambion) according to the manufacturer's instruction. These analyses were accomplished using polyadenylated mRNA extracted from a mixed colony pool of *B. schlosseri*.

Briefly, 1 mg of polyadenylated RNA was treated with calf intestinal phosphatase to remove free 5'-phosphates from truncated or noncapped mRNA, leaving a 5-OH. The RNA was then treated with tobacco acid pyrophosphatase (TAP) to remove the 5-cap from full-length mRNAs. This treatment leaves a 5-phosphate required for ligation. A 5'-RACE RNA adapter oligonucleotide was ligated to the 5'-end of the mRNA using T4 RNA ligase. Subsequently, first-strand cDNA synthesis was made by reverse-transcribing the ligated mRNA with random decamers. After cDNA synthesis the 5'-end of RNA was obtained by two rounds of PCR amplifications as described in Supplemental Figure 1.

To obtain 3'-ends of *B. schlosseri ambra1*, 2 mg total RNA was reverse-transcribed using 3'-RACE adapter primers. After cDNA synthesis, the 3'-end of RNA was obtained by two rounds of PCR amplification as described in Supplemental Figure 1.

The amplification procedure for both 3'- and 5'-RACE consisted of 2 min at 95°C followed by a touch-down PCR reaction with annealing temperatures decreasing from 65°C to 55°C over 10 cycles and the final 30 cycles maintained at 55°C. The extension phase of the last cycle was prolonged by 10 min. The primer sequences are reported in Table 1.

The resultant amplicons were purified from the sliced gel bands and the gel-purified fragments were directly sequenced or ligated into a pGEM-T vector using a pGEM-T Easy vector System according to the supplier's recommendations (Promega). Plasmids from positive colonies were purified and the clones were sequenced.

Primer	Sequence
Bs-AM-F1	5′-CCATCCTATGACAATGAGC-3′
Bs-AM-R1	5′-TCCAATGAGACAGTGACG-3′
Bs-AM-F2	5′-GTCACTGTCTCATTGGAG-3′
Bs-AM-R2	5′-GTTGAATCCACGCACACC-3′
Bs-AM-F3	5′-AATCATGGACGCTCGAGC-3′
Bs-AM-R3	5′-GCAATGGCAAGAACGTGC-3′
Bs-AM-R4	5′-GATTTCTGGCAACTGAAGC-3′
Bs-AM-F5	5′-ATCCTAGATGTGAAGCACC-3′
Bs-AM-R5	5′-CAAACGGGACCGAGCAG-3′
Bs-AM-F6	5′-CAGAGATTCCAACTCGG-3′
Bs-AM-R6	5′-CTGGAGGTCTGTCATCGG-3′
Bs-AM-F7	5′-TATGGATAGTCTAGCTGC-3′
Bs-AM-R7	5′-ACACTGTCGATGGTGTCG-3′

Table 1. List of primers used for the *B. schlosseri ambra1* cloning.

Light and transmission electron microscopy

Colonies were fixed in 1.5% glutaraldehyde buffered with 0.2 M sodium cacodylate, pH 7.4, plus 1.6 % NaCl. After washing in buffer and postfixation in 1% OsO4 in 0.2 M cacodylate buffer, specimens were dehydrated and embedded in Epon Araldite. Sagittal serial sections (1 µm) were counterstained with toluidine blue; thin sections (90 nm) were given contrast by staining with uranyl acetate and lead citrate. Micrographs were taken with a FEI Tecnai G^2 electron microscope (operating at 100 kV). All photos were collected and typeset in Corel Draw X3.

RESULTS

Isolation and characterization of the *B. schlosseri ambra1* gene and its deduced protein

A BLASTN search for *B. schlosseri ambra1* cDNA sequence was initially performed in a ESTs database (which link is no more available) using, as query, the Ambra1 amino acid sequence of different species: *C. intestinalis* Ambra1 (deduced from the KH.L84.31.v1.A.SL1-1 transcript of the KH assembly [25], available at http://ghost.zool.kyoto-u.ac.jp/cgi-bin/gb2/gbrowse/kh/), *D. rerio* Ambra1a (CCE04070), *D. rerio* Ambra1b (CCA61107) and *H. sapiens* AMBRA1 (NP_001254711). Due to the length of the Ambra1 proteins, no full-length clones were found, but only two cDNA fragments that correspond respectively to a portion of the N-terminal region and to a portion of the C-terminal region.

Based on these partial sequences, we designed antisense and sense primers to obtain the 5'- and 3'-UTR regions according to the cloning strategy described in Supplemental Figure 1. Moreover, the central coding region was covered by RT-PCR of overlapping fragments. The resulting sequence has been deposited in the GenBank database with the accession no (not yet assigned).

The deduced amino acid sequence derived from *B. schlosseri ambra1* transcript is based on an ORF (open reading frame) of 3147 bp, which starts from a putative initiation methionine 184-bp downstream from the 5'-end and continues to a stop codon TGA (Figure 2). The first 24 nucleotides of the 5'-UTR correspond to a characteristic 5'-spliced leader sequence [26]. The ORF encodes a 1048 amino acids long protein. The 3'-untranslated terminal region (3'-UTR) contains 83 bases. The 3'-UTR does not contains a canonical poly-A signal, AATAAA, characteristic of the eukaryotic mRNA. However, two putative poly-A signals were identified, AAGAAA and AATATA, that correspond to natural variants of this region [27].

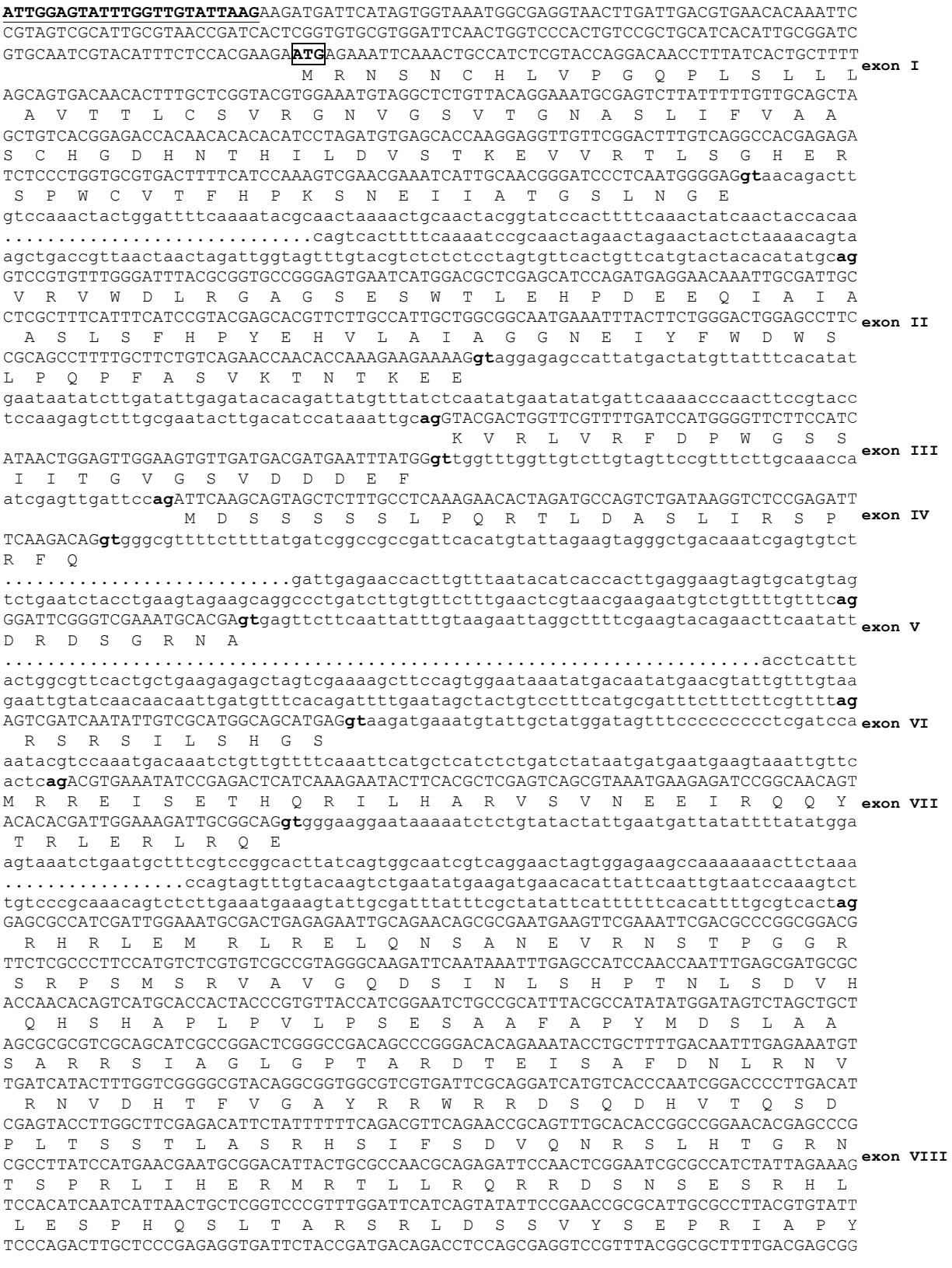
ATTGGAGTATTTGGTTGTATTAAG
ATG
exon I
exon II
exon III
exon IV
exon V
exon VI
exon VII
exon VIII

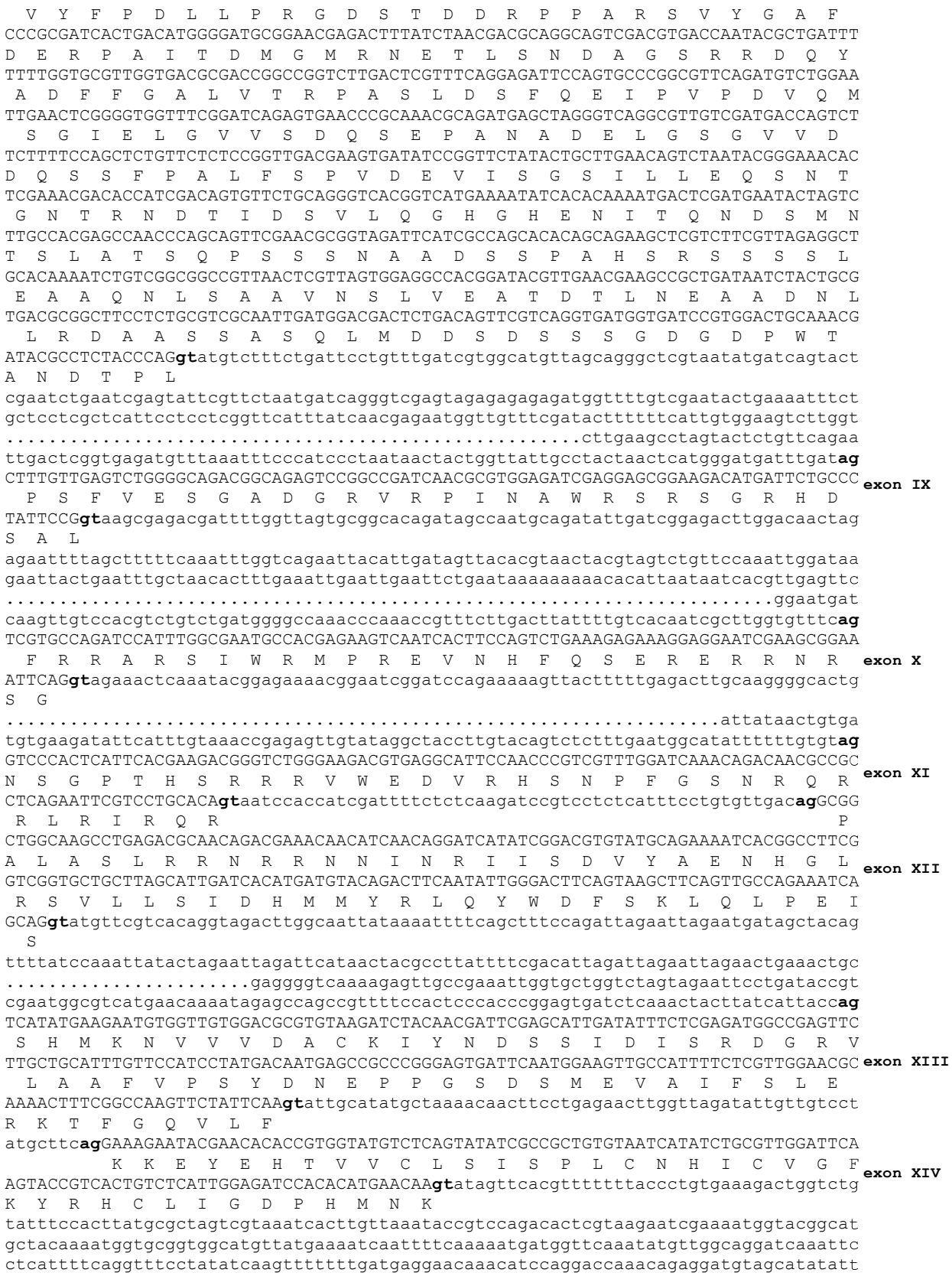
V Y F P D L L P R G D S T D D R P P A R S V Y G A F
CCCGCGATCACTGACATGGGGATGCGGAACGAGACTTTATCTAACGACGCAGGCAGTCGACGTGACCAATACGCTGATTT
D E R P A I T D M G M R N E T L S N D A G S R R D Q Y
TTTTGGTGCGTTGGTGACGCGACCGGCCGGTCTTGACTCGTTTCAGGAGATTCCAGTGCCCGGCGTTCAGATGTCTGGAA
A D F F G A L V T R P A S L D S F Q E I P V P D V Q M
TTGAACTCGGGGTGGTTTCGGATCAGAGTGAACCCGCAAACGCAGATGAGCTAGGGTCAGGCGTTGTCGATGACCAGTCT
S G I E L G V V S D Q S E P A N A D E L G S G V V D
TCTTTTCCAGCTCTGTTCTCTCCGGTTGACGAAGTGATATCCGGTTCTATACTGCTTGAACAGTCTAATACGGGAAACAC
D Q S S F P A L F S P V D E V I S G S I L L E Q S N T
TCGAAACGACACCATCGACAGTGTTCTGCAGGGTCACGGTCATGAAAATATCACACAAAATGACTCGATGAATACTAGTC
G N T R N D T I D S V L Q G H G H E N I T Q N D S M N
TTGCCACGAGCCAACCCAGCAGTTCGAACGCGGTAGATTCATCGCCAGCACACAGCAGAAGCTCGTCTTCGTTAGAGGCT
T S L A T S Q P S S S N A A D S S P A H S R S S S S L
GCACAAAATCTGTCGGCGGCCGTTAACTCGTTAGTGGAGGCCACGGATACGTTGAACGAAGCCGCTGATAATCTACTGCG
E A A Q N L S A A V N S L V E A T D T L N E A A D N L
TGACGCGGCTTCCTCTGCGTCGCAATTGATGGACGACTCTGACAGTTCGTCAGGTGATGGTGATCCGTGGACTGCAAACG
L R D A A S S A S Q L M D D S D S S S G D G D P W T
ATACGCCTCTACCCAG**gt**atgtctttctgattcctgtttgatcgtggcatgttagcagggctcgtaatatgatcagtact
A N D T P L
cgaatctgaatcgagtattcgttctaatgatcagggtcgagtagagagagagatggttttgtcgaatactgaaaatttct
gctcctcgctcattcctcctcggttcatttatcaacgagaatggttgtttcgatacttttttcattgtggaagtcttggt
.....cttgaagcctagtactctgttcagaa
ttgactcggtgagatgtttaaatttcccatccctaataactactggttattgcctactaactcatgggatgatttgat**ag**
CTTTGTTGAGTCTGGGGCAGACGGCAGAGTCCGGCCGATCAACGCGTGGAGATCGAGGAGCGGAAGACATGATTCTGCCC **exon IX**
P S F V E S G A D G R V R P I N A W R S R S G R H D
TATTCCG**gt**aagcgagacgattttggttagtgcggcacagatagccaatgcagatattgatcggagacttggacaactag
S A L
agaattttagctttttcaaatttggtcagaattacattgatagttacacgtaactacgtagtctgttccaaattggataa
gaattactgaatttgctaacactttgaaattgaattgaattctgaataaaaaaaaacacattaataatcacgttgagttc
.....ggaatgat
caagttgtccacgtctgtctgatggggccaaacccaaaccgtttcttgacttattttgtcacaatcgcttggtgtttc**ag**
TCGTGCCAGATCCATTTGGCGAATGCCACGAGAAGTCAATCACTTCCAGTCTGAAAGAGAAAGGAGGAATCGAAGCGGAA
F R R A R S I W R M P R E V N H F Q S E R E R R N R **exon X**
ATTCAG**gt**agaaactcaaatacggagaaaacggaatcggatccagaaaaagttacttttgagacttgcaaggggcactg
S G
.....attataactgtga
tgtgaagatattcatttgtaaaccgagagttgtataggctaccttgtacagtctctttgaatggcatatttttgtgt**ag**
GTCCCACTCATTCACGAAGACGGGTCTGGGAAGACGTGAGGCATTCCAACCCGTCGTTTGGATCAAACAGACAACGCCGC
N S G P T H S R R R V W E D V R H S N P F G S N R Q R **exon XI**
CTCAGAATTCGTCCTGCACA**gt**aatccaccatcgattttctctcaagatccgtcctctcatttcctgtgttgac**ag**GCGG
R L R I R Q R P
CTGGCAAGCCTGAGACGCAACAGACGAAACAACATCAACAGGATCATATCGGACGTGTATGCAGAAAATCACGGCCTTCG
A L A S L R R N R R N N I N R I I S D V Y A E N H G L **exon XII**
GTCGGTGCTGCTTAGCATTGATCACATGATGTACAGACTTCAATATTGGGACTTCAGTAAGCTTCAGTTGCCAGAAATCA
R S V L L S I D H M M Y R L Q Y W D F S K L Q L P E I
GCAG**gt**atgttcgtcacaggtagacttggcaattataaaattttcagctttccagattagaattagaatgatagctacag
S
ttttatccaaattatactagaattagattcataactacgccttattttcgacattagattagaattagaactgaaactgc
.....gaggggtcaaaagagttgccgaaattggtgctggtctagtagaattcctgataccgt
cgaatggcgtcatgaacaaaatagagccagccgttttccactcccacccggagtgatctcaaactacttatcattacc**ag**
TCATATGAAGAATGTGGTTGTGGACGCGTGTAAGATCTACAACGATTCGAGCATTGATATTTCTCGAGATGGCCGAGTTC
S H M K N V V V D A C K I Y N D S S I D I S R D G R V
TTGCTGCATTTGTTCCATCCTATGACAATGAGCCGCCCGGGAGTGATTCAATGGAAGTTGCCATTTTCTCGTTGGAACGC **exon XIII**
L A A F V P S Y D N E P P G S D S M E V A I F S L E
AAAACTTTCGGCCAAGTTCTATTCAA**gt**attgcatatgctaaaacaacttcctgagaacttggttagatattgttgtcct
R K T F G Q V L F
atgcttc**ag**GAAAGAATACGAACACACCGTGGTATGTCTCAGTATATCGCCGCTGTGTAATCATATCTGCGTTGGATTCA
K K E Y E H T V V C L S I S P L C N H I C V G F **exon XIV**
AGTACCGTCACTGTCTCATTGGAGATCCACACATGAACAA**gt**atagttcacgtttttttaccctgtgaaagactggtctg
K Y R H C L I G D P H M N K
tatttccacttatgcgctagtcgtaaatcacttgttaaataccgtccagacactcgtaagaatcgaaaatggtacggcat
gctacaaaatggtgcggtggcatgttatgaaaatcaatttttcaaaaatgatggttcaaatatgttggcaggatcaaattc
ctcattttcaggtttcctatatcaagttttttttgatgaggaacaaacatccaggaccaaacagaggatgtagcatatatt

Figure 2. Nucleotide sequence of *B. schlosseri ambra1* gene and its deduced amino acid sequence. The capital letters correspond to the exon sequence. The 5'-spliced leader sequence at the beginning of the transcript is marked in bold and underlined. The intron sequence is in lower-case letters. The intron dinucleotide acceptor and donor sites for RNA splicing are indicated by lower case, bold letters. One-letter symbols of encoded amino acids are shown below the DNA sequence. The start codon as well as the stop codon are boxed and given in bold type. The positions of putative poly (A)+ signals are underlined. The cDNA sequence has been submitted to the GeneBank under the accession number (not yet assigned).

The alignment of *B. schlosseri* Ambra1 amino acid sequence with those of sea squirt (*C. intestinalis)*, human and mouse showed only a partial conservation of the primary structure of Ambra1 proteins between tunicates and vertebrates. As shown in Figure 3, the WD40 repeat region, that is a marker of this protein in vertebrates, is also present and well conserved in *B. schlosseri* and *C. intestinalis.* However, other conserved regions, such as Beclin 1 binding region, which is highly conserved between mouse, human and zebrafish Ambra1 proteins [11], present a low level of amino acid identity. Nevertheless, in vertebrates, the Beclin 1 binding region also contains a serine-rich region. Although not conserved in their position with respect to mammal proteins, a high number of these amino acids are also present in this region in tunicates (residues marked in bold in Figure 3).

Moreover, due to a reduced length, tunicate Ambra1 proteins lack the two DLC-binding consensus motifs (TQT) that are usually present at the C-terminal region of this protein and that mediate the interaction with dynein light chains (DLCs) [28].

Some of the human Ambra1 phosphorylation sites reported by Fimia and co-workers [10] in the human protein are also conserved in *B. schlosseri* and *C. intestinalis* proteins. Moreover, the lysine ubiquitination site, located at the end of the WD40 domain, and the aspartic acid residue that mediates the Ambra1 caspase cleavage during the apoptotic process [10] are present and maintain the same localization both in tunicate and vertebrate Ambra1 proteins.

Finally, another well-conserved fragment between tunicate and vertebrate sequences is present in the C-terminal region of tunicate protein but no specific functions of this area are up to now known.

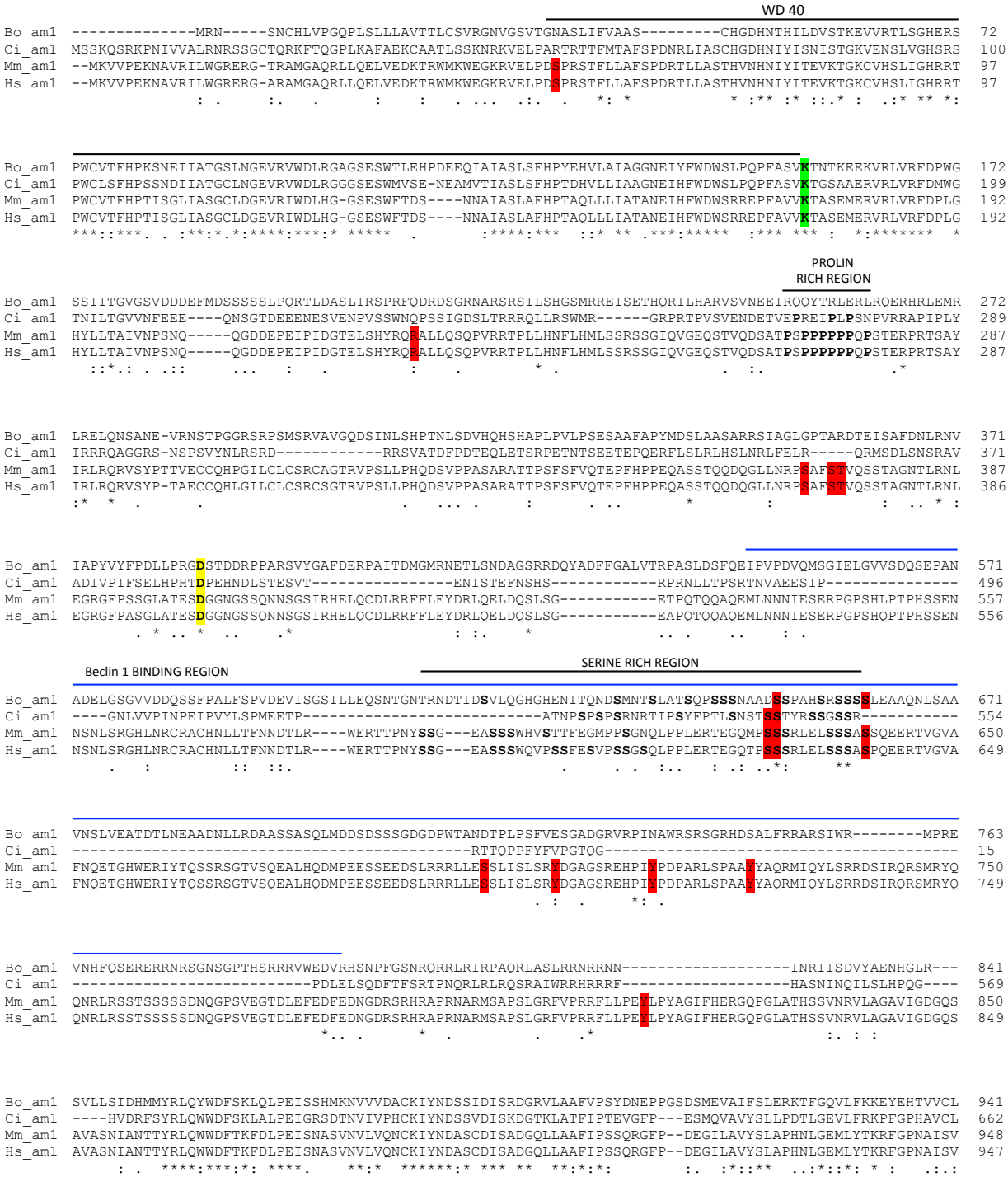
WD 40
PROLIN
RICH REGION
Beclin 1 BINDING REGION
SERINE RICH REGION

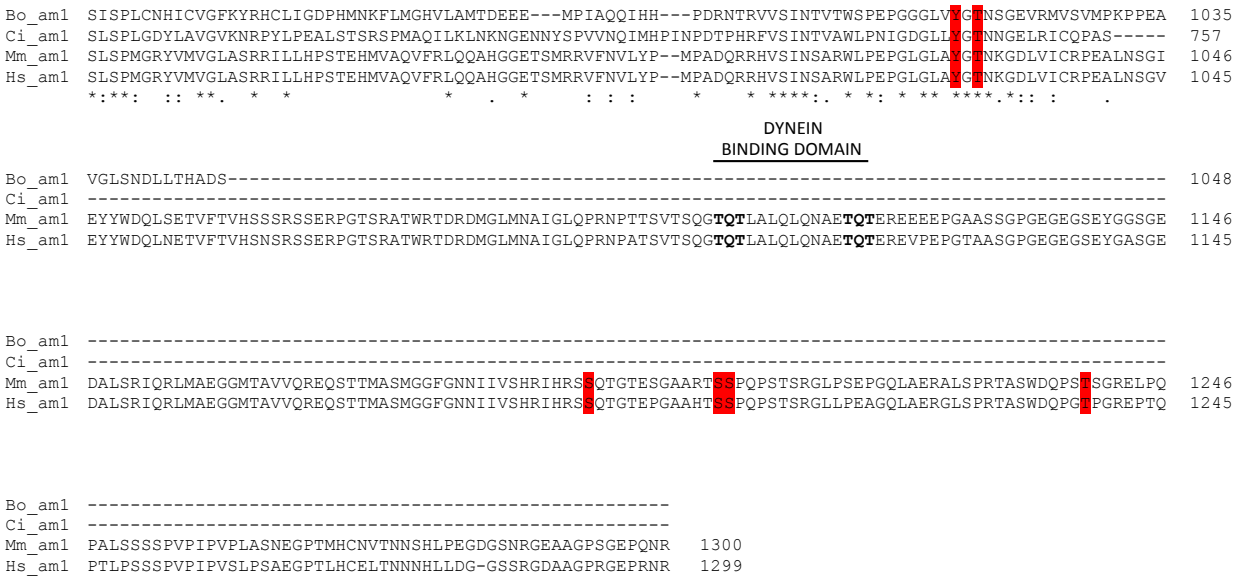

Figure 3. Multiple sequence alignment of human (Hs, *Homo sapiens,* NP_001254711), mouse (Mm, *Mus musculus,* NP_766257), sea squirt (Ci, *C. intestinalis* KH.L84.31.v1.A.SL1-1) and *B. schlosseri* (Bs, number not yet assigned) Ambra 1 proteins was originated with the program ClustalW. In the alignment, identical residues in all sequences are indicated by '*'. Conservative and semi-conservative substitutions are indicated by ':' and '.', respectively. Structural domains, as reported for human Ambra1 by Fimia and co-workers 10], are highlighted by a horizontal line just over the alignment. Post-translational phosphorylation in human and mouse aminoacid residues are shadowed in red, the ubiquitination lysine residue is shadowed in green and the caspase-cleavage aspartic acid residue in yellow.

Genomic organization of *B. schlosseri ambra1* gene

The genomic organization of *ambra1* gene was obtained by BLAST analysis of the *B. schlosseri* genome (http://genepyramid.stanford.edu/botryllusgenome/) with the cDNA sequence just obtained. This analysis found three contig fragments covering completely the new cDNA sequence (botctg036000, botctg051220 and botctg014012). In Figure 4 the *B. schlosseri ambra1* genomic organization is compared with those of the corresponding genes in *H. sapiens* and *C. intestinalis* obtained by analysis of their nucleotide or amino acid sequences with the BLAT program (http://genome.ucsc.edu/cgi-bin/hgBlat?command=start). Moreover, in Table 2, we report the sizes of each of the exons and introns of the *B. schlosseri ambra1* gene as well as data from vertebrates and *Ciona*. As for the other species reported in Table 2, the canonical splice consensus sites "GT" and "AG" are present in all *B. schlosseri ambra1* introns, as shown in Figure 2.

B. schlosseri ambra1 gene contains 16 exons and 15 introns. Differently from vertebrates, in this species, *ambra1* gene lacks a non-coding first exon and the first exon is then partially coding. Data on genomic organization of *C. intestinalis ambra1* were obtained by the Ghost Database (http://ghost.zool.kyoto-u.ac.jp/) that integrates expression and genomic information (Figure 4). Based on this analysis, *C. intestinalis ambra1* gene contains 11 exons and 10 introns and thus presents a reduced number of exon with respect to *B. schlosseri* and mammals.

Although the number of exons is not conserved between vertebrates and tunicates, some features of the genomic organization are preserved: position of the WD40 domain and the ubiquitination lysine residue that are localized in the first exons or the caspase-cleavage aspartic acid residue that is positioned in the longest exon in all the genes analysed (yellow line in Figure 4).

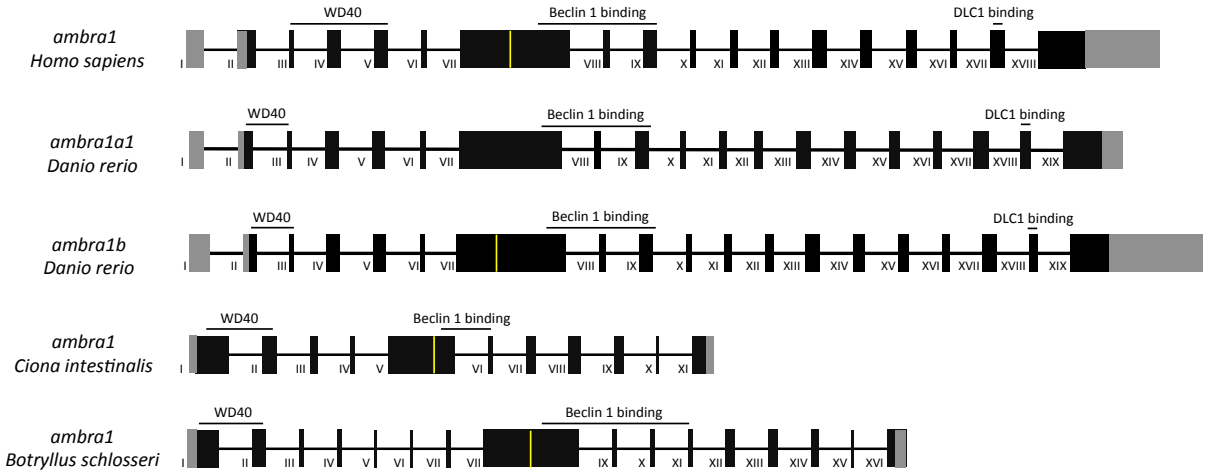

Figure 4. Genomic structure and organization of *B. schlosseri, H. sapiens, D. rerio* and *C. intestinalis ambra1* genes. Plain boxes indicate exons and are numbered with Roman numerals. The coding region is in black whereas the untranslated terminal regions are in grey. The SL (splice leader) sequence is shown as a red linein the first exons. Caspase-cleavage aspartic acid residue is shown as a yellow line in the longest exon. This amino acid residue is not present in the *D. rerio ambra1a1 gene.* The positions of the WD40 domain, Beclin1 and DLC1 binding regions are indicated. Introns, represented as lines, are not drawn to scale, but the corresponding lengths can be found in Table 1 together with the exon sizes.

	1° ex	1° intr	2° ex	2° intr	3° ex	3° intr	4° ex	4° intr	5° ex	5° intr	6° ex	6° intr	7° ex	7° intr	8° ex	8° intr	9° ex	9° intr
Homo sapiens AMBRA1	240	42624	135	370	57	520	186	1336	174	1562	63	576	1455	29131	87	4356	183	13986
Danio rerio ambra1a1	206	3010	233	2168	59	167	184	113	173	986	67	97	1373	7293	87	4736	183	2268
Danio rerio ambra1b	266	801	217	1462	59	104	184	233	173	437	67	115	1463	2937	87	275	183	163
Botryluss schlosseri ambra1	445*	542	204	157	79	56	73	2444	22	2547	32	134	100	677	1376	1530	87	1281
Ciona intestinalis ambra1	489*	387	201	299	118	275	47	258	964	154	94	243	138	2046	177	319	111	172

	10° ex	10° intr	11° ex	11° intr	12° ex	12° intr	13° ex	13° intr	14° ex	14° intr	15° ex	15° intr	16° ex	16° intr	17° ex	17° intr	18° ex	18° intr	19° ex
Homo sapiens AMBRA1	78	415	102	50009	111	8450	189	1220	156	15421	141	7544	93	1569	192	10569	484		
Danio rerio ambra1a1	78	917	101	19177	111	20026	189	3132	155	4999	140	3466	111	3226	209	21056	132	3025	733
Danio rerio ambra1b	81	2285	101	103	111	115	189	412	155	2050	140	4475	99	95	203	2009	123	3125	1802
Botryluss schlosseri ambra1	86	727	100	56	168	693	186	63	111	444	74	2977	254						
Ciona intestinalis ambra1	83	307	456																

Table 1. Exons and introns size of *Homo sapiens*, *Danio rerio ambra1a, Botryllus schlosseri* and *Ciona intestinalis* genes. * The first exon contains SL (splice leader) sequence.

Expression analysis of *ambra1* mRNA in different *B. schlosseri* stages

A preliminary study of the expression pattern of *B. schlosseri ambra1* gene was performed by RT-PCR analysis on cDNA obtained from different stages (Figure 5). A gene-specific primer set was designed to span an intron, in order to reveal any contaminating genomic DNA as a larger-sized PCR fragment. A different number of amplification cycles (30, 35, 40) was used in order to reveal difference in the transcripts contents between different life stages of the *B. schlosseri.*

The analysis revealed that *ambra1* transcripts are expressed both in mid-cycle (samples 1-3) and in the take-over phases (sample 4). Expression is variable inside samples of the same stage and between different stages. However, this was a qualitative analysis and thus, before to make quantitative consideration, we need to set up a real time PCR protocol.

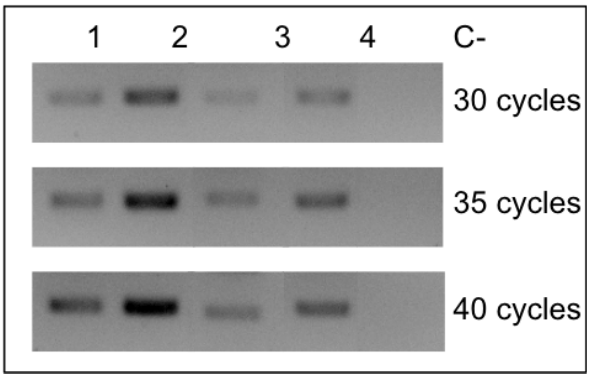

Figure 5. Expression of *B. schlosseri ambra1* transcripts as shown by RT-PCR performed on RNA extracted during different phases of the life cycle and different number of PCR cycles. C- = negative control; 1, 2 = stage 9/8/3; 3 = stage 9/8/4; 4 = stage 11/8/6.

Light and transmission electron microscopy analysis of autophagy in *B. schlosseri*

Taking into account that in *B. schlosseri* autophagic vacuoles were detected during the regression phase [15, 21] and a complex crosstalk exists between autophagy and apoptosis [10], we concentrated our morphological analyses in colonies in takeover. Regressing blastozooid were characterized by contraction of zooids and their internal organs, particularly evident in the branchial sac, and pyknotic nuclei in tissues, suggesting the occurrence of cell death (Figure 6 A, B). Moreover, abundant, large macrophages were circulating in blood lacunae. The Figure 6 C shows a giant phagocyte in blood lacuna, with a phagosome containing an ingested cell (Figure 6 C). The cytoplasm of the ingested cell exhibits clear sign of degeneration, evidenced by the great number of vesicles filling the cytoplasm, the condensed chromatin at the nucleus periphery, and mitochondria with swollen cristae. Cytoplasmic vesicles are heterogeneous in content. Some of them are typical autophagic vacuoles. Figure 6 E shows an autophagosome bordered by a double layer of membranes, containing a mitochondrion. In some cases, cisterns of endoplasmic reticulum are also recognizable close to degenerating organelles (Figure 6 F).

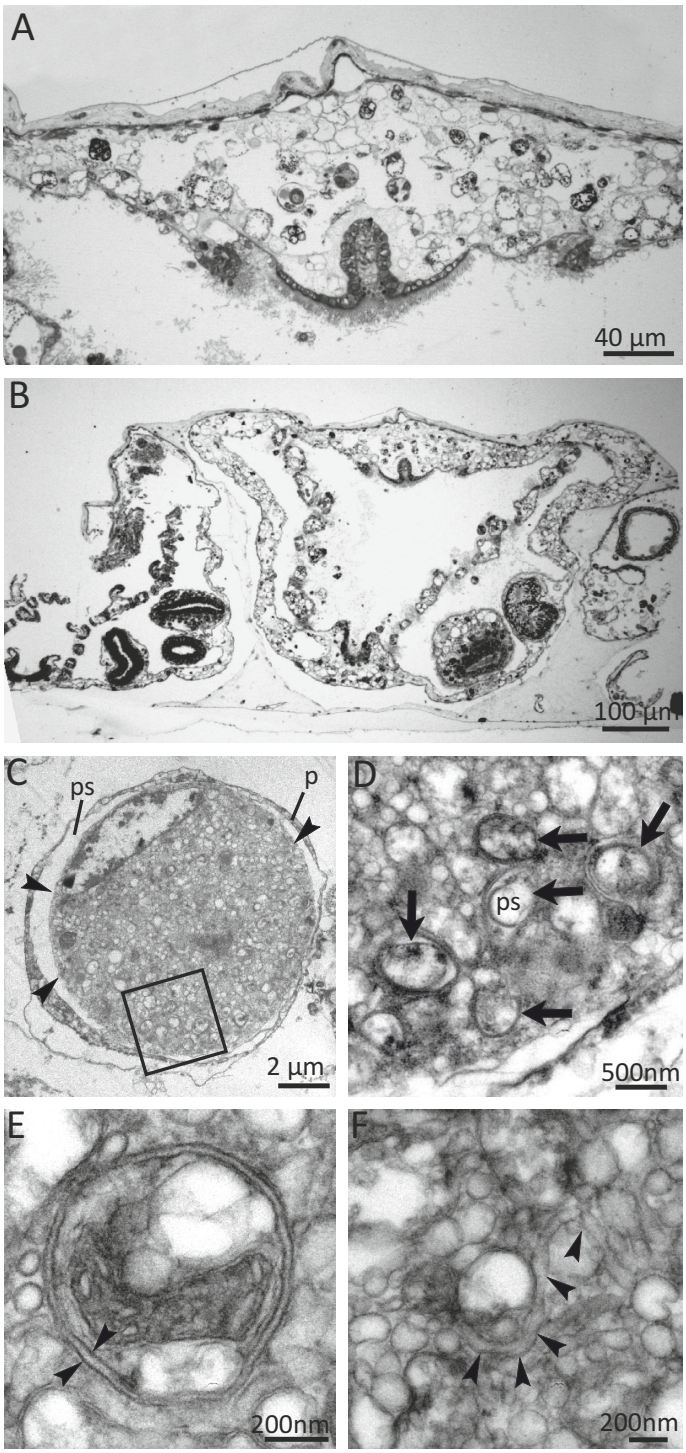

Figure 6. Morphological evidence of autophagy in *B. schlosseri*. A-B. Histological sections of regressing adults belonging to colonies in early take-over. A. Transverse section at branchial chamber (bc) level. Squared area enlarged in B. B. Detail of A, to show the dorsal blood lacuna (bl) containing numerous circulating phagocytes (arrowheads). Note the degenerating epithelium (arrows). e: endostyle; ep: epidermis; i: intestine; peribranchial chamber; st: stomach; t: tunic; te: testis. Toluidine blue. C-F. Transmission electron microscopy of a regressing blastozooid in early take-over. C. A circulating phagocyte (p) with a giant phagosome (ps) containing a degenerating cell (arrowheads). The cytoplasm of the degenerating cell is rich in autophagic vacuoles. Squared area is enlarged in D. D. Autophagosomes (arrows), characterized by the typical double membrane. C. Autophagosome containing a mitochondrion (m). Note the double membrane (arrowheads) encircling the autophagosome. D. Endoplasmic reticulum cistern (arrowheads) partially enveloping a degenerating mitochondrion (dm).

DISCUSSION

Ambra1 gene identification and characterization in *Botryllus schlosseri*

In this study, we report the identification, through genome bioinformatic searches and targeted cloning, of the first complete *ambra1* transcript in a non-vertebrate species, the tunicate *B. schlosseri*. Before this study, expression of *ambra1*, together with expression of other genes important in the mammalian autophagic process but not present in yeast, was demonstrated only in the tunicate, *C. intestinalis* [12]. The authors also showed that *ambra1* expression, as analysed by means of RT-PCR, is developmentally regulated. However, the experimental determination of the complete sequence allowed us, not only to analyse its expression, but also to compare the *B. schlosseri ambra1* sequence with those from vertebrate species.

The deduced amino acid sequence of *B. schlosseri* is shorter than vertebrate sequences till now characterized and lacks completely of the DLC1-binding consensus motifs (TQT) that, in absence of autophagy induction, docked the protein at its specific cytoskeletal site [28]. However, splicing variants, represented by truncated isoforms missing the carboxyl-terminal region and thus the crucial binding site to DLC1, have been identified on zebrafish [11] and are likely present also in human and mouse, as suggested by the occurrence of different Ambra1 protein isoforms in the UniProt website (http://www.uniprot.org/uniprot/). However, looking for alternative splicing in this region, we repeat the 3'-RACE analysis three times and also analysed *B. schlosseri* and *C. intestinalis* EST libraries without finding longer transcripts. Therefore, we assume that in tunicates *ambra1* genes may encode a shorter isoform of the vertebrate Ambra1 proteins.

Differently form the high amino acid identity between vertebrate Ambra1 proteins [11], not all conserved regions are present in the experimentally determined *B. schlosseri* and in the predicted *C. intestinalis* Ambra1 proteins.

Among the conserved features, it is possible to find the caspase cleavage site, always located inside the longest exon, the N-terminal WD40 domain, which is a signature of this protein and the ubiquitination site at its end. The WD40 domain is present in a large family of eukaryotic proteins that normally acts as scaffold by interaction with different proteins [29]. This allows proteins bearing this domain to play specific roles in different processes, as was also proposed for Ambra1 [10].

A low degree of identity was instead found in the fragment corresponding to Beclin 1 binding region. However, based on results obtained with Disorder Predictor Programs (http://www.disprot.org/predictors.php, data not shown) and as also proposed by Nazio and co-workers [30], in vertebrates Ambra1 was found to belong to the class of Intrinsically Disordered Proteins (IDPs). The same result was also obtained with tunicates Ambra1 proteins. IDPs are able to adapt their tridimensional structure to their binding partners, and thus can carry out important biological functions in different cells and in several subcellular organelles. The finding that Ambra1 belongs to this class of proteins, together with the presence of the WD40 domain, could explain why this protein can associate to different

proteins and to act in many cell processes. It is possible that tunicates Ambra1 proteins, despite their low sequence identity with vertebrates Ambra1, retain similar multi-protein complex assembly functions thank to the presence of intrinsically disordered segments in which functionality could be more related to amino acid composition than to conservation of primary sequence [31].

Autophagy in the blastogenic cycle of *B. schlosseri*

Our results confirm that autophagy is a strategy adopted by *B. schlosseri* during its blastogenic cycle. Autophagy in this species was previously shown in different cells and developmental phases. In zymogenic cells of the stomach, autophagic vacuoles were proposed to be related to the control of the cycle of zymogen production, or to the initiation of the general process of involution of these cells when take-over approaches [21]. Similarly, autophagic vacuoles were found in gut cells and in endostyle cells of adult blasotzooids during the regression phase [15]. At larval metamorphosis, a limited number of autophagic vacuoles bounded by single or a double limiting membrane were also found in caudal muscle involuting cells [22]. A number of these vacuoles displayed also a positive reaction for acid phosphatase, the reaction product being often confined to the space between the limiting membranes. Both the take-over and the metamorphosis are dominated by apoptosis in remodelling tissues and organs [16-18,32,33].

In this study, we demonstrate that *ambra1* transcripts are expressed both in mid-cycle and in takeover of *B. schlosseri*. Moreover, we show unequivocal autophagosomes, bounded by a double membrane, in cells during take-over. This reinforces the idea that autophagy is a crucial mechanism operating in the life-cycle. It is to note that we recognized autophagosomes in a degenerating cell phagocyted by a circulating macrophage. This fact highlights the interesting link between autophagy and apoptosis, and allows us to hypothesize that autophagy play a role in the crosstalk between bud and parent, optimizing the colony survival. A quantitative real time PCR protocol will be necessary to understand if expression of *ambra1* transcript is tightly regulated during the life cycle of this species.

In conclusion in this study, we evidence that the autophagic process has a role in the blastogenic cycle of *B. schlosseri*, showing that the *ambra1* gene, coding for a key autophagic factor, is expressed in different phases of the cycle, and that typical autophagosomes can be recognized.

In recent years, *B. schlosseri* has become an emergent model to study dynamics of development and homeostasis [13, 34, 35]. The specificity of its asexual reproduction, based on cyclical changes of generation, rendered this animal particularly suitable to study apoptosis and its regulation [18, 36]. It has been shown that the survival of animal tissues and organs is controlled through both activation and suppression of programmed cell death at takeover: apoptosis is crucial to ensure macromolecular recycling and engineer the reconstitution of a functional asexual generation every week [37, 36]. In the light of the complex relationships between autophagy and apoptosis [10, 38], our data allow considerations on the role of these cellular processes in the homeostasis of the organism. Moreover, taking into account that tunicates are believed the sister group of vertebrates

[39], our data open to new evolutionary considerations on the role and the control of the autophagic mechanism in chordates.

ACKNOWLEDGMENTS

This work was financially supported by University of Padova (RFO-ex 60%) to LDV and by PRIN 2009 Project to LM. Authors wish to thank Prof. A.W. De Tomaso, University of California, S. Barbara, for rendering available his *Botryllus* EST collection.

REFERENCES

1. Mizushima N, Komatsu M. 2011. Autophagy: renovation of cells and tissues. Cell 147, 728–741.

2. Di Bartolomeo S, Nazio F, Cecconi F. 2010. The role of autophagy during development in higher eukaryotes. Traffic 11, 1280–1289.

3. Ravikumar B, Sarkar S, Davies JE, Futter M, Garcia-Arencibia M, Green-Thompson ZW, Jimenez-Sanchez M, et al. 2010. Regulation of mammalian autophagy in physiology and pathophysiology. Physiol Rev 90, 1383–435.

4. King JS. 2012. Autophagy across the eukaryotes. Is S. cerevisiae the odd one out?. Autophagy 8, 1159–1162.

5. Klionsky, D. J. et al. 2003. A unified nomenclature for yeast autophagy-related genes. Dev Cell 5, 539–545.

6. Levine B, Klionsky DJ. 2004. Development by self-digestion: Molecular mechanisms and biological functions of autophagy. Dev Cell 6, 463–477.

7. Calvo-Garrido J, Carilla-Latorre S, Kubohara Y, Santos-Rodrigo N, Mesquita A, Soldati T, Golstein P, Escalante R. 2010. Autophagy 6, 686–701.

8. Fimia GM, Stoykova A, Romagnoli A, Giunta L, Di Bartolomeo S, Nardacci R, et al. 2007. Ambra1 regulates autophagy and development of the nervous system. Nature 447, 1121–1125.

9. He C, Levine B. 2010. The Beclin 1 interactome. Curr. Opin. Cell Biol. 22, 140-149.

10. Fimia GM, Corazzari M, Antonioli M, Piacentini M. 2013. Ambra1 at the crossroad between autophagy and cell death. Oncogene 32, 3311–3318.

11. Benato F, Skobo T, Gioacchini G, Moro I, Ciccosanti F, Piacentini M, Fimia GM, Carnevali O, Dalla Valle L. 2013. Ambra1 knockdown in zebrafish leads to incomplete development due to severe defects in organogenesis. Autophagy 9, 476–495.

12. Godefroy N, Hoa C, Tsokanos F, Le Goff E, Douzery EJ, Baghdiguian S, Martinand-Mari C. 2009. Identification of autophagy genes in Ciona intestinalis: a new experimental model to study autophagy mechanism. Autophagy 5, 805–815.

13. Manni L, Zaniolo G, Cima F, Burighel P, Ballarin L. 2007. *Botryllus schlosseri*: a model ascidian for the study of asexual reproduction. Dev Dyn 236, 335–352.

14. Voskoboynik a., Neff NF, Sahoo D, Newman a. M, Pushkarev D, et al. 2013. The genome sequence of the colonial chordate, Botryllus schlosseri. Elife 2, e00569–e00569.

15. Burighel P, Schiavinato A. 1984. Degenerative regression of the digestive tract in the colonial ascidian Botryllus schlosseri (Pallas). Cell tissue Res 235, 309–318.

16. Cima F, Basso G, Ballarin L. 2003. Apoptosis and phosphatidylserine-mediated recognition during the take-over phase of the colonial life-cycle in the ascidian *Botryllus schlosseri*. Cell Tissue Res 312, 369–376.

17. Lauzon RJ, Patton CW, Weissman IL 1993. A morphological and immunohistochemical study of programmed cell death in Botryllus schlosseri (Tunicata, Ascidiacea). Cell Tissue Res 272, 115–127.

18. Cima F, Manni L, Basso G, Fortunato E, Accordi B, Schiavon F, Ballarin L. 2010. Hovering between death and life: natural apoptosis and phagocytes in the blastogenetic cycle of the colonial ascidian Botryllus schlosseri. Dev Comp Immunol 34, 272–285.

19. Ballarin L, Schiavon F, Manni L. 2010. Natural Apoptosis During the Blastogenetic Cycle of the Colonial Ascidian Botryllus schlosseri: A Morphological Analysis. Zoolog Sci 27, 96–102.

20. Mancuso V, Dolcemascolo G. 1981. Autophagic activity in the mesenchyme cells of Ciona embryo. Acta Embryologiae Et Morphologiae Experimentalis (Halocynthia Association) 2, 3–13.

21. Burighel P, Milanesi C. 1973. Fine structure of the gastric epithelium of the ascidian Botryllus schlosseri vacuolated and zymogenic cells. Z. Zellforsch 145, 541–555.

22. Schiaffino S, Burighel P, Nunzi MG. 1974. Involution of the caudal musculature during metamorphosis in the ascidian, Botryllus schlosseri. Cell Tissue Res 153,293–305.

23. Sabbadin A. 1955. Osservazioni sullo sviluppo, l'accrescimento e la riproduzione di Botryllus schlosseri (Pallas), in condizioni di laboratorio. Boll Zool 22, 243–265.

24. Sabbadin A. 1960. Ulteriori notizie sull'allevamento e sulla biologia dei Botrilli in condizioni di laboratorio. Arch Oceanogr Limnol 12, 97–107.

25. Satou Y, Kawashima T, Shoguchi E, Nakayama A, Satoh N. 2005. An integrated database of the ascidian, Ciona intestinalis: towards functional genomics. Zoolog Sci 22, 837–843.

26. Gasparini F, Shimeld SM. 2011. Analysis of a botryllid enriched-full-length cDNA library: insight into the evolution of spliced leader trans-splicing in tunicates. Dev Genes Evol 220, 329–336.

27. Sheets MD, Ogg SC, Wickens MP. 1990. Point mutations in AAUAAA and the poly(A) addition site: effects on the accuracy and efficiency of cleavage and polyadenylation in vitro, Nucl Acids Res 18, 5799–5805.

28. Di Bartolomeo S, Corazzari M, Nazio F, Oliverio S, Lisi G, Antonioli M, et al. 2010. The dynamic interaction of AMBRA1 with the dynein motor complex regulates mammalian autophagy. J Cell Biol 191, 155–168.

29. Stirnimann CU, Petsalaki E, Russell RB, Müller CW. 2010. WD40 proteins propel cellular networks. Trends in Biochemical Sciences 35, 565–574.

30. Nazio F, Strappazion F, Antonioli M, Bileli P, Cianfanelli V, Bordi M, Gretmeier C, Dengjel J, Piacentini M, Fimia GM, Cecconi F. 2013. Nature Cell Biology 15, 406–416.

31. Ando D, Colvin M, Rexach M, Gopinathan A. 2013. Physical motif clustering within intrinsically disordered nucleoporin sequences reveals universal functional features. PLoS One 8, e73831.

32. Chambon JP, Nakayama A, Takamura K, McDougall A, Satoh N, Ando D, et al. 2007. ERK- and JNK-signalling regulate gene networks that stimulate metamorphosis and apoptosis in tail tissues of ascidian tadpoles. Development 134, 1203–19.

33. Nakayama-Ishimura A, Chambon JP, Horie T, Satoh N, Sasakura Y. 2009. Delineating metamorphic pathways in the ascidian Ciona intestinalis. Dev Biol 326, 357–367.

34. Manni L, Burighel P. 2006. Common and divergent pathways in alternative developmental processes of ascidians. BioEssays 28, 902–912.

35. Lauzon RJ, Kidder SJ, Long P 2007. Suppression of programmed cell death regulates the cyclical degeneration of organs in a colonial urochordate. Dev Biol 301, 92–105.

36. Lauzon RJ, Ishizuka KJ, Weissman IL. 2002. Cyclical generation and degeneration of organs in a colonial urochordate involves crosstalk between old and new: a model for development and regeneration. Dev Biol 249, 333–348.

37. Sabbadin A .1958. Analisi sperimentale dello sviluppo delle colonie di *Botryllus schlosseri* (Pallas). Arch Ital Anat Istol Patol 63, 178–221.

38. Gioacchini G, Dalla Valle L, Benato F, Fimia GM, Nardacci R, Ciccosanti F, et al. 2013. Interplay between autophagy and apoptosis in the development of Danio rerio follicles and the effects of a probiotic. Reproduction, Fertility and Development 25, 1115–1125.

39. Delsuc F, Brinkmann H, Chourrout D, Philippe H. 2006. Tunicates and not cephalochordates are the closest living relatives of vertebrates. Nature 439, 965–968.

40. Ballarin L, Menin A, Tallandini L, Matozzo V, Burighel P, Basso G, et al. 2008. Haemocytes and blastogenetic cycle in the colonial ascidian Botryllus schlosseri: a matter of life and death. Cell Tissue Res 331, 555-564.

SUPPLEMENTARY MATERIAL

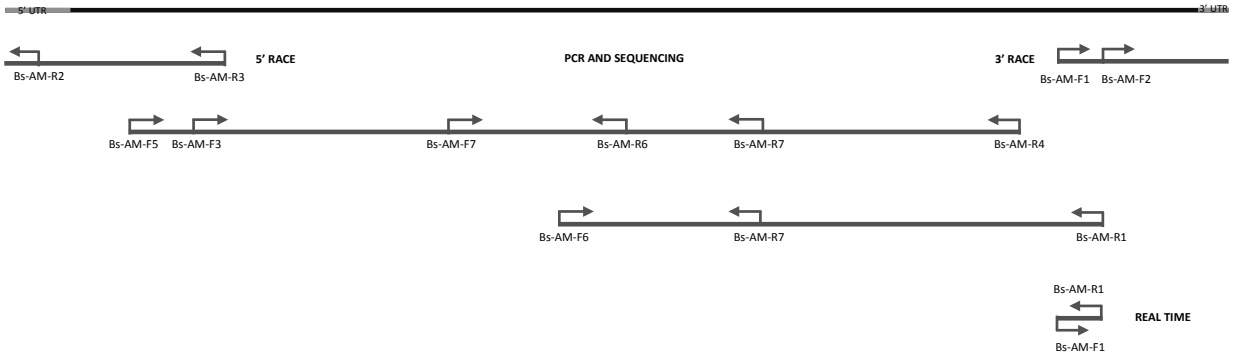

Supplemental Figure 1. Schematic representation of the cloning strategy for the sequencing of *B. schlosseri ambra1* cDNAs. The thick black horizontal line represents the cDNA coding sequence for *ambra1* whereas the 5'- and 3'-UTRs are shown in grey.

This study describes the identification and characterization of two paralogous *ambra1* genes in the zebrafish, their roles during early embryogenesis and muscle development. *Ambra1a* and *ambra1b* arose as part of the fish-specific whole-genome duplication that occurred after the divergence of the fish and tetrapod lineages. These two genes share a similar genomic organization with mammalian *ambra1*. Expression analysis shows that the paralogous gene *ambra1a* is spliced in four alternative transcripts, whereas only one *ambra1b* transcript has been identified. The finding of alternatively spliced transcript variants in zebrafish suggests that some specific Ambra1 functions may depend on distinct protein isoforms able to interact with other proteins in different ways with respect to the complete isoform. This assumption found support in a recently published paper that describes the occurrence of Atg16L1 splice variants playing different functions in the autophagic process [1].

Interestingly, alternatively spliced transcripts for Ambra1 seem to be common also in mammals, as revealed by bioinformatics analysis of databases containing human and murine cDNA sequences. One remarkable and very peculiar splicing variant, identified on zebrafish but likely present also in human and mouse, is represented by a truncated isoform lacking the carboxyl-terminal region and thus the crucial binding site to DLC1. Physiological significance of these different alternative forms is, for the moment, unknown. A new potential goal in the Ambra1 research field could be the detailed characterization of the tissue-specific expression of the different protein isoforms and their specific binding capabilities, to get knowledge on their functions in different physiological and pathological processes. In order to do this, zebrafish represents a good model organism, also for the presence of two paralogous genes in which the multiple roles of the mammalian Ambra1 orthologous seem to have been partitioned.

At the molecular level, also in zebrafish, the down-regulation of Ambra1 expression leads to impairment of the autophagy process associated with hyperproliferation and increased cell death, confirming the crucial role of Ambra1, previously demonstrated in mouse, in the crosstalk among these processes during embryogenesis. The functional link between proliferation, apoptosis and autophagy suggests that these processes are coordinately regulated in early development in order to limit uncontrolled cell demise and/or cell growth during the profound remodelling occurring in the course of organogenesis.

Only few aspects of the involvement of these proteins in zebrafish development has been, up to now, analysed more deeply, starting with their functions during muscle development. Data obtained from *ambra1a* and *ambra1b* zebrafish morphant embryos and from Ambra1$^{gt/gt}$ mouse embryos indicate that this autophagy related-protein plays a critical function during skeletal muscle development in agreement with other recent studies indicating that autophagy plays a key role in skeletal muscles. While the presence of abnormal organelles is likely associated to the well-known role of Ambra1 in the first steps of the autophagic process, the altered morphology and the hyper-cellularity of the developing skeletal muscles may be due to a different function of Ambra1. Further studies

will be necessary to fully elucidate the functional role of Ambra1 in the developing and postnatal skeletal muscles, in order to understand the role of this protein in muscle homeostasis and identify possible human muscle pathologies linked to Ambra1 mutations. Moreover, Ambra1 morphants defects are not limited to the skeletal muscle but involve also the cardiac muscle as morphants embryos exhibit a small string like heart with severe pericardial edema, likely due to developmental heart malformation (work in process).

Another aspect that requires further analyses is the involvement of Ambra1 in head cartilages formation as these structures resulted strongly altered after morpholinos knockdown of *ambra1a* and *ambra1b* expression (data not shown). According to they origin from neural crest cells, *in situ* hybridization analyses with markers specific show modifications in their migration and expression pattern (work in process).

Collectively, our findings confirm an important developmental role for Ambra1 in early vertebrate embryogenesis.

In this study, we also report the identification, through genome bioinformatic searches and targeted cloning, of the first complete *ambra1* transcript in a non-vertebrate species, the tunicate *B. schlosseri*. *ambra1* expression was demonstrated by RT-PCR analysis whereas autophagosomes were visualised by electron microscopy in a degenerating cell phagocyted by a circulating macrophage. This fact highlights the interesting link between autophagy and apoptosis, and allows us to hypothesize that autophagy, in this species, play a role in the crosstalk between bud and parent, optimizing the colony survival. Moreover, taking into account that tunicates are believed the sister group of vertebrates, our data open to new evolutionary considerations on the role and the control of the autophagic mechanism in chordates.

REFERENCES

1. Jiang T, Qin B, He J, Lin S, Ding S. 2013. Three isoforms of the Atg16L1 protein contribute different autophagic properties. Mol Cell Biochem 378,257–266

- Pikulkaew S., Benato F., Celeghin A., Zucal C., **Skobo T.**, Colombo L., Valle LD. The knockdown of maternal glucocorticoid receptor mRNA alters embryo development in zebrafish. 2011. Dev Dyn. Apr 240(4), 874-89.

- Benato F., **Skobo T.**, Gioacchini G., Moro I., Ciccosanti F., Piacentini M., Fimia G.M., Carnevali O., Dalla Valle L. Ambra1 knockdown in zebrafish leads to incomplete development due to severe defects in organogenesis. 2013 Autophagy 9(4).

- Benato F., Dalla Valle L., **Skobo T.**, Alibardi L. 2013. Biomolecular identification of beta-defensin-like peptides from the skin of the soft-shelled turtle Apalone spinifera. JEZ Part B: Molecular and Developmental Evolution.

- Dalla Valle L., Michieli F., Benato F., **Skobo T**., Alibardi L. 2013. Molecular characterization of alpha-keratins in comparison to associated beta-proteins in soft-shelled and hard-shelled turtles produced during the process of epidermal differentiation. JEZ Part B: Molecular and Developmental Evolution.

Participation meetings

- L. Dalla Valle, F. Benato, **T. Skobo**, G. Gioacchini, M. Piacentini, G.M.Fimia, O. Carnevali. "Occurrence of two zebrafish paralogous Ambra 1 (activating molecule in beclin 1-regulated autophagy) transcripts and knockdown effects on development in Danio rerio embryos". **LVII Convegno - Gruppo Embriologico Italiano (GEI);** 5- 8 June 2011, Monteortone, Italy.

- **T. Skobo**, S. Pikulkaew, F. Benato, A. Celeghin, P. Belvedere, L. Colombo Lorenzo, L. Dalla Valle. "The knockdown of the maternal glucocorticoid receptor mRNA affects transcript contents and development in zebrafish embryos". **2nd IRB Barcelona PhD Symposium; LIFE IN MOTION: Dynamics of Molecules and Systems;** 17- 18 November 2011, Barcelona, Spain.

- **T. Skobo**, F. Benato, G. Gioacchini, F. Ciccosanti, M. Piacentini, G. M. Fimia, O. Carnevali, L. Dalla Valle. "Occurrence of two paralogous AMBRA1 transcript and knockdodw effects on zebrafish development". **26th Conference of European Comparative Endocrinologists;** 21- 25 August 2012, Zurich, Switzerland.

- F. Benato, **T. Skobo**, E. Colleti, E. Moro, F. Argenton, L. Dalla Valle. "Visualization of glucocorticoid receptor activity in vivo**". 26th Conference of European Comparative Endocrinologists;** 21- 25 August 2012, Zurich, Switzerland.

- **T. Skobo**, F. Benato, P. Grumati, P. Bonaldo, F. Cecconi, L. Dalla Valle. "*Ambra1* knockdown in zebrafish leads to defects in skeletal muscle development and organization". **8th European Zebrafish Meeting**; 9- 13 July 2013, Barcelona, Spain.

- F. Benato, **T. Skobo**, E. Colleti, E. Moro, F. Argenton, L. Dalla Valle. "Generation of a transegenic zebrafish line for studying the GRE mediated glucocorticoid activity *in vivo*". **8th European Zebrafish Meeting**; 9- 13 July 2013, Barcelona, Spain

- Miccoli, G. Gioacchini, F. Maradonna, F. Benato, **T. Skobo**, L. Dalla Valle, O. Carnevali. "Parental microbial changes affect eggs quality by the modulation of maternal factors involved in autophagic and apoptotic process during Danio rerio development". **17th International Congress of Comparative Endocrinology, ICCE 2013**; 15- 19 July 2013, Barcelona, Spain.

- Miccoli, G. Gioacchini, F. Maradonna, F. Benato, **T. Skobo**, L. Dalla Valle, O. Carnevali. "Parental microbial changes affect eggs quality by the modulation of maternal factors involved in autophagic and apoptotic process during Danio rerio development". **4th International Workshop on Biology of Fish Gametes;** 17- 20 September 2013, Albufeira –Faro, Portugal.

- FEBS Advanced Lecture Course; **Spetses Summer School, Nuclear Receptor Signalling in Physiology and Disease;** August 28- September 2, 2011, Island of Spetses, Greece.

- **Programma Summer School; Scuole di Dottorato di Ricerca dell'Area Medica**- ciclo 26, 26-30 September 2011, Padova, Italy.

- Advanced Lecture Course; **l Logics in developmental biology**; March 2012, Padova, Italy.

- The NUS/TLL/NIBB workshop "**Genetics, genomics and imaging in zebrafish and medaka**" 22-31 July 2012, Singapore, Singapore.

- Advanced Lecture Course; **Paradigm of Cell Fate Specification**; November 2013, Padova, Italy.